

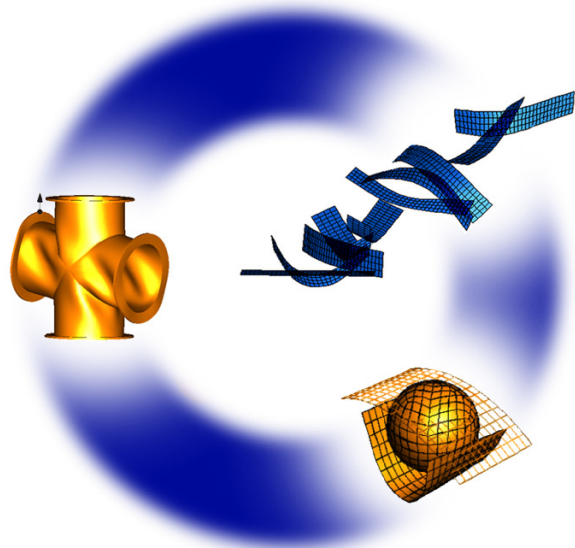


Technische Universität München

Analytical and Numerical Approaches for the Computation of Aeroelastic Sensitivities Using the Direct and Adjoint Methods

Lukas Scheucher, B.Sc.

Master Thesis



SUPERVISOR:

Dr.-Ing. Alexander Popp, Dr.-Ing. Georg Hammerl
popp@lnm.mw.tum.de

Own work declaration

Hereby I confirm that this is my own work and I referenced all sources and auxiliary means used and acknowledged any help that I have received from others as appropriate.

(location, date)

(signature)

Abstract

This is the most often read section. It will determine if someone actually bothers to read more of what you've written. Only write this section after you have completed your report. The abstract consist of only one paragraph, mostly limited to 200-300 words. Literally, a summary of your work. Write a sentence or two about each of the main sections of your report, as discussed in this section. When summarizing results, make the reader aware of the most important results (including numbers when applicable) and important conclusions or questions that follow from these.

Zusammenfassung

german version of your abstract.

Contents

1 About this template	1
2 Fluid mechanics	3
2.1 Eulerian and Lagrangian view	3
2.1.1 Material derivative	3
2.1.2 Eulerian derivative	3
2.2 Basic equations of fluid mechanics	4
2.2.1 Incompressible Navier Stokes Equations	4
2.2.2 Compressible Navier Stokes Equations	5
2.2.3 Euler equations	5
2.2.4 Conservative Form	6
2.2.5 Euler equations	8
2.2.6 Equations of State	8
2.2.7 Reynolds Averaged Navier-Stokes Equations	8
3 Numerical solution	11
3.1 General	11
3.2 Finite Volume method for fluid mechanics	12
3.3 Mixed Finite Volumes (FV)-Finite Elements (FE) formulation	12
3.4 Derivation of the mixed FV-FE formulation	15
3.4.1 Geometric considerations	16
4 The immersed boundary method	17
5 Fluid structure interaction	19
5.1 Coupled three-field formulation	19
5.1.1 Staggered algorithm	21
6 Optimization	25
6.1 Optimization Model	26
6.2 Design Model	28
6.3 Analysis Model	29
7 Fluid Sensitivity Analysis (SA)	33
7.1 Connection between discretization and differentiation	33
7.2 Sensitivity derivation	33
7.2.1 Calculation of $\frac{\partial q_j}{\partial s_i} \Big _{w_0}$	34
7.2.2 Calculation of $\frac{\partial q_j}{\partial w} \Big _{w_0}$	35
7.2.3 Calculation of $\frac{dw}{ds_i} \Big _{w_0}$	35
7.3 Full sensitivity equation	37

8 Derivatives of the fluid residual	39
8.1 Fluid Jacobian $\frac{\partial \mathbf{R}}{\partial \mathbf{w}}$	39
8.1.1 Derivative of the convective Jacobian $\frac{\partial \mathbf{R}^c}{\partial \mathbf{w}}$	39
8.1.2 Derivative of the viscous Jacobian $\frac{\partial \mathbf{R}^v}{\partial \mathbf{w}}$	40
8.2 Analytic Jacobian of the Roe flux	41
8.3 Derivative with respect to the abstract variable $\frac{\partial \mathbf{R}}{\partial s}$	49
8.3.1 Convective contribution $\frac{\partial \mathbf{R}^c}{\partial s}$	49
8.3.2 Viscous contribution $\frac{\partial \mathbf{R}^v}{\partial s}$	50
9 Aero-elastic Sensitivity Analysis	51
9.1 Direct vs. adjoint approach	52
9.1.1 Direct Sensitivity Analysis for the Euler equations	53
9.1.2 Adjoint Sensitivity Analysis for the Euler equations	55
10 The Embedded Boundary Method	57
10.1 Setup	57
10.2 Evaluation of the inviscid term at the interface	57
10.2.1 FIVER-1	58
10.2.2 FIVER-2	59
10.3 Evaluation of the viscous terms at the interface	59
10.3.1 Reconstruction of the fluid-state at ghost-nodes	60
10.4 Evaluation of forces	60
10.5 Level-set method	61
11 Verification	63
11.1 Verification approach	63
12 Verification of mach-sensitivity	64
13 Verification shape sensitivity	64

List of Figures

1	aaa	1
2	FV semi-discretization of an unstructured mesh. Vertex i is the center of dual cell C_i . The boundary of the dual cell is denoted as ∂C_{ij}	13
3	One Triangle T out of the set of triangles \sum_T , that are connected to vertex i . C denotes the dual cell related to vertex i	16
4	Staggered algorithm scheme	21
5	Optimization block-diagram	25
6	Design-model: geometrical approach	30
7	Design element visualization	31
8	Sensitivity Analysis approaches	33
9	aa	50
10	FIVER setup	58
11	Riemann Sketch	59
12	Ghost Point population	61
13	Verification $\frac{dw}{dM_\infty}$ Euler equations body-fitted	65
14	Verification $\frac{dw}{dM_\infty}$ Laminar equations body-fitted	66
15	Verification $\frac{dw}{dM_\infty}$ RANS equations body-fitted	67
16	Verification $\frac{dw}{dM_\infty}$ Euler equations embedded	68
17	Verification $\frac{dw}{dM_\infty}$ Laminar equations embedded	69
18	Verification $\frac{dw}{dM_\infty}$ RANS equations embedded	70
19	Comparison of analytic $\frac{dw}{dM_\infty}$ for all equation types body-fitted	71
20	Comparison of analytic $\frac{dw}{dM_\infty}$ for all equation types embedded	72
21	Verification $\frac{dw}{ds}$ Euler equations body-fitted	73
22	Verification $\frac{dw}{ds}$ Laminar equations body-fitted	74
23	Verification $\frac{dw}{ds}$ RANS equations body-fitted	75
24	Verification $\frac{dw}{ds}$ Euler equations embedded	76
25	Verification $\frac{dw}{ds}$ Laminar equations embedded	77
26	Verification $\frac{dw}{ds}$ RANS equations embedded	78
27	Comparison of analytic $\frac{dw}{dM_\infty}$ for all equation types embedded-fitted	79
28	Comparison of analytic $\frac{dw}{dM_\infty}$ for all equation types embedded-fitted	80
29	Validation of the Lift and Drag results for mach-sensitivity: body-fitted Laminarequations	81
30	Validation of the Lift and Drag results for shape-sensitivity: body-fitted Eulerequations	82
31	Validation of the Lift and Drag results for shape-sensitivity: body-fitted Laminarequations	83
32	Validation of the Lift and Drag results for shape-sensitivity: body-fitted RANSequations	84

Nomenclature

Operators

Algebraic operations

A^T	Transpose of a tensor	T
A^{-1}	Inverse of a tensor	inv
\bar{a}	Average component of a quantity	av
a'	Fluctuating component of a quantity	fluc
$\ a\ $	Norm of a quantity	norm

Analytic operations

\ddot{A}	Second time derivative at a fixed reference position	dderivtime
\dot{A}	First time derivative at a fixed reference position	derivtime
$\frac{\partial A}{\partial B}$	partial derivative of one argument with respect to the other	pdfrac
$\frac{\partial^2 A}{\partial B^2}$	Second partial derivative of one argument with respect to the other	ppdfrac
$\frac{DA}{DB}$	Material time derivative	mfrac
$\frac{dA}{dB}$	First total derivative of one argument with respect to the other	tfrac

Representation of scalars, tensors and other quantities

a	Scalar quantity	s
\mathbf{a}	Vector quantity	v
\mathbf{A}	Matrix quantity	m
A, a	continuous quantity	c
A, a	discrete quantity	d
$a^{(k)}$	Iteration index in the optimization loop	it
$a^{(k)}$	Iteration index in the optimization loop	ito
$a^{(n)}$	Iteration index in the staggered algorithm	its
\bar{A}	Fictitious entity	fic
$\mathcal{O}(A)$	Order of magnitude	order

Symbols

3-field formulations

\mathbf{T}_p	Interface projection matrix from fluid to structure mesh	ifaceprojFt
\mathbf{H}_2	Second order Jacobian	jactwo
\mathbf{S}	Turbulence term	turbmat
\mathbf{T}_u	Interface projection matrix from structure to fluid mesh	ifaceprojSt
\mathbf{R}^c	Convective part of the flux matrix	fluxmatconv
\mathbf{w}	Discrete fluid state vector	dfstate
\mathcal{D}_{gov}	State equation of the mesh	EOSmesh
\mathbf{P}	Fluid load TODO	load
\mathbf{a}_u	Adjoint structure displacement	structdispa
\mathbf{w}	Fluid state vector	fstate
\mathbf{P}_F	Fluid load	fload
\mathcal{S}_{gov}	State equation of the structure	EOSstruct
\mathbf{a}_w	Adjoint fluid state vector	fstatead
$\tilde{\mathbf{w}}$	Primitive fluid state vector	fstateprim
$\dot{\mathbf{x}}$	Fluid mesh motion	mms
\mathbf{G}	diffusive part of the flux matrix	fluxmatdiff
\mathcal{F}_{gov}	State equation of the fluid	EOSfluid
\mathbf{S}	Source term in the Reynolds Averaged Navier-Stokes (RANS) equations	turbulences
\mathbf{a}_x	Adjoint fluid mesh motion	mmsad
\mathbf{w}_{RANS}	Augmentes fluid state vector in the RANS formulation	fstaterans
\mathbf{P}_T	Structure load	sload
\mathbf{u}	Structure displacement	structdisp
\mathbf{A}	Diagonal matrix with vell volumes	cellvolmat
χ	Additional fluid state variable introduced by the turbulence model	turbparamve

Fluid Structure Interaction

\mathcal{P}	State equation of the structure	strucstateq
\mathcal{D}	State equation of the mesh motion	mmsstateeq
\mathcal{F}	State equation of the fluid	fluidstateq

Structural Analysis

\mathbf{K}	FE stiffness matrix	stiffmat
\mathbf{u}	Displacement vector	disp
\mathbf{d}	Interface displacement	ifacedispsvec
\mathbf{u}	Discrete displacement vector	dispsvec
\mathbf{x}	Mesh motion	motion

Optimization

s	Abstract optimazation variable	absvar
q	Optimization criterium	optcrit
ϵ^{SA}	Specified tolerance in the Sensitivity analysis	tolsa
η	Lagrange multipliers of the equality constraints	lagmultseq
L	Lagrangian function of the optimization problem	Lagfunc
s	Vector of abstract optimization variables	absvars
g	Non-equality constraints	neqctr
γ	Lagrange multipliers of the inequality constraints	lagmultsneq
q	Vector of optimization criteria	optcrits
d	Physical design parameters	physvars
z	Target cost function	costfunc
n_g	Number of non-equality constraints	numneqctr
h	Equality constraints	eqctr
a	Adjoint solutions	adjoints
n_h	Number of equality constraints	numeqctr

Fluid Mechanics

p	Pressure	pres
\mathcal{F}	Convective fluxes	fluxesconv
\mathbf{P}	Matrix that contains the eigenvectors of the jacobian matrix of \mathbf{R}^c	jaceigvecs
T	Fluid temperature	temp
v_3	Fluid velocity in z-direction	fluidvelz
Λ	Diagonal matrix that contains the eigenvalues of the jacobian matrix of \mathbf{R}^c	jaceigvals
\mathcal{H}	Jacoian matrix	jac
ρ	Density	dens
μ	Dynamic viscosity	viscosdyn
\mathbf{I}	Identity matrix	eye
ν	Kinematic viscosity	viscoskin
\mathcal{A}	Flux Jacobian	fluxjac
τ	Deviatoric fluid stress tensor	fluidstress
\mathcal{G}	Diffusive fluxes	fluxesdiff
q	Heat flux componenent	heatfluxcomp
k	Thermal conductivity of the fluid	thermcond
E	Total energies	energytot
R_e	Reynolds number	reynolds
\mathbf{q}	Heat flux vector	heatflux
γ	Specific heat ratio	specheatratio
v_2	Fluid velocity in y-direction	fluidvely
e	Internal energy	energyint
v	Fluid velocity vector	fluidvelcomp
v_1	Fluid velocity in x-direction	fluidvelx
\mathbf{M}	Averaging function associated with the Roe flux	roeavgfunc

Abbreviations

SQP Sequential Quadratic Programming

GSE Global Sensitivity Equations

SA Sensitivity Analysis

VOF Volume of Fluid Method

GFM Ghost Fluid Method

GFMP Ghost Fluid Method of the Poor

EOS Equation of State

JWL Jones-Wilkins-Lee

PG Perfect Gas

SG Stiffened Gas

MUSCL Monotonic Upwind scheme for Conservation Laws

FIVER Finite Volume Method with exact two-phase Riemann Integrals

RANS Reynolds Averaged Navier-Stokes

FV Finite Volumes

FD Finite Differences

FE Finite Elements

SA Sensitivity Analysis

LNM Lehrstuhl für Numerische Mechanik (Institute for Computational Mechanics)

TUM Technical University of Munich

CFD Computational Fluid Dynamics

ALE Arbitrary Lagrangian Eulerian

VOF Volume of Fluid Methods

DFP Davidon-Fletcher-Powell formula

BFGS Broyden-Fletcher-Goldfarb-Shanno algorithm

LDR Lift over Drag Ratio

NSE Navier Stokes Equations

NSME Momentum Equation of the Navier Stokes Equations

NSCE Continuity Equation of the Navier Stokes Equations

NSEE Energy Equation of the Navier Stokes Equations

PDE Partial Differential Equation

CG Conjugate Gradient

PCG Preconditioned Conjugate Gradient

SA Sensitivity Analysis

CFD Computational Fluid Dynamics

FSI Fluid Structure Interaction

FRG Farhat Research Group

1 About this template

The purpose of this document is two-fold:

Firstly, this is a plain and simple template with the most basic L^AT_EX-commands and structures introduced that are needed for writing a thesis in L^AT_EX. It should be sufficient for 95% of the theses submitted at LNM - this means that completeness is not claimed. It is recommended to stick to these basic suggestions, knowing that other - possibly better - philosophies or styles exist. In case a more complex structure is needed, refer to literature or the web, although you should think twice about introducing a much more complex structure.

Secondly, this report gives some basic suggestions on what the structure of the report should look like and also some brief description about typically expected content.

Figure 1: aaa bbb

Please note:

- Significant changes to the document style, layout and structure should only be done according to prior agreement with your supervisor.
- compile the template with the following command
`latex LaTeX_template_v04.tex && dvipdfm LaTeX_template_v04.dvi`
- if you encounter problems with dvipdfm, you can also use
`latex LaTeX_template_v04.tex && dvi2ps LaTeX_template_v04.dvi && ps2pdf LaTeX_template_v04.ps`
- if you use texmaker, or a similar LaTeX editor, declare `LaTeX_template_v04.tex` as master document
- the latex compiler might require 2 or 3 runs, until newly created references are resolved correctly
- the bibtex file has to be compiled separately

1 ABOUT THIS TEMPLATE

2 Fluid mechanics

2.1 Eulerian and Lagrangian view

In time dependent analytical physics there are two basic concepts of how to view a system of interest: the Eulerian and the Lagrangian approach. It shall be stressed here, that Eulerian view and Euler equations are two totally separate things.

One view this issue from different perspectives, but what the difference boils down to is the interpretation of the time derivative. Since we will be using the different derivatives frequently in this thesis, a short introduction shall be provided.

2.1.1 Material derivative

The material derivative of a property, is a derivative(rate of change), that follows a specific particle 'p'. That means that at every time instance the material derivative gives as the current value of the property of a specific particle. Since in general, a particle will move its position in time quite a lot, some mean is required to track the particles motion. The material derivative is also known as the Lagrangian concept, and is commonly used in Solid mechanics, since the motion of the solid particles is typically little, or at least nearly uniform over the body, which makes position tracking easy.

2.1.2 Eulerian derivative

The Eulerian derivative takes a different approach. It refers to a fixed frame of reference in the domain, and gives the rate of change at that specific position. Due to the particle movement, it typically refers to different particles at different times. Material and Eulerian derivatives can be linked via the so-called convective rate of change as:

$$\underbrace{\frac{D\mathbf{G}}{Dt}}_{\text{Lagrangian rate of change}} = \underbrace{\frac{\partial \mathbf{G}}{\partial t}}_{\text{Eulerian rate of change}} + \underbrace{\mathbf{v} \cdot \nabla \mathbf{G}}_{\text{Convective rate of change}} \quad (1)$$

In fluid mechanics the Eulerian concept is typically preferred.

However, when looking at fluid-structure interaction problems, the interface is typically moving. To account for that motion in the fluid, one either has to come up with some cell-intersection approach, or the fluid-mesh has to be deformed to.

An appealing and straightforward approach to do so, is the so called Arbitrary Lagrangian Eulerian(Arbitrary Lagrangian Eulerian ([ALE](#))) approach. As the name suggest, it is a hybrid between Eulerian and Lagrangian point of view. The [ALE](#) approach allows to utilize the best of both approaches. The mesh can either be fixed, moved with the continuum in an Eulerian manner, or be moved in some arbitrarily specified manner inbetween. The [ALE](#) method can handle larger distortions than a pure Eulerian would, while still allowing to keep interface continuity between the structure and the fluid, such that no intersection of fluid cells is necessary.

In this thesis, both Eulerian and ALE methods will be covered. In general, no recommendation on to prefer one or the other method can be given. Instead, one should always be aware of the pros and cons of either method and choose the appropriate one for a specific problem accordingly.

2.2 Basic equations of fluid mechanics

The physics of fluid motion are governed by the so-called Navier Stokes Equations (NSE). These equations were derived independently of one another by Claude-Louis Navier and George Gabriel Stokes as a generalization of the Euler-equations that now includes viscosity effects. In general one distinguishes the incompressible and the compressible NSE. The validity of their application depends on the problem setup. As a rule of thumb, flows with Mach-numbers lower than 0.3 can usually be safely approximated by the incompressible NSE.

The Navier stokes equation consist of the Momentum Equation of the Navier Stokes Equations (NSME), the Continuity Equation of the Navier Stokes Equations (NSCE) and, if the compressible equations are solved, the Energy Equation of the Navier Stokes Equations (NSEE). In the literature, the term NSE is often synonymously used for the NSCE, in this thesis however, with NSE we will always refer to the full set of equations and will explicitly name the momentum, continuity or energy equation otherwise.

2.2.1 Incompressible Navier Stokes Equations

The incompressible NSE are derived by putting a few assumptions on the Cauchy stress tensor:

- Galilean invariance of the fluid stress tensor
- Isotropy of the fluid
- The stokes stress constitutive equation applies: $\tau = 2\mu\epsilon$ with $\epsilon = \frac{1}{2}(\nabla\mathbf{v} + (\nabla\mathbf{v})^T)$

In convective form, the incompressible NSME can be written as

$$\underbrace{\frac{\partial \mathbf{v}}{\partial t} + (\mathbf{v} \cdot \nabla) \mathbf{v}}_{\substack{\text{Inertia per volume} \\ \text{Variation}}} - \underbrace{\nu \nabla^2 \mathbf{v}}_{\substack{\text{Divergence of stress} \\ \text{Convection}}} = - \underbrace{\nabla w}_{\substack{\text{Internal source}}} + \underbrace{g}_{\substack{\text{External source}}} \quad \text{eq:nsg_incompressible (2)}$$

where w is the specific thermodynamic work, which satisfies

$$\nabla w = \frac{1}{\rho} \nabla p \quad (3)$$

And the incompressible NSCE can be written as

$$\nabla \cdot \mathbf{v} = 0 \quad (4)$$

It shall be noted, that in the incompressible NSE, the pressure can only be solved up to a certain constant. The pressure at a certain point therefore has to be fixed, or the system will be singular.

2.2.2 Compressible Navier Stokes Equations

Compared to the incompressible NSE, the compressible NSE introduce one additional unknown, since the density can now vary. To close the system, one additional equation is required: the energy equation.

The compressible NSE are derived by making the following assumptions:

- Galilean invariance of the stress tensor
- Linearity of the stress in the velocity gradient: $\tau(\nabla \mathbf{v}) = \mathbf{C} : (\nabla \mathbf{v})$, where \mathbf{C} is called the viscosity or elasticity tensor.
- Isotropy of the fluid

The compressible NSME can be written as

$$\frac{\partial \mathbf{v}}{\partial t} + \mathbf{v} \cdot \nabla \mathbf{v} = -\frac{\partial \rho}{\partial p} \nabla p + \nu \nabla^2 \mathbf{v} + \frac{1}{3} \nu \nabla (\nabla \cdot \mathbf{v}) + g \quad \text{eq:nsg_compressible (5)}$$

where it shall be noted that for the special case of an incompressible flow, the volume of the fluid elements is constant, resulting in a solenoidal velocity field. Thus $\nabla \cdot \mathbf{v} = 0$ and $\nabla p = 0$, which gives equation 2.

The NSCE now takes into accounts for the variable density

$$\frac{\partial \rho}{\partial t} = \nabla \cdot (\rho \mathbf{v}) = 0 \quad (6)$$

And finally the NSEE writes

$$\frac{\partial s}{\partial t} = -\mathbf{v} \cdot \mathbf{s} + \frac{Q}{T} \quad (7)$$

where s is the entropy per unit mass, Q is the heat transferred, and T is the temperature.

2.2.3 Euler equations

The Euler equations can be regarded as a special case of the Navies stokes equations where the diffusive(viscous) contributions are neglected. Dimension analysis [?] reveals that this is usually justified for high Mach numbers and distant from walls. In fact, boundary Layer theory suggests that a lot of problems can be well approximated by solving the full, diffusive equations only near the wall boundary and using the Euler equations everywhere else. Although the Euler equations can be derived for both incompressible and compressible flows, the statement above suggests that only the compressible ones give actual, physically correct results. We therefore restrict

our considerations to the compressible Euler equations.

Summing up, these equations can be written in convective form as

$$\left\{ \begin{array}{ll} \frac{\partial \rho}{\partial t} + \mathbf{v} \cdot \nabla \rho + \rho \nabla \cdot \mathbf{v} = 0 & \text{Continuity equation} \\ \frac{\partial \mathbf{v}}{\partial t} + \mathbf{v} \cdot \nabla \mathbf{v} + \frac{p}{\rho} = \mathbf{g} & \text{Momentum equation} \\ \frac{\partial e}{\partial t} + \mathbf{v} \cdot \nabla e + \frac{p}{\rho} \nabla \cdot \mathbf{v} = 0 & \text{Energy equation} \end{array} \right. \quad (8)$$

2.2.4 Conservative Form

For the purpose of **FV** discretization one usually brings the equations into the so-called conservative form, which can be written generally as

$$\frac{d\boldsymbol{\xi}}{dt} + \nabla \cdot f(\boldsymbol{\xi}) = \mathbf{0} \quad \text{eq:conservative_form_general} \quad (9)$$

$$(10)$$

where $\boldsymbol{\xi}$ is the conserved quantity of interest and $f(\boldsymbol{\xi})$ is denoted as "flux function". This equation can then be transformed into an integral form using the divergence theorem

$$\frac{d}{dt} \int_V \boldsymbol{\xi} dV + \int_{\partial V} f(\boldsymbol{\xi}) \cdot \mathbf{n} dS \quad \text{eq:conservation_form_integral} \quad (11)$$

This equation states that the rate of change of the integral of the quantity $\boldsymbol{\xi}$ over an arbitrary control volume V is equal to the negative of the "flux" through the boundary of the control volume ∂V .

A simple choice for f would be $f(\boldsymbol{\xi}) = \boldsymbol{\xi} \mathbf{v}$, which means that the quantity $\boldsymbol{\xi}$ follows the fluid field and gives the so-called "advection equation".

Although one form is derived from the other, these two are not equivalent. Particularly, it is possible to find solutions to the integral equations that are non-differentiable and therefore not a solutions to the differential form. This leads to so called "weak solutions" and is the cause for many numerical difficulties in the finite volume simulation of such problems.

This thesis focuses on the compressible **NSE** only. They can be brought to conservative form as:

$$\frac{\partial \mathbf{w}}{\partial t} + \nabla \cdot \mathcal{F}(\mathbf{w}) + \nabla \cdot \mathcal{G}(\mathbf{w}) = \mathbf{0} \quad \text{eq:nsg_conservative_form} \quad (12)$$

where, comparing to the general conservative form, one can see that $\boldsymbol{\xi} = \mathbf{w}$ and $f(\boldsymbol{\xi}) = \mathcal{F}(\mathbf{w}) + \mathcal{G}(\mathbf{w})$

In the conservative form of the **NSE** the so-called "fluid state vector" \mathbf{w} is defined as

$$\mathbf{w} = \begin{bmatrix} \rho \\ \rho \mathbf{v} \\ E \end{bmatrix} \quad \text{eq:fstate_definition} \quad (13)$$

2.2 Basic equations of fluid mechanics

with

$$\mathbf{v} = \begin{bmatrix} v_1 \\ v_2 \\ v_3 \end{bmatrix} \quad \text{eq:fluidvel_definition (14)}$$

denoting the fluid velocity vector.

The total energy E can be computed as a sum of the so called internal energy and the kinematic energy due to fluid velocity as

$$\underbrace{E}_{\text{total energy}} = \underbrace{\rho e}_{\text{internal energy}} + \underbrace{\frac{1}{2} \mathbf{v}^T \mathbf{v}}_{\text{kinematic energy}} \quad \text{eq:energytot (15)}$$

Bringing the convective form of the compressible NSE (5) into the conservative form (12), one can derive the convective fluxes \mathcal{F} as

$$\begin{aligned} \mathcal{F} &= \mathbf{w} \mathbf{v}^T + p \begin{bmatrix} 0 \\ \mathbf{I} \\ \mathbf{v}^T \end{bmatrix} & \text{eq:fluxesconv (16)} \\ &= \begin{bmatrix} \rho \mathbf{v}^T \\ \rho (\mathbf{v} \mathbf{v}^T) + p \mathbf{I} \\ (E + p) \mathbf{v}^T \end{bmatrix} \end{aligned} \quad (17)$$

$$= \begin{bmatrix} \rho v_1 & \rho v_2 & \rho v_3 \\ p + \rho v_1^2 & \rho v_1 v_2 & \rho v_1 v_3 \\ \rho v_2 v_1 & p + \rho v_2^2 & \rho v_2 v_3 \\ \rho v_3 v_1 & \rho v_3 v_2 & p + \rho v_3^2 \\ v_1(E + p) & v_1(E + p) & v_1(E + p) \end{bmatrix} \quad (18)$$

depending on the algorithm, one or another form can be advantageous.

The diffusive fluxes can be written as

$$\begin{aligned} \mathcal{G} &= \begin{bmatrix} \mathbf{0} \\ \boldsymbol{\tau} \\ \boldsymbol{\tau} \mathbf{v} + \mathbf{q} \end{bmatrix} & \text{eq:fluxes_diff (19)} \\ &= \begin{bmatrix} 0 & 0 & 0 \\ -\tau_{xx} & -\tau_{yx} & -\tau_{zx} \\ -\tau_{xy} & -\tau_{yy} & -\tau_{zy} \\ -\tau_{xz} & -\tau_{yz} & -\tau_{zz} \\ -q_x - v_1 \tau_{xx} - v_1 \tau_{yx} - v_1 \tau_{zx} & -q_y - v_1 \tau_{xy} - v_1 \tau_{yy} - v_1 \tau_{zy} & -q_z - v_1 \tau_{xz} - v_1 \tau_{yz} - v_1 \tau_{zz} \end{bmatrix}^T \end{aligned} \quad (20)$$

The definition of the stress tensor depends of the fluid model used. For the simple case of a Newtonian fluid, it can be written as

$$\boldsymbol{\tau} = \mu (\nabla \mathbf{v} + (\nabla \mathbf{v})^T) + \lambda (\nabla \cdot \mathbf{v}) \mathbf{I} \quad \text{eq:fluidstress (21)}$$

For the relation between Temperature and heat flux an assumption has to be made. Most often, a simple Fourier's law is assumed

$$\mathbf{q} = -k\nabla T \quad \text{eq:heatflux} \quad (22)$$

2.2.5 Euler equations

The euler equations are a simplified form of the Navier-Stokes Equations (2)(5), where the viscous effects are neglected by setting $\mathcal{G} = \mathbf{0}$.

$$\frac{\partial \mathbf{w}}{\partial t} + \nabla \cdot \mathcal{F}(\mathbf{w}) = \mathbf{0} \quad \text{eq:euler} \quad (23)$$

The Euler equations are appropriate for a wide range of applications. A typical indicator is the Reynolds number, which describes the ratio between inertial forces and viscous forces:

$$R_e = \frac{\rho \mathbf{v} L}{\mu} = \frac{\mathbf{v} L}{\nu} \quad \text{eq:reynolds} \quad (24)$$

where L describes a characteristic length.

A high Reynolds number thus indicates that the flow is dominated by inertial forces, thus the Euler Equations should give satisfying results. However, an Euler flow lacks the ability to represent stick wall boundary conditions, thus it is unable to represent boundary layers.

2.2.6 Equations of State

Looking at the above Equations, one might notice that the number of unknowns is greater than the number of equations. Particularly, the pressure only appears in Equation (16) and is not linked to the other formulas. This problem is solved by introducing an Equation of State (EOS) that relates pressure, internal energy and density. The EOS depends on the fluid model, some well-known ones are: Perfect Gas (PG), Stiffened Gas (SG), Jones-Wilkins-Lee (JWL).

For the simplest one, PG, the EOS can be written as

$$p = (\gamma - 1)\rho e \quad \text{eq:eos_pg} \quad (25)$$

2.2.7 Reynolds Averaged Navier-Stokes Equations

The Reynolds Averaged Navier-Stokes (RANS) Equations are time-averaged equations of motion for the fluid.

$$\mathbf{w} \rightarrow \bar{\mathbf{w}} = \lim_{T \rightarrow \infty} \frac{1}{T} \int_{t^0}^{t^0+T} \mathbf{w} dt \quad \text{eq:rans_averaging} \quad (26)$$

The main idea of the approach is to decompose an instantaneous quantity into time-averaged and fluctuating components

$$\mathbf{w} = \underbrace{\bar{\mathbf{w}}}_{\text{time-average}} + \underbrace{\mathbf{w}'}_{\text{fluctuation}} \quad \text{eq:rans_decomposition} \quad (27)$$

2.2 Basic equations of fluid mechanics

When substituting this decomposition back into the [NSE](#)(and injecting several other approximations), a closure problem induced by the arising non-linear Reynolds stress term $R_{eij} = -v_i'v_j'$ arises. Additional modeling is therefore required to close the [RANS](#) equations, which has led to many different turbulence models.

Whatever turbulence model is chosen, the fluid-state vector is augmented by the m parameters of the turbulence model

$$\boldsymbol{w}_{RANS} \leftarrow \begin{bmatrix} \boldsymbol{w} \\ \chi_1 \\ \vdots \\ \chi_m \end{bmatrix} = \begin{bmatrix} \rho \\ \rho \boldsymbol{v}^T \\ E \\ \chi_1 \\ \vdots \\ \chi_m \end{bmatrix} \quad (28)$$

The [RANS](#) equations can then be written as

$$\frac{\partial \bar{\boldsymbol{w}}}{\partial t} + \nabla \cdot \mathcal{F}(\bar{\boldsymbol{w}}) + \nabla \cdot \mathcal{G}(\bar{\boldsymbol{w}}) = \mathcal{S}(\bar{\boldsymbol{w}}, \chi_1, \dots, \chi_m) \quad \text{eq:rans_eqautions} \quad (29)$$

2 FLUID MECHANICS

3 Numerical solution

3.1 General

Like Finite Differences (**FD**) or Finite Elements (**FE**), the Finite Volumes (**FV**) method is a mean of solving a Partial Differential Equation (**PDE**) by transforming it into a discrete algebraic form. In the field of fluid mechanics, the finite volume method is the most popular approach. Other than **FD** or **FE**, the finite volume is conservative by construction. In contrast to **FD** it can easily be implemented for unstructured grids. Compared to the **FE** method, where boundary conditions come naturally from the formulation, this causes some difficulties in **FV**.

It shall also be mentioned that the introduction of stabilization schemes (like streamline upwinding), is much easier in an **FV** formulation. Overall, for Computational Fluid Dynamics (**CFD**), **FV** has so far shown to be the best compromise between accuracy, stability and efficiency.

Finite volume methods are typically derived from the so called conservative form of a **PDE**. It is shown in Section 2.2.4, that the **NSE** equation can be brought to the conservative form. In general, the conservative form can be written as:

$$\frac{d\boldsymbol{\xi}}{dt} + \nabla \cdot \mathbf{f}(\boldsymbol{\xi}) = \mathbf{0} \quad \text{eq:general_conservative_form} \quad (30)$$

$$(31)$$

where $\boldsymbol{\xi}$ represents a vector of states and f is the so-called flux tensor.

After subdividing the domain into finite volumes, also called cells, one can write for each particular cell i

$$\int_{V_i} \frac{d\boldsymbol{\xi}}{dt} dV_i + \int_{V_i} \nabla \cdot \mathbf{f}(\boldsymbol{\xi}) dV_i \quad (32)$$

It shall be stressed again that reformulating the equations in integral form has already changed the space of admissible solutions. Particularly, the integral form is capable of capturing discontinuities, like shocks whereas the derivative term would be undefined at a shock in equation (30).

After applying the divergence theorem to the second term this gives:

$$\frac{d}{dt} \int_{V_i} \boldsymbol{\xi} dV_i + \int_{\partial V_i} \mathbf{f}(\boldsymbol{\xi}) \cdot \mathbf{n} dS_i \quad (33)$$

And after integration the first term to get the volume average

$$V_i \frac{d\bar{\boldsymbol{\xi}}}{dt} + \int_{\partial V_i} \mathbf{f}(\boldsymbol{\xi}) \cdot \mathbf{n} dS_i \quad (34)$$

So that finally, the equation can be written as

$$\frac{d\bar{\boldsymbol{\xi}}}{dt} + \frac{1}{V_i} \int_{\partial V_i} \mathbf{f}(\boldsymbol{\xi}) \cdot \mathbf{n} dS_i \quad \text{eq:final_fv_general} \quad (35)$$

which can easily be interpreted. The cell average of the conserved properties changes according to the total flux through the cells surface. Of course, the conservative value is defined as being constant within one cell, so there will be different values on faces or edges, depending on which side one is looking at. There are different approaches on how to choose an appropriate value. And the choice may greatly effect the numerical properties. In a **FV** solver, the numerical flux at the interface is typically constructed such, that upwinding is achieved.

3.2 Finite Volume method for fluid mechanics

It has already been shown in Section 2.2.4, that the **NSE** can be brought into the conservative form (12). The flux has been shown to consist of a convective and a diffusive part(16)(19). For this thesis, a Monotonic Upwind scheme for Conservation Laws (**MUSCL**) type **FV** framework for unstructured three-dimensional grids, as described in [?] has been used.

In equivalent manner as in equations (30) to (35) one can now write the conservative form of the **NSE** as

$$\frac{\partial \bar{\mathbf{w}}_i}{\partial t} + \frac{1}{\|\Omega_i\|} \int_{\partial\Omega_i} \mathcal{F}(\mathbf{w}) \cdot dS + \frac{1}{\|\Omega_i\|} \int_{\partial\Omega_i} \mathcal{G}^{\text{eq:NSE full FV formulation}}(\bar{\mathbf{w}}, \nabla \bar{\mathbf{w}}) \cdot dS = \mathbf{0} \quad (36)$$

3.3 Mixed **FV-FE** formulation

It would be totally correct to now solve both terms with classical **FV** methods. However, we note two things. First, there is no need for upwinding in the diffusive term due to its elliptic nature. Secondly, the integration of the second term also becomes much more cumbersome than the first one to the gradient of the fluid state vector demanding at least a first order representation.

For this reasons, we introduce the following, mixed **FV-FE** formulation

$$\frac{\partial \mathbf{w}_i}{\partial t} + \int_{\partial\mathcal{C}_i} \mathcal{F}(\mathbf{w}) \cdot dS - \int_{\sum T_i} \mathbb{K} \mathbf{w} \nabla \phi_i dx = \mathbf{0} \quad \text{eq_mixed_FV_FE} \quad (37)$$

where \mathbb{K} is the diffusive tensor introduced in **TODO** and ϕ_i is a linear P1 shape-function over the triangle. Please also note that the convective term is now integrated over the dual cell related to vertex i , whereas the diffusive term integrated over all primal triangles connected to vertex i .

We will justify this re-formulation in section 3.4.

As can be seen from Figure 2, the dual cells themselves can have very random shapes. This makes the integration over the boundary of the second term in Equation (37) more cumbersome than in a primal approach. Also, the volume integral in the **FE**-like expression has to be splitted into regular shaped subdomains, e.g. tetrahedra, such that standard integration rules, like gauss-rule, can be applied.

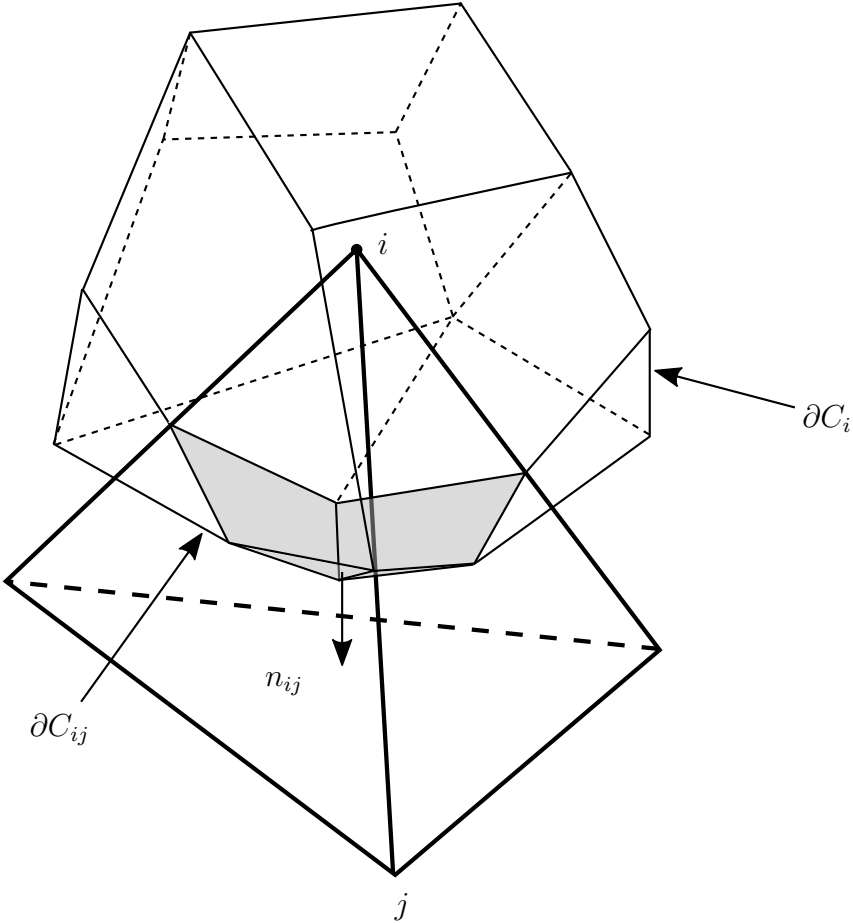


Figure 2: FV semi-discretization of an unstructured mesh. Vertex i is the center of dual cell C_i . The boundary of the dual cell is denoted as ∂C_{ij}

For a closer look into the convective fluxes integral, we decompose the boundary as $\partial\Omega_i = \sum_{j \in \kappa(i)} \partial\Omega_{ij}$, where $\kappa(i)$ denotes the set of vertices connected by an edge to vertex i .

In this thesis, the surface integral in equation (37) is than approximated using a Riemann solver and a MUSCL [?] technique. This approximation can be written as

$$\int_{\partial\Omega_i} \mathcal{F}(\mathbf{w}) \cdot dS \approx \sum_{j \in \kappa(i)} \phi_{ij} \overset{\text{eq:convective term_approximation}}{=} (\mathbf{w}_{ij}, \mathbf{w}_{ji}, \mathbf{n}_{ij}) \quad (38)$$

where ϕ_{ij} denotes the chosen numerical flux function along the edge $i - j$ and the two extrapolated fluid states at the i and the j -side of the the intersection of the cell boundary $\partial\Omega_{ij}$ and edge $i - j$ are denoted by \mathbf{w}_{ij} and \mathbf{w}_{ji} respectively. The area-weighted normal of edge $i - j$ is denoted as \mathbf{n}_{ij} .

A popular choice for the numerical approximation of the convective fluxes is the so-called Roe flux. Appropriate upwinding is directly built into the definition of the Roe flux [?]. In 1D it is defined as:

$$\phi_{ij} = \frac{1}{2} (\mathcal{F}(\mathbf{w}_j) + \mathcal{F}(\mathbf{w}_i)) - \frac{1}{2} |\mathbf{A}| (\mathbf{w}_j - \mathbf{w}_i) \quad (39)$$

3 NUMERICAL SOLUTION

To evaluate a roe-flux between two points in 2D or 3D, a normal vector is required to project the higher, dimensional flux on the connecting line.

As for the volume integral of the diffusive term in Equation (37), it shall be noted that the shape function is still denoted in the primal cell. Since the gradient of the test function is constant, as is the diffusive flux itself, the integral becomes a summation of the primal sub-tetrahedral contributions.

The final numerical approximation can therefore be summarized as

$$\frac{\partial \bar{\mathbf{w}}_i}{\partial t} + \sum_{j \in \kappa(i)} \phi_{ij}(\mathbf{w}_{ij}, \mathbf{w}_{ji}, \boldsymbol{\nu}_{ij}) - \sum_{T_i \in \lambda(i)} \int_{T_j} \mathbb{K}^{\text{eq:nse}} \nabla \mathbf{w} \nabla \phi_j dx = \mathbf{0} \quad (40)$$

where $\kappa(i)$ is the set of vertices connected to vertex i by an edge, and $\lambda(i)$ is the set of primal elements connected to vertex i .

3.4 Derivation of the mixed FV-FE formulation

The equivalence of the finite volume representation of the viscous term, with the finite element-like representation provided in Equation (37) might not be obvious to the reader. This section is therefore denoted to a FE discretization of the governing equations, that can then be reformulated such that the mixed FV-FE formulation is obtained.

First, we start with the full NSE in conservative form, as provided in Equation (12). Next, a test function is defined. We chose the function $(\chi_i)_{i \in \mathcal{P}_h}$ where \mathcal{P}_h represents the primal mesh, as step functions over the dual cells of \mathcal{D}_h . A multiplication with the test-functions and subsequent integration thus gives the following weak form

$$\int_{\Omega} \frac{\partial \mathbf{w}}{\partial t} \chi_i dx + \int_{\Omega} \nabla \cdot \mathcal{F}(\mathbf{w}) \chi_i dx + \int_{\Omega} \nabla \cdot \mathcal{G}(\mathbf{w}, \nabla \mathbf{w}) \chi_i dx \stackrel{\text{f v weak form felike}}{=} \mathbf{0} \quad (41)$$

$$(42)$$

where by using the divergence theorem, we obtain

$$\int_{\Omega} \nabla \cdot \mathcal{F}(\mathbf{w}) \chi_i dx = \int_{\partial C_i} \mathcal{F}(\mathbf{w}) \cdot \mathbf{n} ds \stackrel{\text{eq:divtheorem_felike}}{=} (43)$$

$$\int_{\Omega} \nabla \cdot \mathcal{G}(\mathbf{w}, \nabla \mathbf{w}) \chi_i dx = \underbrace{\int_{\partial C_i} \mathbb{K} \nabla \mathbf{w} \cdot \mathbf{n} ds}_{II} \quad (44)$$

Where the first term is already equivalent to what we have derived by the FV approach in (36).

If the diffusive tensor \mathbb{K} is approximated to be constant over the triangle, which is justified in TODO, the product $\mathbb{K}\mathbf{w}$ is constant, one can now write the above integral as

$$II = \sum_{T \in \mathcal{D}_i} \mathbb{K} \nabla \mathbf{w} \int_{\partial C_i \cap T} \mathbf{n}_C ds \quad (45)$$

Now, we use a particular geometric relation, that holds for primitive elements like triangles and tetrahedra, and is derived in Section 3.4.1

$$\int_{C_i \cap T} \mathbf{n} ds = \frac{\mathbf{n}_i^T}{2} \quad (46)$$

where \mathbf{n}_i^T is the normal to the primal mesh triangle T on the edge opposite of node i . This is where the geometric considerations of section 3.4.1 come into place. As shown in equations (55), the integral over the dual face edge can be written via the normal of the primal mesh triangle as

$$-\sum_{T \in \mathcal{D}_i} \mathbb{K} \nabla \mathbf{w} \frac{\mathbf{n}_i^T}{2} \quad (47)$$

3 NUMERICAL SOLUTION

Also, we have shown in Section 3.4.1, that for the case of a simple triangle (but equally applicable to tetrahedra), the last term of the above equation can be written as

$$-\sum_{T \in \mathcal{D}_i} \mathbb{K} \nabla \mathbf{w} \int_T \nabla \phi_i dx \quad (48)$$

where ϕ_i is the P1 shape-function defined in (50). Finally we can go the opposite way, and join the summations over integrals over triangular contributions back to an overall integral over the whole dual cell. Doing this finally leads to

$$II = - \int_{\mathcal{D}_i} \mathbb{K} \nabla \mathbf{w} \cdot \nabla \phi_i dx \quad (49)$$

which is exactly the term provided in equation (40). Since we used the same step-function based test-functions for all terms in equation (41), this approach is not only consistent, for the special case, of linear triangles we have shown that our finite element term is equivalent to a FV approximation.

3.4.1 Geometric considerations

This section is dedicated to the derivation of a particular link between the shape-function of a linear triangle/tetrahedra and its outward facing normals that we use in chapter 3.4 to proof the equivalence of the FE-formulation of the finite volume term with the FV formulation.

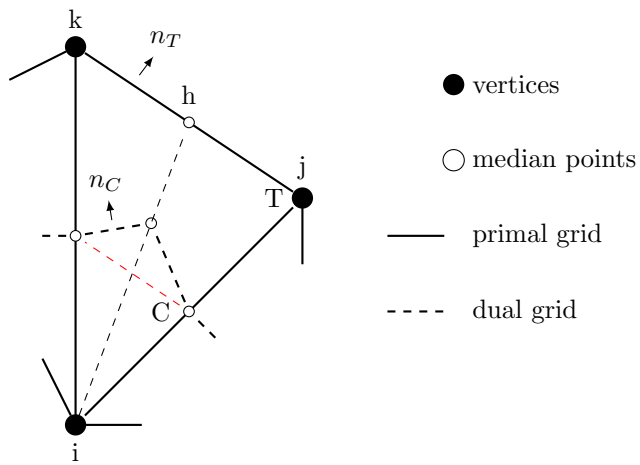


Figure 3: One Triangle T out of the set of triangles \sum_T , that are connected to vertex i . C denotes the dual cell related to vertex i .

We first look at one triangle of the set of triangles \sum_T that belong to node i . The setup is visualized in Figure 3.

The reader can easily verify, that a linear shape-function of node i can be written as:

$$\phi_i(\mathbf{x}) = \frac{\mathbf{h}\mathbf{x} \cdot \mathbf{h}\mathbf{i}}{\|\mathbf{h}\mathbf{i}\|^2} \quad \text{eq:p1_triangle-(50)}$$

where \mathbf{hx} is the vector from point h to any point x in the triangle, and \mathbf{hi} is the vector from point h to point i . For this particular representation of the shape function, the gradient can be elegantly written as

$$\nabla \phi_i(\mathbf{x}) = \frac{\mathbf{hi}}{\|\mathbf{hi}\|^2} = \frac{\hat{\mathbf{hi}}}{\|\mathbf{hi}\|} \quad \text{eq:p1_triangle-(51)}$$

where $\hat{\mathbf{hi}}$ is the normalized vector in $h - i$ direction. Moreover, simple geometry tells us that

$$\|\mathbf{hi}\| \|\mathbf{kj}\| = 2|T| \quad \text{eq:p1_triangle-(52)}$$

where $|T|$ is the area of the triangle T

Substituting equation 52 into equation 51 therefore leads to

$$\nabla \phi_i(\mathbf{x}) = \mathbf{hi} \cdot \frac{\|\mathbf{kj}\|}{2|T|} = -\frac{\boldsymbol{\nu}}{2|T|} \quad \text{eq:p1_triangle-(53)}$$

where $\boldsymbol{\nu}$ is the weighted outward facing normal to edge jk .

$$\boldsymbol{\nu} = -\hat{\mathbf{hi}} \|\mathbf{kj}\| = - \int_{[jk]} \mathbf{n}_T d\Gamma \quad (54)$$

Referring to previous chapter we remind the reader that in the vertex based **FV** approach, and integration over the dual face interface (dashed line in Figure 3) via the weighted interface normal is typically performed.

By simple geometrical considerations we can now determine, that the following relation holds

$$\begin{aligned} \int_{\Gamma_C \cap T} \text{const. } \mathbf{n}_c &= \frac{1}{2} \int_{\Gamma_T} \text{const. } \mathbf{n}_T \\ &= \frac{\boldsymbol{\nu}_i^T}{2} \end{aligned} \quad \text{eq:final_relation-(55)}$$

4 The immersed boundary method

Traditionally internal fluid boundaries, like physical walls imposed by a structure, are represented by meshing the fluid such that it coincides with the structure surface. This approach, that shall be denoted by "explicit boundary method" here, is intuitive and the imposition of boundary conditions comes naturally. In the case of fluid structure interaction, where we expect the structure to move and deform, an explicit boundary treatment prohibits the use of an Eulerian formulation, as described in section REF. Instead every move or shape-change of the structure requires an appropriate update of the fluid mesh. Therefore, Fluid Structure Interaction (**FSI**) problems with explicit boundaries are typically solved via an acALE formulation. Details can be found in section REF.

4 THE IMMERSED BOUNDARY METHOD

However, using an ALE-formulation has some sever disadvantages. First and most importantly for the context of shape-optimization, only minor changes to the topology are admissible. The mesh motion or mesh-update algorithm is only capable of moving the fluid nodes in a spatial manner, the main connectivity of the mesh does not change, however. Therefor, the method can neither cover large distortions, nor is it possible to fundamentally change the structure shape, e.g. removing material in a non-critical region of the structure.

Additionally, creating body-fitted meshed can be cumbersome and time consuming, especially for complex structure geometries.

An elegant solution to this problem is the so-called "immersed boundary method", first described in the context of flow-computations in the human heart in [?]. In an immersed boundary method, the structure surface does not coincide with fluid faces. Therefore, no mesh-movement algorithm is required, and the fluid mesh no longer needs to be specifically designed with a certain structure in mind. In fact, combining this approach with an adaptive mesh refinement completely eliminated any cost in the fluid mesh generation.

The two different approaches are visualized in Figure REF. Due to the attractiveness of the immersed boundary method in the context of shape optimization, special emphasis has been put on the immersed boundary method in this thesis.

TODO figure

5 Fluid structure interaction

Fluid Structure Interaction ([FSI](#)) describes the aeroelastic response of a mechanical system under fluid load, as well as the interaction between fluid and structure itself. Synonymously the term "Aeroelasticity" is often used.

For this thesis, we first will focus on an [ALE](#) formulation, a closer look into this topic in the context of en Embedded formulation will follow.

5.1 Coupled three-field formulation

In an aeroelastic ALE problem, three solution fields have to be considered. Firstly, the usual fluid problem has to be solved. Over the [FSI](#) interface, the fluid now interacts with the structure, imposing a Neumann problem on it. Finally, since we are considering [ALE](#) here, a governing equation for the fluid mesh motion has to be introduced, which closes the system.

Generally speaking, there exist two main approaches for solving this problem. Firstly, one can solve all three problems in one joint system, leading to a so-called monolithic algorithm. The advantage is, that the formulation is consistent and compared to the subsequently introduced staggered algorithm it does not introduce errors in the coupling. However, the solution of the monolithic system is cumbersome, since completely different physics are involved.

In practice, using a so-called "staggered algorithm" has shown to be a more robust choice. In a staggered algorithm, fluid- and structure problem are updated from time step n to $n + 1$ one after the other. Therefore, consistency is lost, and (if no correction is applied) accuracy drops to first order. On the other hand each problem by itself can be treated by well established, optimized, existing solvers so the solution procedure is more robust.

This thesis utilizes the staggered approach. We have coupled a three-dimensional second order finite volume code [?] with a second order accurate finite element code[?] according to the popular three-field formulation of [?].

The three-field formulation of [ALE](#) aeroelasticity can be written as:

$$\begin{aligned} \text{governing equation of structure: } & \mathcal{S}_{gov}(\mathbf{s}, \mathbf{u}, \dot{\mathbf{x}}, \mathbf{w}) \stackrel{\text{eq:3field_structure}}{=} \mathbf{0} & (57) \\ \text{governing equation of meshmotion: } & \mathcal{D}_{gov}(\mathbf{s}, \mathbf{u}, \dot{\mathbf{x}}) \stackrel{\text{eq:3field_mesh}}{=} \mathbf{0} & (58) \\ \text{governing equation of the fluid: } & \mathcal{F}_{gov}(\mathbf{s}, \dot{\mathbf{x}}, \mathbf{w}) \stackrel{\text{eq:3field_fluid}}{=} \mathbf{0} & (59) \end{aligned} \quad (60)$$

Governing equation of the structure: For a simple linear case, that is assumed in this thesis, the structure state equation can be written as

$$\mathcal{S}_{gov} = \mathbf{K}\mathbf{u} - \mathbf{P}(\dot{\mathbf{x}}, \mathbf{w}) \quad \stackrel{\text{eq: eos_struct}}{=} (61)$$

5 FLUID STRUCTURE INTERACTION

where \mathbf{K} represents the finite element stiffness matrix and \mathbf{P} denotes the external load vector that combines aerodynamic loads \mathbf{P}_F that are inflected to the structure by the fluid, and gravity loads \mathbf{P}_0

$$\mathbf{P} = \mathbf{P}_0 + \mathbf{P}_F \quad (62)$$

Governing equation of the mesh motion: In an Arbitrary Lagrangian Eulerian formulation, the fluid mesh deforms with the structure. A governing equation is thus required to describe that deformation. Typically a simple linear pseudo finite element approach or a spring analogy method [?] is used to do so. A Dirichlet problem is solved to move the mesh.

$$\mathcal{D}_{gov} = \bar{\mathbf{K}}\dot{\mathbf{x}} \quad \text{with } \dot{\mathbf{x}} = \mathbf{u} \text{ on } \Gamma_{F|S} \quad \text{eq: eos_mesh} \quad (63)$$

Governing equation of the fluid: The state equation of the fluid depends on the flow model used, as well as on whether a Eulerian or Lagrangian approach is used. A quick overview is provided in Section 2.2.

Please note, that the frame of reference(Eulerian, Lagrangian, Arbitrary Lagrangian Eulerian) has nothing to do with the fluid equation type.

The state equation of the fluid(Equation three in ??)) can be expressed as

$$\mathcal{F}_{gov} = \begin{array}{|c|c|c|} \hline & \text{Euler} & \frac{\partial \mathbf{w}}{\partial t} + \nabla \mathcal{F}(\mathbf{x}, \mathbf{w}) \\ \hline & \text{NSE} & \frac{\partial \mathbf{w}}{\partial t} + \nabla \mathcal{F}(\mathbf{x}, \mathbf{w}) + \nabla \mathcal{G}(\mathbf{x}, \mathbf{w}) \\ \hline & \text{RANS} & \frac{\partial \mathbf{w}}{\partial t} + \nabla \mathcal{F}(\mathbf{x}, \mathbf{w}) + \nabla \mathcal{G}(\mathbf{x}, \mathbf{w}) - \mathcal{S}(\mathbf{x}, \mathbf{w}, \chi) \\ \hline \text{Eulerian} & \text{Euler} & \frac{\partial \mathbf{Jw}}{\partial t} + \mathbf{J} \nabla_{\xi} \mathcal{F}^c(\mathbf{x}, \dot{\mathbf{x}}, \mathbf{w}) \\ \hline & \text{NSE} & \frac{\partial \mathbf{Jw}}{\partial t} + \mathbf{J} \nabla_{\xi} \mathcal{F}^c(\mathbf{x}, \dot{\mathbf{x}}, \mathbf{w}) + \mathbf{J} \nabla_{\xi} \mathcal{G}^c(\mathbf{x}, \dot{\mathbf{x}}, \mathbf{w}) \\ \hline & \text{RANS} & \frac{\partial \mathbf{Jw}}{\partial t} + \mathbf{J} \nabla_{\xi} \mathcal{F}^c(\mathbf{x}, \dot{\mathbf{x}}, \mathbf{w}) + \mathbf{J} \nabla_{\xi} \mathcal{G}^c(\mathbf{x}, \dot{\mathbf{x}}, \mathbf{w}) - \mathcal{S}^c(\mathbf{x}, \dot{\mathbf{x}}, \mathbf{w}, \chi) \\ \hline \text{ALE} & & \\ \hline \end{array} = \mathbf{0} \quad (64)$$

where

$$\mathcal{F}^c(\mathbf{w}) = \mathcal{F}(\mathbf{w}) - \dot{\xi} \mathbf{w} \quad (65)$$

After **FV** discretization of the convective part, and **FE** discretization of the diffusive part, as explained in section **TODO**, the discrete system can be written as

$$\mathcal{F}_{gov} = \begin{array}{|c|c|c|} \hline & \text{Euler} & \frac{\partial \mathbf{w}}{\partial t} + \mathbf{R}^c(\mathbf{x}, \mathbf{w}) \\ \hline & \text{NSE} & \frac{\partial \mathbf{w}}{\partial t} + \mathbf{R}^c(\mathbf{x}, \mathbf{w}) + \mathbf{G}(\mathbf{x}, \mathbf{w}) \\ \hline & \text{RANS} & \frac{\partial \mathbf{w}}{\partial t} + \mathbf{R}^c(\mathbf{x}, \mathbf{w}) + \mathbf{G}(\mathbf{x}, \mathbf{w}) - \mathbf{S}(\mathbf{x}, \mathbf{w}, \chi) \\ \hline \text{Eulerian} & \text{Euler} & \frac{\partial \mathbf{A(x)w}}{\partial t} + \mathbf{R}^c(\mathbf{x}, \dot{\mathbf{x}}, \mathbf{w}) \\ \hline & \text{NSE} & \frac{\partial \mathbf{A(x)w}}{\partial t} + \mathbf{R}^c(\mathbf{x}, \dot{\mathbf{x}}, \mathbf{w}) + \mathbf{G}(\mathbf{x}, \dot{\mathbf{x}}, \mathbf{w}) \\ \hline & \text{RANS} & \frac{\partial \mathbf{A(x)w}}{\partial t} + \mathbf{R}^c(\mathbf{x}, \dot{\mathbf{x}}, \mathbf{w}) + \mathbf{G}(\mathbf{x}, \dot{\mathbf{x}}, \mathbf{w}) - \mathbf{S}(\mathbf{x}, \dot{\mathbf{x}}, \mathbf{w}, \chi) \\ \hline \text{ALE} & & \\ \hline \end{array} = \mathbf{0} \quad (66)$$

Where we remind the reader that, as explained in section 3.2, for a FV discretization, the fluid state \mathbf{w} has to be interpreted as average value over the cell. We often take the cell average to be equal to the value at the cell center, a n approximation that is second order accurate.

In the above equations \mathbf{R}^c denotes the vector of Roe fluxes resulting from a second-order finite volume discretization of the convective part of the NSE, see section 3.2. Likewise, \mathbf{G} likewise denotes an approximation of the diffusive part. As explained in section 3.3 we chose a FE approximation over a FV one for this term.

\mathbf{A} denotes the matrix of cell volumes and \mathbf{S} denotes the matrix resulting from the additional turbulence closures in the RANS equations (see Section 2.2.7).

The above table also gives a very nice overview over the different equation types and the used simplifications. The Euler equations are obviously obtained by neglecting the diffusive part of the NSE. One can also see that the RANS equations are more difficult than the NSE themselves. However, as explained in 2.2.7, the advantage is that RANS can operate on much coarser meshes that do not have to resolve the small scale turbulence phenomena, which makes them more numerically efficient overall in many applications.

5.1.1 Staggered algorithm

The three-field coupled system of equations (57)-(59), can be solved very efficiently with an iterative staggered procedure, such as the one proposed by [?]. This work utilizes the second-order staggered algorithm described in Figure 4.

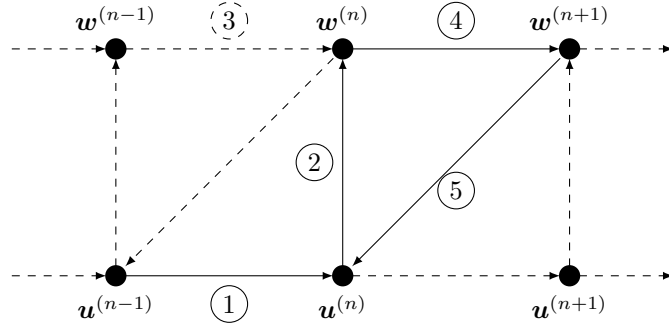


Figure 4: Scheme for the staggered algorithm. The picture depicts the sequential structure(\mathbf{u}) and fluid(\mathbf{w}) solves. First, the structure is updated to a new time step. With this information, a corresponding fluid solution is obtained. After the fluid is progressed in time, the structure solutions is being corrected with that information. A detailed description of all steps follows below.

① **Determining structural response** For a given external load $\mathbf{P}^{(n)}$, the structural response $\mathbf{u}^{(n)}$ is determined by solving the state equation of the structure (57).

To increase stability, and under-relaxation is typically performed:

$$\mathbf{u}^{(n)} = (1 - \theta)\mathbf{u}^{(n-1)} + \theta\tilde{\mathbf{u}} \quad (67)$$

$$\tilde{\mathbf{u}} = \mathbf{K}^{-1}\mathbf{P}^{(n)} \quad (68)$$

Typically, the relaxation factor is chosen as $0.5 \leq \theta \leq 0.9$

② Motion transfer to wet surface The motion of the wet surface of the structure has to be transformed to the fluid.

$$\mathbf{u}_T^{(n)} = \mathbf{T}_u \mathbf{u}^{(n)} \quad (69)$$

where \mathbf{T}_u is a transfer matrix that also accounts for potentially non-matching meshes [?].

③ Fluid mesh motion update The fluid mesh motion is then updated by solving an auxiliary pseudo-Dirichlet problem on the fluid mesh. This step is at the very heart of the ALE algorithm.

$$\bar{\mathbf{K}}\dot{\mathbf{x}}^{(n)} = 0 \quad \dot{\mathbf{x}}^{(n)} = \mathbf{u}_T^{(n)} \text{ on } \Gamma_{F|S} \quad (70)$$

where the Dirichlet conditions are introduced into the system via a decomposition:

$$\bar{\mathbf{K}} = \begin{bmatrix} \bar{\mathbf{K}}_{\Omega\Omega} & \bar{\mathbf{K}}_{\Omega\Gamma} \\ \bar{\mathbf{K}}_{\Gamma\Omega} & \bar{\mathbf{K}}_{\Gamma\Gamma} \end{bmatrix}, \quad \dot{\mathbf{x}} = \begin{bmatrix} \dot{\mathbf{x}}_\Omega \\ \dot{\mathbf{x}}_\Gamma \end{bmatrix} \quad (71)$$

Here, the subscript Γ denotes the fluid grid points at the FSI interface and the subscript Ω denotes the remainder. Hence, the fluid mesh is updated in two steps, by first transferring the structure motion to the fluid interface, and then solving the auxiliary pseudo Dirichlet problem:

$$\dot{\mathbf{x}}_\Gamma^{(n)} = \mathbf{T}_u \mathbf{u}^{(n)} \quad \text{eq:mms_update_1} \quad (72)$$

$$\bar{\mathbf{K}}_{\Omega\Omega}\dot{\mathbf{x}}_\Omega^{(n)} = -\bar{\mathbf{K}}_{\Omega\Gamma}\dot{\mathbf{x}}^{(n)} \quad \text{eq:mms_update_2} \quad (73)$$

It shall be noted that an exact solution of the preceding equation is not required. In fact it is an arbitrarily chosen auxiliary pseudo-problem anyway. Therefor, a valid update of the mesh motion, that does not produce crossovers is enough. Such an update can be obtained at low cost by allying a few Preconditioned Conjugate Gradient (PCG) iterations to Equation (73).

④ Update fluid state vector After the mesh has been deformed, the fluid state \mathbf{w} vector can be updated by allying a singe Newton Rapsodon iteration to

equation TODO, which leads to.

Eulerian	Euler	$\mathbf{R}^c(\mathbf{x}^{(n+1)}, \mathbf{w}^{(n)}) + \frac{\partial \mathbf{R}^c}{\partial \mathbf{w}}(\mathbf{x}^{(n+1)}, \mathbf{w}^{(n+1)} - \mathbf{w}^{(n)})$	$= 0 \quad (74)$
	NSE	$\langle \text{term above} \rangle + \frac{\partial \mathbf{G}}{\partial \mathbf{w}}(\mathbf{x}^{(n+1)}, \mathbf{w}^{(n+1)} - \mathbf{w}^{(n)})$	
	RANS	$\langle \text{term above} \rangle - \frac{\partial \mathbf{S}}{\partial \mathbf{w}}(\mathbf{x}^{(n+1)}, \mathbf{w}^{(n+1)} - \mathbf{w}^{(n)}, \boldsymbol{\chi})$	
ALE	Euler	$\mathbf{R}^c(\mathbf{x}^{(n+1)}, \dot{\mathbf{x}}^{(n+1)}, \mathbf{w}^{(n)}) + \frac{\partial \mathbf{R}^c}{\partial \mathbf{w}}(\mathbf{x}^{(n+1)}, \dot{\mathbf{x}}^{(n+1)}, \mathbf{w}^{(n+1)} - \mathbf{w}^{(n)})$	$= 0 \quad (74)$
	NSE	$\langle \text{term above} \rangle + \frac{\partial \mathbf{G}}{\partial \mathbf{w}}(\mathbf{x}^{(n+1)}, \dot{\mathbf{x}}^{(n+1)}, \mathbf{w}^{(n+1)} - \mathbf{w}^{(n)})$	
	RANS	$\langle \text{term above} \rangle - \frac{\partial \mathbf{S}}{\partial \mathbf{w}}(\mathbf{x}^{(n+1)}, \dot{\mathbf{x}}^{(n+1)}, \mathbf{w}^{(n+1)} - \mathbf{w}^{(n)}, \boldsymbol{\chi})$	

is this correct? What do I do with the turbulence parameter?

⑤ Determining structural responses Once the new fluid-state vector has been determined, the pressure $p^{(n+1)}$ can be recovered. The pressure on the fluid interface side, than mifht need to be transferred to the structure via a transfer matrix \mathbf{T}_u to account for potentially non-matching fluid-structure interfaces.

5 FLUID STRUCTURE INTERACTION

6 Optimization

As mentioned in REF, the overall motivation for this thesis is optimization. A typicall optimization process, not restricted to fluid problems, is depicted in Figure 5.

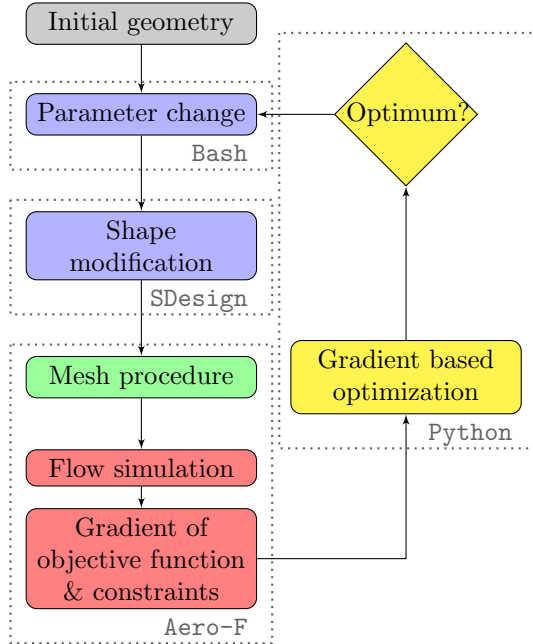


Figure 5: Flow chart of an optimization process in the context of flow simulations. If regards the flow-computation block as a black-box to compute gradients of an objective function and the shape-modification block more general as parameter modification, this optimization routine is applicable to all kinds of problems. In our case, we begin with an initial geometry created by a standard mesh-generation software. We also parametrize the initial mesh in terms of design elements in this first step. This is done via SDesign in this thesis. All further modifications to the geometry are obtained via the design element concept. The mesh-movement, steady-state siumulations and Sensitivity Analysis (SA) are then performed in AERO-F. For the optimizer itself, python has been chosen in this thesis, more specifically the TODO module. The codes communicate via result-files. These files are used to monitor and investigate the optimization process.

A generic, aeroelastic optimization problem can be written as

$$q(\mathbf{s}, \mathbf{u}, \mathbf{w}) \left\{ \begin{array}{l} \min_{\mathbf{s}} z(\mathbf{s}) \\ \mathbf{h}(\mathbf{s}) = \mathbf{0}, \quad \mathbf{h} \in \mathbb{R}^{n_h} \\ \mathbf{g}(\mathbf{s}) > \mathbf{0}, \quad \mathbf{g} \in \mathbb{R}^{n_g} \\ \mathbf{s} = \{\mathbf{s} \in \mathbb{R}^{n_s} \mid \mathbf{s}_L \leq \mathbf{s} \leq \mathbf{s}_U\} \end{array} \right. \begin{array}{l} \text{eq:generic_optimization_problem 1} \\ (75) \\ \text{eq:generic_optimization_problem 2} \\ (76) \end{array}$$

Here, z is an arbitrary cost function that should be minimized. Note that a maximization problem can easily be obtained by multiplying the cost function by a factor

of -1 . In aerodynamics, a typical example for a cost function would be the Lift over Drag Ratio (**LDR**) ratio of an airfoil. The cost-function is described in terms of so-called *abstract variables*. These can have some physical interpretation, but don't necessarily have to(see Section 6.2). Since typically, these optimization problems have no finite solution on an unbounded domain, some restrictions/conditions are introduced. In the airfoil example, we would probably specify a minimum lift that is required to support the configuration. Also a maximum stress for the structure will likely have to be specified. These are classical examples of non-equality constraints, denoted by $\mathbf{g}(\mathbf{s})$ in the above formulation. Constraints can also be formulated in an equality sense, for instance geometrical restrictions due to the turbine suspensions. Furthermore, the abstract optimization variables \mathbf{s} themselves are typically restricted by lower(\mathbf{s}_L) and upper(\mathbf{s}_U) bounds.

The combinations of objective function z and constraints \mathbf{h} and \mathbf{g} is typically denoted as optimization criteria q .

$$\begin{aligned} q &= q(\mathbf{s}, \mathbf{u}, \mathbf{w}) \\ \mathbf{u} &= \mathbf{u}(\mathbf{s}), \quad \mathbf{w} = \mathbf{w}(\mathbf{s}) \end{aligned} \quad \text{eq:optimization_criteria} \quad (77)$$

This thesis follows the *nested analysis and design approach*, meaning that we assume that \mathbf{u} and \mathbf{w} always satisfy the aeroelastic state equations. This means that the state equations are not included in the set of constraints, but the structural displacements \mathbf{u} and the fluid state variables \mathbf{w} are determined in each iteration. As [?] write, the aeroelastic optimization problem can typically be solved by combining three different numerical approaches:

- Optimization Model
- Design Model
- Analysis Model

The optimization model describes the solution of the generic optimization problem(75)-(76). For this thesis, a Sequential Quadratic Programming (**SQP**) has been chosen [?].

The design model links abstract optimization variables \mathbf{s} to actual shapes, structures, geometries or aerodynamics design parameters. For this purpose SDESIGN, a programm specifically written for **SA** purpose in the Farhat Research Group (**FRG**), has been used during this thesis. Its basic concepts an ideas are described in [?].

Finally, the analysis model provides concepts of evaluation the optimization criteria. Typically, the optimization criteria depend on \mathbf{u} and \mathbf{w} which is why a coupled system of equations has to be solved in every design optimization process. The Sensitivity Analysis (**SA**) is also part of this model. Aeroelastic analysis and Sensitivity analysis are discussed in Section 9.

6.1 Optimization Model

Optimization problems are typically solved by gradient-based methods. The methods are divided into

6.1 Optimization Model

- Primal
- Dual
- Penalty-barrier and
- Lagrange approaches

This thesis focuses on Lagrange approaches. For a thorough analysis and comparison of the different approaches, the interested reader is referred to [?].

The Lagrangian approach formulates the optimization problem(75)(76) as an extreme value problem of the Lagrangian:

$$L(\mathbf{s}, \boldsymbol{\eta}, \boldsymbol{\gamma}) = z(\mathbf{s}) \stackrel{\text{eq:lagrangian_of_optimization}}{=} \boldsymbol{\eta}^T \mathbf{h}(\mathbf{s}) + \boldsymbol{\gamma}^T \mathbf{g}(\mathbf{s}) \quad (78)$$

$$\quad \quad \quad (79)$$

Here, $\boldsymbol{\eta}$ denote the Lagrange multipliers for the equality constraints and $\boldsymbol{\gamma}$ the Lagrange multipliers for the non-equality constraints. In fact, one can easily see that the original optimization problem can be obtained as saddle point of the Lagrangian:

$$\frac{\partial L}{\partial \mathbf{s}} = \frac{\partial z}{\partial \mathbf{s}} = \boldsymbol{\eta}^T \frac{\partial \mathbf{h}}{\partial \mathbf{s}} + \boldsymbol{\gamma}^T \frac{\partial \mathbf{g}}{\partial \mathbf{s}} \stackrel{\text{eq:saddlepoint_optimization}}{=} 0 \quad (80)$$

$$\frac{\partial L}{\partial \boldsymbol{\eta}} = \mathbf{h} = 0 \quad (81)$$

$$\frac{\partial L}{\partial \boldsymbol{\gamma}} = \mathbf{g} = 0 \quad (82)$$

The **SQP** method, mention before uses a Newton-Rhapsodon algorithm to solve the above system.

$$\begin{bmatrix} \frac{\partial^2 L}{\partial \mathbf{s}^2} & \frac{\partial \mathbf{g}}{\partial \mathbf{s}}^{(k)} & \frac{\partial \mathbf{h}}{\partial \mathbf{s}}^{(k)} \\ \boldsymbol{\gamma}^{(k)} \frac{\partial \mathbf{g}}{\partial \mathbf{s}}^{(k)} & \mathbf{h}^{(k)} & \mathbf{0} \\ \frac{\partial \mathbf{h}}{\partial \mathbf{s}}^{(k)} & \mathbf{0} & \mathbf{0} \end{bmatrix} \begin{bmatrix} \Delta \mathbf{s} \\ \Delta \boldsymbol{\gamma} \\ \Delta \boldsymbol{\eta} \end{bmatrix} = - \begin{bmatrix} \frac{\partial L}{\partial \mathbf{s}}^{(k)} \\ \boldsymbol{\gamma}^{(k)} \mathbf{g}^{(k)} \\ \mathbf{h}^{(k)} \end{bmatrix} \stackrel{\text{eq:saddlepoint_newtonform}}{=}$$

$$(83)$$

Here $(\cdot)^{(k)}$ denotes the iteration index of the optimization loop.

The linear Equations (83) can also be formulated as an equivalent quadratic minimization problem:

$$\min_{\mathbf{s}} \left(\frac{1}{2} \Delta \mathbf{s}^T \frac{\partial^2 L}{\partial \mathbf{s}^2}^{(k)} \Delta \mathbf{s} + \frac{\partial L}{\partial \mathbf{s}}^{(k)} \right) \stackrel{\text{eq:quadratic_minimization_problem_1}}{=} \quad (84)$$

$$\frac{\partial \mathbf{g}}{\partial \mathbf{s}}^{(k)} \Delta \mathbf{s} + \mathbf{g}^{(k)} \geq \mathbf{0} \stackrel{\text{eq:quadratic_minimization_problem_2}}{=} \quad (85)$$

$$\frac{\partial \mathbf{h}}{\partial \mathbf{s}}^{(k)} \Delta \mathbf{s} + \mathbf{h}^{(k)} = \mathbf{0} \stackrel{\text{eq:quadratic_minimization_problem_3}}{=} \quad (86)$$

In the above formulation, the evaluation of the second derivative of the Lagrangian (Hessian of L) is the numerically most expensive part. Usually it is preferred to approximate it by a first-order information, for example by the Davidon-Fletcher-Powell formula (**DFP**) or by the Broyden-Fletcher-Goldfarb-Shanno algorithm (**BFGS**) method. However, this simplification introduces an error that one should be aware of. Some correction methods have been proposed trying to minimize the error. In this thesis we adapt the one proposed by [?]:

$$\begin{bmatrix} \boldsymbol{s}^{(k+1)} \\ \boldsymbol{\eta}^{(k+1)} \\ \boldsymbol{\gamma}^{(k+1)} \end{bmatrix} = \begin{bmatrix} \boldsymbol{s}^{(k)} \\ \boldsymbol{\eta}^{(k)} \\ \boldsymbol{\gamma}^{(k)} \end{bmatrix} + \alpha^{(k)} \begin{bmatrix} \Delta\boldsymbol{s}^{(k)} \\ \Delta\boldsymbol{\eta}^{(k)} \\ \Delta\boldsymbol{\gamma}^{(k)} \end{bmatrix} \quad \text{eq:correction_step (87)}$$

The appropriate step size $\alpha^{(k)}$ is determined by a line search. AS [?] write, due to this insufficiencies, the Lagrangian can not be used to measure an improvement. Instead, a merit function is introduced that is minimized by the line-search. A local minimum is reached by following a sequence of decreasing merit function values. Convergence of the process can be measured via the \mathcal{L}_2 -norm of the residual of the Kuhn-Tucker conditions([80](#)).

By construction, the constraints are satisfied only when the optimum point is reached.

6.2 Design Model

The design model represent the essential link between the described optimization model and the analysis model. Generally speaking, it relates physical design parameters to abstract ones.

$$\boldsymbol{d} = \boldsymbol{d}(\boldsymbol{s}), \quad \boldsymbol{d} \in \mathbb{R}^{n_d} \quad \text{eq:physvarsToabsvars (88)}$$

Here, n_d denotes the number of physical design parameters. To define a relation between the abstract optimization variables and the motion of the nodes, the following design model is introduced:

$$\dot{\boldsymbol{x}} = \dot{\boldsymbol{x}}(\boldsymbol{s}) \quad (89)$$

As [?] explain, it is unpractical to identify an abstract variable directly with an increment of the coordinate of a grid point. Instead, two approaches, namely geometrical and mechanical can be adopted for constructing the generic design model.

Mechanical approach In the mechanical approach, the shape variation is identified with a superposition of fictitious structural deformations $\bar{\boldsymbol{u}}_j$ due to fictitious

loads $\mu \bar{\mathbf{P}}_j$ and fictions support conditions

$$\dot{\mathbf{x}} = \sum_j \bar{\mathbf{u}}_j = \sum_j \bar{\mathbf{K}}_j^{-1} \mu_j \bar{\mathbf{P}}_j \quad \text{eq:mechanical_approach (90)}$$

where $\bar{\mathbf{K}}_j$ is a fictitious pseudo structure stiffness matrix representing the fluid domain compatible to the current fictions support conditions.

Geometrical approach The geometrical approach describes the geometry of the structure or the fluid boundary the design element concept. Here, the shape of a body \mathbf{X} is approximated by so-called design elements as follows:

$$\mathbf{X} = \sum_j \phi_j(\xi) \hat{\mathbf{X}}_j \quad \text{eq:geometrical_approach (91)}$$

Here, $\phi_j(\xi)$ is a shape function, $\hat{\mathbf{X}}_j$ is the vector of control nodes and ξ represents the reference coordinate. In the design element concept, the variation of the control nodes of the design element is used to vary the shape of the body. The variation of the control nodes position denoted as "mesh-motion" is given as $\dot{\mathbf{x}} = \Delta \hat{\mathbf{X}}$

$$\dot{\mathbf{x}} = \sum_j \phi_j(\xi) \dot{\hat{\mathbf{x}}}_j \quad \text{eq:mms (92)}$$

Just as in Finite Elements, where the shape-functions can not only be used to describe the solution field, but also the body's geometry and material parameters, the design element concept can be applied to prescribe parameter distributions and their variations in the optimization process. A simple sketch of the concept is provided in Figure 6

Both approaches have pros and cons, that are quickly discussed in [?], this thesis utilizes the geometrical approach solemnly.

6.3 Analysis Model

In the analysis model, the optimization criteria q are determined for a given set of optimization variables s . Since the optimization algorithm chosen in this thesis is based on gradients, the gradients of the optimization criteria with respect to the abstract variables are determined in this step. A main focus on this thesis has been the appropriate evaluation of these derivatives, we therefore denote the subsequent chapter 7 to the issue.

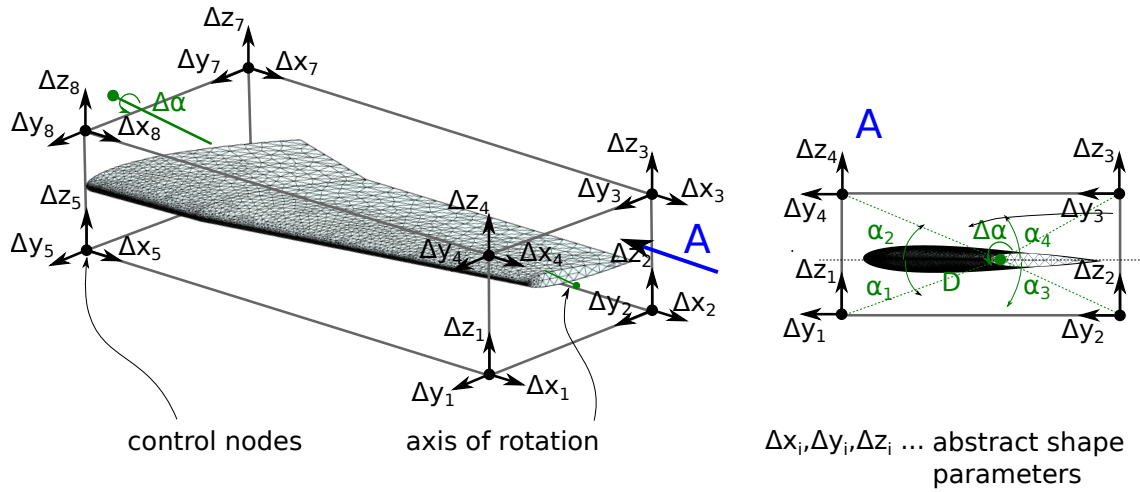


Figure 6: Geometrical approach for the design model as explained in Section 6.2. A NACA type airfoil is considered here as an example. The airfoil is embedded in a bounding box defined by eight so-called control nodes. The position of these control nodes can be varied, which alternates the shape of the airfoil according to some interpolation functions defined on the nodes. The 24 displacement unknowns are denoted as "abstract shape parameters". Abstract shape variables can be arbitrarily defined. As an example, a rotation axis is defined through the wing.

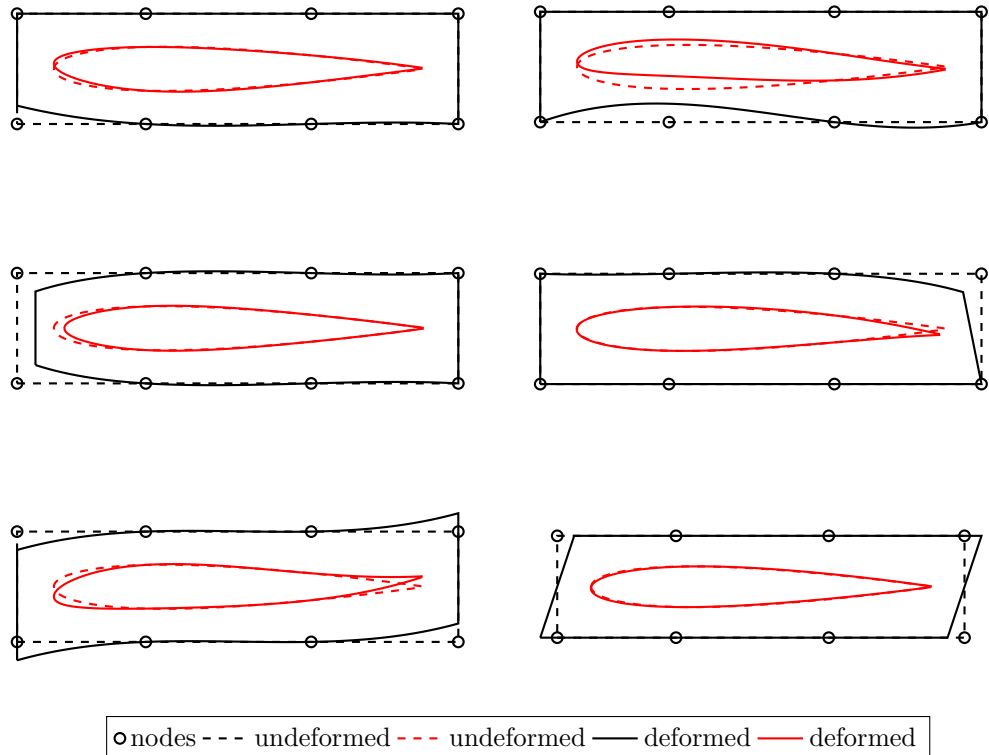


Figure 7: Visualization of the design element concept, exemplarily shown on a NACA0012 airfoil. For simplicity, a single design element(cubic in the horizontal direction and linear in the vertical direction) is used. Both the initial configuration(dashed lines) and the deformed configuration(full lines) are plotted. Although only eight design element nodes are provided, the function space of the design element allows for a great variation of the airfoil shape. Also, the size of the parameter space is now independent of the airfoil mesh size. From this perspective, the design element concept can be regarded as an model reduction for the shape variation.

6 OPTIMIZATION

7 Fluid Sensitivity Analysis (SA)

As explained in section 6, optimization is based on the calculations of gradients, also denoted as Sensitivity Analysis (SA).

7.1 Connection between discretization and differentiation

When it comes to calculating the gradients of a solution of a PDE, there are two fundamentally different approaches one could take.

Firstly one could think of first deriving the continuous equation and then applying the discretization scheme. On the other hand its equally legitimate to first apply the discretization and compute the gradients of that, approximated solution. This thesis focuses uses the latter one, the reasons being explained in Figure 8.

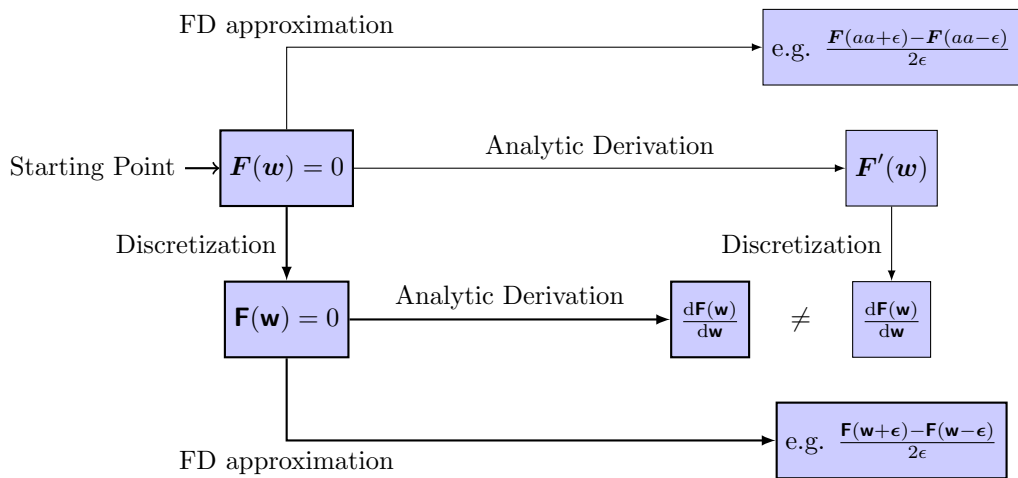


Figure 8: Two different approaches of SA. The question here is whether to discretize the system of equations first and then compute the derivatives of the approximate solution, or whether the continuous system of equation is first derived and discretized afterwards. Both approaches are valid, the final result however will generally not be the same. We have solemnly focused on the case of derivation after discretization in this thesis(thick lines). There are several reason to this. Firstly, if one chose to first derive and then compute a discretized solution, one would solve a completely different equation. If on the other hand the discretization(e.g. Finite Volumes) is done first, standard solvers can be utilized. What is more, approximating the derivative by a Finite difference becomes much easier, since the finite difference evaluation involves only a evaluation of \mathbf{F} , which a standard fluid solver is perfectly capable of, whereas the FD approximation in the other case would involve evaluations of the continuous function and the discretization of the obtained expression which would be much more cumbersome. **Think about whether this is correct**

7.2 Sensitivity derivation

When it comes to SA within the context of CFD, one also has to distinguish between SA of the non-coupled fluid problem and the SA in the fully coupled aeroelastic case.

The latter case is much more involved, since it requires additional terms from the Structure and mesh motion equations. In the following we will therefore begin with the SA of a regular fluid problem. A generalization to a coupled FSI problem will follow.

As mentioned in Section 6, we typically deal with an optimization criteria q_j , that is in this case dependent on the fluid state variables \mathbf{w} that themselves may depend on abstract variables s_i

$$q_j = q_j(\mathbf{w}(s_i)) \quad (93)$$

$$\frac{dq_j}{ds_i} \Big|_{\mathbf{w}_0} = \underbrace{\frac{\partial q_j}{\partial s_i} \Big|_{\mathbf{w}_0}}_{\text{directly derived from the definition of } q} + \underbrace{\frac{\partial q_j}{\partial \mathbf{w}} \Big|_{\mathbf{w}_0}}_{\substack{\text{derived analytically or} \\ \text{by FD}}} \underbrace{\frac{\partial \mathbf{w}}{\partial s_i} \Big|_{\mathbf{w}_0}}_{\text{eq:sensitivity_startingpoint(94) derived from dynamic fluid equilibrium}}$$

7.2.1 Calculation of $\frac{\partial q_j}{\partial s_i} \Big|_{\mathbf{w}_0}$

In this thesis, we restrict ourselves to Lift(L), Drag(D) and combinations of these quantities (e.g. Lift-Drag ration $\frac{L}{D}$) as optimization criteria q . As abstract variables we only consider the free stream mach-number M_∞ , the free-stream angle of attack α_∞ and an airfoil shape parameter as explained in section 6.2. The formula for the lift over an airfoil can be written as

If Γ_{FS} denotes the fluid structure interface, which in the ALE context coincides with the airfoil surface, one can formulate the lift and drag of an airfoil in a steady state as:

$$\begin{aligned} L &= \int_{\Gamma_{FS}} p(\mathbf{w}, \mathbf{x}) \mathbf{n}(\mathbf{x}) \cdot \mathbf{e}_L dS \\ D &= \int_{\Gamma_{FS}} p(\mathbf{w}, \mathbf{x}) \mathbf{n}(\mathbf{x}) \cdot \mathbf{e}_D dS \end{aligned} \quad \text{eq:lift_and_drag_integrals(95)}$$

where \mathbf{e}_D is the unit vector pointing in the direction of the free stream, and \mathbf{e}_L is the unit vector perpendicular to that. We therefor note, that $\frac{\partial L}{\partial s_i}$ and $\frac{\partial D}{\partial s_i}$ are zero for $s_i = M_\infty$ and $s_i = \alpha_\infty$ and non-zero if s_i is a shape parameter.

Also, having determined the derivatives $\frac{\partial L}{\partial s_i}$ and $\frac{\partial D}{\partial s_i}$, the derivative of the Lift-Drag ratio follows simply as

$$-\frac{\partial(\frac{L}{D})}{\partial s_i} \Big|_{\mathbf{w}_0} = -\frac{D_0 \frac{\partial L}{\partial s_i} \Big|_{\mathbf{w}_0} - L_0 \frac{\partial D}{\partial s_i} \Big|_{\mathbf{w}_0}}{D_0^2} \quad \text{eq:lifttodrag_by_absvar(97)}$$

7.2.2 Calculation of $\frac{\partial q_j}{\partial \mathbf{w}} \Big|_{\mathbf{w}_0}$

The derivative of the optimization criteria with respect to the fluid state vector can again be splitted into Lift and Drag part. For an aeroelastic simulations, the biggest difficulty here is the dependence on the fluid state by the fluid-structure interface itself. We are therefore faced with a derivative of an integral quantity, where the integration area itself is dependent on the quantiti of interest.

For this purpose, we recall the leibnitz rule from calculus:

$$\frac{d}{dx} \left(\int_{a(x)}^{b(x)} f(x, t) dt \right) = f(x, b(x)) \cdot \frac{d}{dx} b(x) - f(x, a(x)) \cdot \frac{d}{dx} a(x) + \int_{a(x)}^{b(x)} \frac{d}{dx} f(x, t) dt \quad \text{eq:Leibnitz_rule (98)}$$

Alternatively, we can directly switch to the discrete form, where the calculation of Lift and drag as outlined in Equation (95) can be performed as

$$L = \sum_{e \in \sum_{FS}} \sum_{i=1}^{n_g} g_i p(\mathbf{w}_i, \mathbf{x}_i) \mathbf{n}_e \cdot e_L D = \sum_{e \in \sum_{FS}} \sum_{i=1}^{n_g} \bar{g}_i p(\mathbf{w}_i, \mathbf{x}_i) \bar{\mathbf{n}}_e \cdot \bar{e}_D \quad \text{eq:discrete lift and drag formulas (99)}$$

where \sum_{FS} is the set of surface elements on the fluid-structure interface, n_g is the number of gauss-points and g_i are the gauss weights. The dependency of the surface shape, on the fluid state vector is now reflected in non-zero derivatives of the gauss point locations.

Finally, the derivative of the lift-to-drag ratio can be obtained analogously to equation (97) as

$$\frac{\partial (\frac{L}{D})}{\partial \mathbf{w}} \Big|_{\mathbf{w}_0} = \frac{D_0 \frac{\partial L}{\partial \mathbf{w}} \Big|_{\mathbf{w}_0} - L_0 \frac{\partial D}{\partial \mathbf{w}} \Big|_{\mathbf{w}_0}}{D_0^2} \quad \text{eq:lifttodrag_by_dfstate (100)}$$

7.2.3 Calculation of $\frac{d\mathbf{w}}{ds_i} \Big|_{\mathbf{w}_0}$

Also, we keep in mind, that the state equation of the fluid can be expressed as

$$\mathcal{F}_{gov}(\mathbf{w}(s_i), \dot{\mathbf{x}}(s_i), s_i) = \frac{\partial \mathbf{w}(s_i)}{\partial t} + \nabla \cdot \mathcal{F}(\mathbf{w}(s_i)) + \nabla \mathcal{G}(\mathbf{w}(s_i)) + S = \mathbf{0} \quad (101)$$

After discretization, we have derived our discrete governing equation as

$$\frac{\partial \bar{\mathbf{w}}_i}{\partial t} + \sum_{j \in \kappa(i)} \phi_{ij}(\mathbf{w}_{ij}, \mathbf{w}_{ji}, \boldsymbol{\nu}_{ij}) - \sum_{T_i \in \lambda(i)} \int_{T_j} \mathbb{K} \nabla \mathbf{w} \nabla \phi_j dx = \mathbf{0} \quad \text{eq:nse_final_discretized_2 (102)}$$

For the pupose of Sensitivity analysis around a given steady state, the fluid-state vector does not change in time, and can thus be ommitted, also we summaraze the

convective and the diffusive part as \mathbf{R}

$$\cancel{\frac{\partial \bar{\mathbf{w}}_i}{\partial t}^0} + \underbrace{\sum_{j \in \kappa(i)} \phi_{ij}(\mathbf{w}_{ij}, \mathbf{w}_{ji}, \nu_{ij})}_{\mathbf{R}^i} - \underbrace{\sum_{T_i \in \lambda(i)} \int_{T_j} \mathbb{K} \nabla \mathbf{w} \nabla \phi_j dx}_{\mathbf{R}^v} = \mathbf{0} \quad \text{eq: nse final discretized notation change (103)}$$

where \mathbf{R}^i denotes the inviscid residual and \mathbf{R}^v the viscous contribution. We now can express the steady state equation in very compact form as:

$$\mathbf{R} = \mathbf{0} \quad \text{eq: discrete steady state (104)}$$

In general, this residual depends on the fluid state solution \mathbf{w} as well as on a potential mesh movement \mathbf{x} , both of which can be dependent on the abstract design variable. Additionally, a direct dependence on s might be encountered too.

$$\mathbf{R}(\mathbf{w}(s), \mathbf{x}(s), s) = \mathbf{0} \quad (105)$$

The total derivative of the residual with respect to the design variable can thus be expanded via the chain rule to

$$\frac{d\mathbf{R}}{ds_i} = \mathbf{0} = \frac{d\mathbf{R}}{ds_i} + \frac{\partial \mathbf{R}}{\partial \mathbf{w}} \frac{d\mathbf{w}}{ds_i} + \frac{\partial \mathbf{R}}{\partial \mathbf{x}} \frac{d\mathbf{x}}{ds_i} \quad (106)$$

Therefore the total derivative of the fluid state with respect to the shape variable, needed in equation (94), can be obtained by solving

$$\frac{\partial \mathbf{R}}{\partial \mathbf{w}} \frac{d\mathbf{w}}{ds_i} = - \frac{d\mathbf{R}}{ds_i} - \frac{\partial \mathbf{R}}{\partial \mathbf{x}} \frac{d\mathbf{x}}{ds_i} \quad \text{eq: dfstate_by_absvart (107)}$$

In this equation, $\frac{\partial \mathbf{R}}{\partial s_i}$ can be computed analytically or by FD. This part is the most cumbersome part of the whole sensitivity analysis, which is why we denoted a full chapter(8) to it.

The derivative of the mesh motion with respect to the abstract variables is often denoted as "shape gradient". It can be divided into two components:

- The interface component $\frac{d\dot{\mathbf{x}}_\Gamma}{ds_i}$, which is associated with the grid points lying on the fluid boundary
- The interior component $\frac{d\dot{\mathbf{x}}_\Omega}{ds_i}$, which is associated with the grid points located in the interior Ω of the computational domain.

The interface component is determined by the structure. Having obtained this one, the interior component can be computed by solving an auxiliary, fictitious Dirichlet problem:

$$\frac{d\dot{\mathbf{x}}_\Omega}{ds_i} = - \left[\bar{\mathbf{K}}_{\Omega\Omega}^{-1} \bar{\mathbf{K}}_{\Omega\Gamma} \right] \frac{d\dot{\mathbf{x}}_\Gamma}{ds_i} \quad (108)$$

where $\bar{\mathbf{K}}$ is a pseudo stiffness matrix that can be obtained by a simple spring analogy or similar approaches. In general, the mesh-motion algorithm should be chosen consistently with the one used in the calculation of the steady state solution. For the later introduced Embedded framework, $\frac{d\dot{\mathbf{x}}}{ds_i}$ is the position vector of the embedded discrete surface

7.3 Full sensitivity equation

After inserting (97), (100) and (107) into (94), one can derive the final sensitivity equations for the special case of a rigid or non-existing structure as

$$\frac{dq_j}{ds_i} \Big|_{\mathbf{w}_0} = - \frac{dq_j}{d\mathbf{w}} \Big|_{\mathbf{w}_0} \left[\frac{\partial \mathbf{R}}{\partial \mathbf{w}} \Big|_{\mathbf{w}_0} \right]^{-1} \left(\frac{\partial \mathbf{R}}{\partial s_i} \Big|_{\mathbf{w}_0} + \left[\alpha \frac{\partial \mathbf{R}}{\partial \dot{\mathbf{x}}_\Omega} \Big|_{\mathbf{w}_0} \quad \frac{\partial \mathbf{R}}{\partial \dot{\mathbf{x}}_\Gamma} \Big|_{\mathbf{w}_0} \right] \begin{matrix} \alpha \bar{\mathbf{K}}_{\Omega\Omega}^{-1} \bar{\mathbf{K}}_{\Omega\Gamma} \\ \mathbf{I} \end{matrix} \frac{d\dot{\mathbf{x}}_\Gamma}{ds_i} \right) \quad \text{eq:full_sa_nostruct} \quad (109)$$

$$\alpha = \begin{cases} 1 & \text{in ALE framework} \\ 0 & \text{in Embedded framework} \end{cases} \quad (110)$$

8 Derivatives of the fluid residual

This section is denoted to a thorough derivation of the partial derivatives $\frac{\partial \mathbf{R}}{\partial \mathbf{w}}$ and $\frac{\partial \mathbf{R}}{\partial s}$ of the fluid residual equation. These are the main quantities needed in order to compute the sensitivity of the state vector $\frac{\partial \mathbf{w}}{\partial s}$ as shown in equation 109. We need this derivative in order to solve for $\frac{\mathbf{w}}{s}$ in equation (??).

8.1 Fluid Jacobian $\frac{\partial \mathbf{R}}{\partial \mathbf{w}}$

According to (103), the total residual is comprised of a convective(inviscid) part and a viscous contributions. Thanks to the distributive property of the derivative operator, we can thus compute the derivative of the total residual as the sum of the derivatives of the components. This is particulary important for us, since we used two different discretization routines for the viscous and the inviscid part.

8.1.1 Derivative of the convective Jacobian $\frac{\partial \mathbf{R}^c}{\partial \mathbf{w}}$

Also, we will only discuss the special case of intersected elements in the following, since the special case of an non-intersected cell follows trivially from that.

For more details on the evaluation of the inviscid residual the reader is refered to section 3, specifically section 3.2 and section ?? for the incorporation of the immersed boundary conditions.

For the convective part of the Jacobian, \mathbf{R}^c we can be therefor write

$$\mathbf{R}_{ij}^{c,i} = \phi_{ij}^i(\tilde{\mathbf{w}}_{ij}, \tilde{\mathbf{w}}_{ij}^*, \mathbf{n}_{ij}) \quad (111)$$

Since the fluid normal is dependent on the mesh position this can also be written as

$$\mathbf{R}_{ij}^{c,i} = \phi_{ij}^i(\tilde{\mathbf{w}}_{ij}, \tilde{\mathbf{w}}_{ij}^*, \mathbf{x}) \quad (112)$$

If the edge $i - j$ is intersected however, the half-Riemann problem approach as discussed in section REF is applied. Also, the quantity \mathbf{w}_{ij} on the interface can be reconstructed in several way. In this thesis we applied a MUSCL technique. Of course, the reconstruction and limitation has to be taken into account as well.

Putting this all together, one can write

$$\frac{\partial \mathbf{R}_{ij}^i}{\partial \mathbf{w}_k} = \frac{\partial \mathbf{R}_{ij}^i}{\partial \tilde{\mathbf{w}}_{ij}^*} \frac{\partial \tilde{\mathbf{w}}_{ij}^*}{\partial \tilde{\mathbf{w}}_k} \frac{\partial \tilde{\mathbf{w}}_k}{\partial \mathbf{w}_k} + \frac{\partial \mathbf{R}_{ij}^i}{\partial \tilde{\mathbf{w}}_{ij}} \frac{\partial \tilde{\mathbf{w}}_{ij}}{\partial \tilde{\mathbf{w}}_k} \frac{\partial \tilde{\mathbf{w}}_k}{\partial \mathbf{w}_k} + \underbrace{\frac{\partial \mathbf{R}_{ij}^{c,i}}{\partial \mathbf{x}} \frac{\partial \mathbf{x}}{\partial \mathbf{n}_{ij}}}_{=0 \text{ for embedded}} \quad (113)$$

- Analytical Jacobian of the (Roe's) centering flux
- Analytical derivative of the solution of the 1D half-Riemann problem
- Analytical derivative of the MUSCL reconstruction and limitation

where, $(\tilde{\cdot})$ denotes primitive quantitivs, $\frac{\partial \tilde{\mathbf{w}}_k}{\partial \mathbf{w}_k}$ accounts for the conversion between primitive and conservative state vector, $\frac{\partial \mathbf{R}_{ij}^{c,i}}{\partial \tilde{\mathbf{w}}_{ij}^*}$ is the analytical derivative of the MUSCL reconstruction and limitation and a is the analytical Jacobian of the Roe flux. Finally, $\frac{\partial \tilde{\mathbf{w}}_{ij}^*}{\partial \tilde{\mathbf{w}}_k}$ accounts for the analytical derivative of the solution of the 1D half-Riemann problem. This also accounts for the only really new derivative to be considered in comparison to the cells far from the immersed boundaries.

The analytic Jacobian of the Roe flux is provided in section 8.2, the derivative of the solution of the 1D hgalf-Riemann problem is discussed in section TODO, the derivative of the MUSCL reconstruction in section TODO and finally, the derivative of the conversion to primitive variables is discussed in section TODO.

8.1.2 Derivative of the viscous Jacobian $\frac{\partial \mathbf{R}^c}{\partial \mathbf{w}}$

For the discussion of the viscous Jacobian, we first remind the reader that an FE approach is used to evaluate this term, in contrast to the FV approach used for the inviscid contribution. For a detailed discussion the reader is referred to section 3.3 and the following sections.

As far as the residual evaluation itself goes, we recall that, once the ghost points have been populated(see section TODO), the residual is evaluated as though it had never been intersected in the first place. We can therefore write the viscous residual of an intersected cell as

$$\mathbf{R}^c(\tilde{\mathbf{w}}^a, \tilde{\mathbf{w}}^g(\tilde{\mathbf{w}}^a)) = \mathbf{0} \quad (114)$$

where $\tilde{\mathbf{w}}^a$ represents the fluid states of the active node, and $\tilde{\mathbf{w}}^g$ are the fluid states of the ghost nodes, which can themselves be expressed in terms of the active nodes. An thus the derivative becomes:

$$\frac{\partial \mathbf{R}^v(\tilde{\mathbf{w}}^a, \tilde{\mathbf{w}}^g(\tilde{\mathbf{w}}^a))}{\partial \tilde{\mathbf{w}}} = \underbrace{\frac{\partial \mathbf{R}^v}{\partial \tilde{\mathbf{w}}^a}}_{\text{can be re-used from ALE after the ghost-point population}} + \frac{\partial \mathbf{R}^v}{\partial \tilde{\mathbf{w}}^g} \cdot \overbrace{\frac{\partial \tilde{\mathbf{w}}^g}{\partial \tilde{\mathbf{w}}^a}}^{\text{obtained during the population process}} \quad (115)$$

For the analytic viscous Jacobian contribution we don't have to make a difference between $\frac{\partial \mathbf{R}^c}{\partial \tilde{\mathbf{w}}^a}$ and $\frac{\partial \mathbf{R}^v}{\partial \tilde{\mathbf{w}}^g}$.

We recall the definition of the viscous residual as

$$\mathbf{R}_i^v = - \sum_{T_i \in \lambda(i)} \int_{T_j} \mathbb{K} \nabla \mathbf{w} \nabla \phi_j dx \quad (116)$$

again, we switch to primitive variables for easier evaluation

$$\mathbf{R}_i^v = - \sum_{T_i \in \lambda(i)} \int_{T_j} \mathbb{K} \nabla \mathbf{w} \nabla \phi_j dx \quad (117)$$

Applying a numerical integration such as gauss rule, this becomes

$$\mathbf{R}_i^v = - \sum_{T_i \in \lambda(i)} \sum_{i=1}^{n_g} w_i \tilde{\mathbb{K}} \nabla \tilde{\mathbf{w}}(\mathbf{x}_i) \nabla \phi_j(\mathbf{x}_i) dx \quad \text{eq:aaa(118)}$$

Thus, due the constant nature of the diffusive tensor $\tilde{\mathbb{K}}$ the derivative can be written straightforwardly as

$$\frac{\partial \mathbf{R}_i^v}{\partial \tilde{\mathbf{w}}} = - \sum_{T_i \in \lambda(i)} \sum_{i=1}^{n_g} w_i \tilde{\mathbb{K}} \nabla \tilde{\mathbf{w}}(\mathbf{x}_i) \nabla \phi_j(\mathbf{x}_i) dx \quad \text{eq:aaa(119)}$$

8.2 Analytic Jacobian of the Roe flux

This section provides a detailed step by step derivation of the analytic convective Jacobian. This section is lengthy and not necessarily required for understanding the rest of the thesis. For this reason it has been moved at the end of chapter 8. Nonetheless, in the authors opinion, it provides some crucial insight into the basics of SA, and it is certainly of great help and serves as a reference for anyone who wants to implement those derivatives himself.

$$\frac{\partial \mathbf{R}_i^c}{\partial \mathbf{w}} = \sum_{j \in \kappa(i)} \underbrace{\frac{\partial \text{meas}(C_{ij})}{\partial \mathbf{w}} \phi_{ij}(\mathbf{w}_{ij}, \mathbf{w}_{ji}, \boldsymbol{\nu}_{ij})}_{=0 \text{ for embedded}} + \text{meas}(C_{ij}) \frac{\partial \phi_{ij}(\mathbf{w}_{ij}, \mathbf{w}_{ji}, \boldsymbol{\nu}_{ij})}{\partial \mathbf{w}} \quad (120)$$

where the first term is always zero for embedded simulations.

TODO ask Farhat what to do with the first derivative.

First, we recall the definition of the numerical flux as

$$\boldsymbol{\phi}(\mathbf{w}_i, \mathbf{w}_j, \mathbf{n}_{ij}) = \frac{1}{2} [\mathcal{F}(\mathbf{w}_i) \cdot \mathbf{n}_{ij} + \mathcal{F}(\mathbf{w}_j) \cdot \mathbf{n}_{ij}] - \frac{1}{2} |\mathbf{A}_{\text{Roe}}(\mathbf{w}_i, \mathbf{w}_j, \mathbf{n}_{ij})| (\mathbf{w}_j - \mathbf{w}_i) \quad \text{eq:roe_flux(121)}$$

Similar to the MUSCL procedure we transform the fluid state vector to primitive form

$$\mathbf{w} = \begin{pmatrix} \rho \\ \rho \mathbf{v} \\ E \end{pmatrix} \xrightarrow{\text{U}} \tilde{\mathbf{w}} = \begin{pmatrix} \rho \\ \mathbf{v} \\ p \end{pmatrix} \quad (122)$$

Of course, this transformation involves the EOS of the fluid. We will use $(\tilde{\cdot})$ from now on top mark any quantity as based on/formulated in primitive variables.

The primitive state vector is also much more appealing when it comes to the implementation of boundary conditions, since the solution variables are separated there.

8 DERIVATIVES OF THE FLUID RESIDUAL

Next we recall the conservative form of the Euler equations, which was presented in section 2.2.4 as

$$\frac{\partial \mathbf{w}}{\partial t} + \nabla \cdot \mathcal{F}(\mathbf{w}) = \mathbf{0} \quad \text{eq:t1} \quad (123)$$

Where the convective flux matrix \mathcal{F} is provided in equation (16), and can be written as

$$\mathcal{F}(\mathbf{w}) = \begin{pmatrix} \mathcal{F}_x(\mathbf{w}) & \mathcal{F}_x(\mathbf{w}) & \mathcal{F}_x(\mathbf{w}) \end{pmatrix} \quad (124)$$

Therefore, applying the Nabla operator in Equation (123) gives

$$\frac{\partial \mathbf{w}}{\partial t} + \underbrace{\frac{\partial \mathcal{F}_x(\mathbf{w})}{\partial \mathbf{w}} \frac{\partial \mathbf{w}}{\partial x}}_A + \underbrace{\frac{\partial \mathcal{F}_y(\mathbf{w})}{\partial \mathbf{w}} \frac{\partial \mathbf{w}}{\partial y}}_B + \underbrace{\frac{\partial \mathcal{F}_z(\mathbf{w})}{\partial \mathbf{w}} \frac{\partial \mathbf{w}}{\partial z}}_C = \mathbf{0} \quad \text{eq:conservative_splitted} \quad (125)$$

where the matrices A, B and C are called the *flux Jacobians*.

In Section 7, we have derived that for any sensitivity calculation, the derivative of the flux matrix with respect to the fluid state vector $\frac{\partial \mathbf{R}^c}{\partial \mathbf{w}}$ is required.

We have derived in Section 3.3 that at an interior vertex point of the fluid mesh, we have

$$[\mathbf{R}^c(\mathbf{w}, \mathbf{x}, \dot{\mathbf{x}})]_i = \sum_{j \in \kappa(i)} \text{mes}(\partial C_{ij}) \phi(\mathbf{w}_i, \mathbf{w}_j, \mathbf{n}_{ij}) \quad \text{eq:convective_term_approximation2} \quad (126)$$

Since an equilibrium point is considered, $\dot{\mathbf{x}} = \mathbf{0}$ and is neglected in the following derivations.

In equation (38) we have introduced ϕ as the numerical flux function. In this thesis, we consider the popular Roe flux, which is defined as given in equation (121).

Let us remind, that \mathbf{R}_i^c is the convective residual at vertex i , $\kappa(i)$ is the set of vertices connected to vertex i by an edge, C_i is the control volume of the dual cell centered at vertex i and ∂C_{ij} is the segment of the boundary that intersects edge (ij) and \mathbf{n}_{ij} is the outward-facing weighted normal to ∂C_{ij} . See figure 2 for a visualization of the setup.

From Equation (126) it is obvious that when looking for the derivative $\frac{\partial \mathbf{R}^c}{\partial \mathbf{w}}$, the derivative of the numerical flux with respect to the fluid state vector $\frac{\partial \phi}{\partial \mathbf{w}}$ is required. To make things easier we will in the following derive the primitive version of that quantity $\frac{\partial \tilde{\phi}}{\partial \tilde{\mathbf{w}}}$

As [?] demonstrates, primitive version of the numerical Roe flux can be expressed as

$$\tilde{\phi}(\tilde{\mathbf{w}}_i, \tilde{\mathbf{w}}_j, \mathbf{n}_{ij}) = \frac{1}{2} \left(\tilde{\mathcal{F}}(\tilde{\mathbf{w}}_i) \cdot \mathbf{n}_{ij} + \tilde{\mathcal{F}}(\tilde{\mathbf{w}}_i) \cdot \mathbf{n}_{ij} \right) - \frac{1}{2} \mathbf{P}^{-1}(\sim) |\Lambda(\sim)| \mathbf{P}(\sim) (\tilde{\mathbf{w}}_j - \tilde{\mathbf{w}}_i) \quad \text{eq:primitive_roe_flux} \quad (127)$$

where, for ease of notation we omit the function arguments by simply writing (\sim) as follows

$$\begin{aligned}\mathbf{P}^{-1}(\sim) &= \mathbf{P}^{-1}(\mathbf{M}(\sim), \mathbf{n}_{ij}) \\ \mathbf{M}(\sim) &= \mathbf{M}(\tilde{\mathbf{w}}_i, \tilde{\mathbf{w}}_j) \\ \mathbf{\Lambda}(\sim) &= \mathbf{\Lambda}(\mathbf{M}(\sim), \mathbf{n}_{ij}) \\ \mathbf{P}(\sim) &= \mathbf{P}(\mathbf{M}(\sim), \mathbf{n}_{ij})\end{aligned}\quad \text{eq:split_roeaveragingmatrix}_{(128)}$$

Here, $\mathbf{M}(\tilde{\mathbf{w}}_i, \tilde{\mathbf{w}}_j)$ is the averaging function associated with the roe flux. It can be written as

$$\mathbf{M}(\tilde{\mathbf{w}}_i, \tilde{\mathbf{w}}_j) = \frac{1}{\sqrt{\rho_i} + \sqrt{\rho_j}} \left(\sqrt{\rho_i} \begin{bmatrix} \rho_i \\ \mathbf{v}_i \\ \mathbf{H}_i \end{bmatrix} + \sqrt{\rho_j} \begin{bmatrix} \rho_j \\ \mathbf{v}_j \\ \mathbf{H}_j \end{bmatrix} \right) \quad (129)$$

and \mathbf{P} is the matrix whose columns are the right eigenvectors of the Jacobian matrix \mathcal{A} of \mathcal{F} . The Jacobi matrix in primitive form can be written as

$$\tilde{\mathcal{A}} = \frac{\partial(\tilde{\mathcal{F}} \cdot \mathbf{n})}{\partial \tilde{\mathbf{w}}} \quad (130)$$

$$= \begin{bmatrix} \mathbf{v} \cdot \mathbf{n} & \rho n_x & \rho n_y & \rho n_z & 0 \\ v_1(\mathbf{v} \cdot \mathbf{n}) & \rho(\mathbf{v} \cdot \mathbf{n}) + \rho v_1 n_1 & \rho v_1 n_2 & \rho v_1 n_3 & n_1 \\ v_2(\mathbf{v} \cdot \mathbf{n}) & \rho v_2 n_1 & \rho(\mathbf{v} \cdot \mathbf{n}) + \rho v_2 n_2 & \rho v_2 n_3 & n_2 \\ v_3(\mathbf{v} \cdot \mathbf{n}) & \rho v_3 n_1 & \rho v_3 n_2 & \rho(\mathbf{v} \cdot \mathbf{n}) + \rho v_3 n_3 & n_2 \\ A_{51} & A_{52} & A_{53} & A_{54} & A_{55} \end{bmatrix}$$

$$\mathcal{A}_{51} = H(\mathbf{v} \cdot \mathbf{n}) - \rho \mathbf{v} \cdot \mathbf{n} \frac{\gamma p}{\rho(\gamma)}$$

$$\mathcal{A}_{52} = \rho \mathbf{v} \cdot \mathbf{n} v_1 + \rho H n_1$$

$$\mathcal{A}_{53} = \rho \mathbf{v} \cdot \mathbf{n} v_2 + \rho H n_2$$

$$\mathcal{A}_{54} = \rho \mathbf{v} \cdot \mathbf{n} v_3 + \rho H n_3$$

$$\mathcal{A}_{55} = \rho \mathbf{v} \cdot \mathbf{n} \frac{\gamma}{\rho(\gamma - 1)}$$

$$(131)$$

8 DERIVATIVES OF THE FLUID RESIDUAL

For this Jacobian, one can now symbolically derive an eigenvalue decomposition, such that

$$\mathcal{A} = \mathbf{P}^{-1} \boldsymbol{\Lambda} \mathbf{P} \quad (132)$$

The total specific enthalpy for a perfect gas is given as

$$\mathsf{H} = \frac{\gamma p}{\rho(\gamma - 1)} + \frac{1}{2} \mathbf{v}^T \mathbf{v} \quad (133)$$

where we note the following derivatives

$$\frac{\partial \mathsf{H}}{\partial \rho} = -\frac{\gamma p}{\rho^2(\gamma - 1)} \quad \frac{\partial \mathsf{H}}{\partial v_i} = v_i \quad \frac{\partial \mathsf{H}}{\partial p} = \frac{\gamma}{\rho(\gamma - 1)} \quad (134)$$

Therefore, the derivative of the averaging function with respect to the primitive fluid state vector can be calculated as

$$\begin{aligned} \frac{\partial \mathbf{M}(\sim)}{\partial \rho_i} &= \frac{1}{2\sqrt{\rho_i}(\sqrt{\rho_i} + \sqrt{\rho_j})} \left(-\mathbf{M}(\sim) + \begin{bmatrix} 3\rho_i & 2\sqrt{\rho_i}\mathbf{v}_i & 2\mathsf{H}_i - 2\rho_i \frac{\gamma p}{\rho^2(\gamma - 1)} \end{bmatrix}^T \right) \\ \frac{\partial \mathbf{M}(\sim)}{\partial v_i} &= \frac{1}{(\sqrt{\rho_i} + \sqrt{\rho_j})} \sqrt{\rho_i} \begin{bmatrix} 0 & \mathbf{e}_i^T & v_i \end{bmatrix}^T \\ \frac{\partial \mathbf{M}(\sim)}{\partial p_i} &= \frac{1}{(\sqrt{\rho_i} + \sqrt{\rho_j})} \sqrt{\rho_i} \begin{bmatrix} 0 & \mathbf{0}^T & \frac{\gamma}{\rho(\gamma - 1)} \end{bmatrix}^T \\ \frac{\partial \mathbf{M}(\sim)}{\partial \tilde{\mathbf{w}}_i} &= \begin{bmatrix} 3\rho_i - \frac{\sqrt{\rho_i}\rho_i + \sqrt{\rho_j}\rho_j}{\sqrt{\rho_i} + \sqrt{\rho_j}} & 0 & 0 & 0 & 0 \\ v_{1i} - \frac{\sqrt{\rho_i}v_{1i} + \sqrt{\rho_j}v_{1j}}{\sqrt{\rho_i} + \sqrt{\rho_j}} & 2\rho_i & 0 & 0 & 0 \\ v_{2i} - \frac{\sqrt{\rho_i}v_{2i} + \sqrt{\rho_j}v_{2j}}{\sqrt{\rho_i} + \sqrt{\rho_j}} & 0 & 2\rho_i & 0 & 0 \\ v_{3i} - \frac{\sqrt{\rho_i}v_{3i} + \sqrt{\rho_j}v_{3j}}{\sqrt{\rho_i} + \sqrt{\rho_j}} & 0 & 0 & 2\rho_i & 0 \\ \frac{\mathbf{v}^T \mathbf{v}}{2} - \frac{\gamma p}{\rho(\gamma - 1)} - \frac{\sqrt{\rho_i}\mathsf{H}_i + \sqrt{\rho_j}\mathsf{H}_j}{\sqrt{\rho_i} + \sqrt{\rho_j}} & 2\rho_i v_{1i} & 2\rho_i v_{1i} & 2\rho_i v_{1i} & \frac{2\gamma}{\gamma - 1} \end{bmatrix} \end{aligned} \quad (135)$$

8.2 Analytic Jacobian of the Roe flux

The matrix \mathbf{P} can be written as

$$\mathbf{P} = \begin{bmatrix} \left(\mathbf{n} - \frac{(\gamma-1)\mathbf{v}^T \mathbf{v}}{2c^2} \mathbf{n} + \mathbf{n} \times \mathbf{v} \right) \cdot \mathbf{e}_1 & n_1(\gamma-1)\frac{v_1}{c^2} & n_1(\gamma-1)\frac{v_2}{c^2} + n_3 & n_1(\gamma-1)\frac{v_3}{c^2} - n_2 & -n_1\frac{\gamma-1}{c^2} \\ \left(\mathbf{n} - \frac{(\gamma-1)\mathbf{v}^T \mathbf{v}}{2c^2} \mathbf{n} + \mathbf{n} \times \mathbf{v} \right) \cdot \mathbf{e}_2 & n_2(\gamma-1)\frac{v_1}{c^2} - n_3 & n_2(\gamma-1)\frac{v_2}{c^2} & n_2(\gamma-1)\frac{v_3}{c^2} + n_1 & -n_2\frac{\gamma-1}{c^2} \\ \left(\mathbf{n} - \frac{(\gamma-1)\mathbf{v}^T \mathbf{v}}{2c^2} \mathbf{n} + \mathbf{n} \times \mathbf{v} \right) \cdot \mathbf{e}_3 & n_3(\gamma-1)\frac{v_1}{c^2} + n_2 & n_3(\gamma-1)\frac{v_2}{c^2} - n_1 & n_3(\gamma-1)\frac{v_3}{c^2} & -n_2\frac{\gamma-1}{c^2} \\ (\gamma-1)\frac{\mathbf{v}^T \mathbf{v}}{c^2} - c\mathbf{v} \cdot \mathbf{n} & -(\gamma-1)v_1 + cn_1 & -(\gamma-1)v_2 + cn_2 & -(\gamma-1)v_3 + cn_3 & \gamma-1 \\ (\gamma-1)\frac{\mathbf{v}^T \mathbf{v}}{c^2} - c\mathbf{v} \cdot \mathbf{n} & -(\gamma-1)v_1 - cn_1 & -(\gamma-1)v_2 - cn_2 & -(\gamma-1)v_3 - cn_3 & \gamma-1 \end{bmatrix} \quad (136)$$

where c is the speed of sound given by $c = \sqrt{\frac{\gamma p}{\rho}}$

The matrix Λ derives to

$$\Lambda = \text{diag}([\mathbf{v} \cdot \mathbf{n}, \mathbf{v} \cdot \mathbf{n}, \mathbf{v} \cdot \mathbf{n}, \mathbf{v} \cdot \mathbf{n} + c, \mathbf{v} \cdot \mathbf{n} - c])^{\text{eq:jaceigvals_definition}} \quad (137)$$

$$\frac{\partial \mathbf{P}^{-1}}{\partial \tilde{\mathbf{w}}}(\tilde{\mathbf{w}}, \mathbf{n}) \cdot b = \left[\frac{\partial r_1}{\partial \tilde{\mathbf{w}}}(\tilde{\mathbf{w}}, \mathbf{n}) \cdot b \quad \dots \frac{\partial r_{\text{state}}}{\partial \tilde{\mathbf{w}}}(\tilde{\mathbf{w}}, \mathbf{n}) \cdot b \right]^{\text{pdfrac_jaceigvalsBYfstate}} \quad (138)$$

$$\frac{\partial r_1}{\partial \tilde{\mathbf{w}}}(\tilde{\mathbf{w}}, \mathbf{n}) = \begin{bmatrix} 0 & 0 & 0 & 0 & 0 \\ 0 & \mathbf{n}_x & 0 & 0 & 0 \\ 0 & 0 & \mathbf{n}_x & 0 & 0 \\ 0 & 0 & 0 & \mathbf{n}_x & 0 \\ 0 & v_1 n_1 & v_2 n_1 + n_3 & v_3 n_1 - n_2 & 0 \end{bmatrix}^{\text{pdfrac_jaceigvecsBYfstate_comp1}} \quad (139)$$

$$\frac{\partial r_2}{\partial \tilde{\mathbf{w}}}(\tilde{\mathbf{w}}, \mathbf{n}) = \begin{bmatrix} 0 & 0 & 0 & 0 & 0 \\ 0 & \mathbf{n}_y & 0 & 0 & 0 \\ 0 & 0 & \mathbf{n}_y & 0 & 0 \\ 0 & 0 & 0 & \mathbf{n}_y & 0 \\ 0 & v_1 n_2 - n_3 & v_2 n_2 & v_3 n_2 - n_1 & 0 \end{bmatrix}^{\text{pdfrac_jaceigvecsBYfstate_comp2}} \quad (140)$$

$$\frac{\partial r_3}{\partial \tilde{\mathbf{w}}}(\tilde{\mathbf{w}}, \mathbf{n}) = \begin{bmatrix} 0 & 0 & 0 & 0 & 0 \\ 0 & \mathbf{n}_z & 0 & 0 & 0 \\ 0 & 0 & \text{eq:pdffrac_jaceigvecsBYfstate_comp3} \\ 0 & 0 & \mathbf{n}_z & 0 & 0 \\ 0 & 0 & 0 & \mathbf{n}_z & 0 \\ 0 & v_1 n_3 + n_2 & v_2 n_3 - n_1 & v_3 n_3 & 0 \end{bmatrix} \quad (141)$$

$$\frac{\partial r_4}{\partial \tilde{\mathbf{w}}}(\tilde{\mathbf{w}}, \mathbf{n}) = \begin{bmatrix} \frac{1}{2\gamma p} & 0 & 0 & 0 & -\frac{\rho}{2\gamma p^2} \\ \frac{v_1}{2\rho c^2} + \frac{n_1}{4\rho c} & \frac{1}{2c^2} & 0 & 0 & -\frac{v_1}{2pc^2} - \frac{n_1}{4pc} \\ \frac{v_2}{2\rho c^2} + \frac{n_2}{4\rho c} & 0 & \frac{1}{2c^2} & 0 & -\frac{v_2}{2pc^2} - \frac{n_2}{4pc} \\ \frac{v_3}{2\rho c^2} + \frac{n_3}{4\rho c} & 0 & 0 & \frac{1}{2c^2} & -\frac{v_3}{2pc^2} - \frac{n_3}{4pc} \\ \frac{1}{2\gamma} + \frac{\mathbf{v} \cdot \mathbf{n}}{4\rho c} & \frac{n_1}{2c} & \frac{n_2}{2c} & \frac{n_3}{2c} & -\frac{\mathbf{v} \cdot \mathbf{n}}{4pc} \end{bmatrix} \quad (142)$$

$$\frac{\partial r_5}{\partial \tilde{\mathbf{w}}}(\tilde{\mathbf{w}}, \mathbf{n}) = \begin{bmatrix} \frac{1}{2\gamma p} & 0 & 0 & 0 & -\frac{\rho}{2\gamma p^2} \\ \frac{v_1}{2\rho c^2} - \frac{n_1}{4\rho c} & \frac{1}{2c^2} & 0 & 0 & -\frac{v_1}{2pc^2} + \frac{n_1}{4pc} \\ \frac{v_2}{2\rho c^2} - \frac{n_2}{4\rho c} & 0 & \frac{1}{2c^2} & 0 & -\frac{v_2}{2pc^2} + \frac{n_2}{4pc} \\ \frac{v_3}{2\rho c^2} - \frac{n_3}{4\rho c} & 0 & 0 & \frac{1}{2c^2} & -\frac{v_3}{2pc^2} + \frac{n_3}{4pc} \\ \frac{1}{2\gamma} - \frac{\mathbf{v} \cdot \mathbf{n}}{4\rho c} & -\frac{n_1}{2c} & -\frac{n_2}{2c} & -\frac{n_3}{2c} & \frac{\mathbf{v} \cdot \mathbf{n}}{4pc} \end{bmatrix} \quad (143)$$

Due to its shape, the derivation of Λ can be simplified to a differentiation of the eigenvalues λ_i .

$$\frac{\partial \lambda_1}{\partial \tilde{\mathbf{w}}}(\tilde{\mathbf{w}}, \mathbf{n}) = \frac{\partial \lambda_2}{\partial \tilde{\mathbf{w}}}(\tilde{\mathbf{w}}, \mathbf{n}) = \frac{\partial \lambda_3}{\partial \tilde{\mathbf{w}}}(\tilde{\mathbf{w}}, \mathbf{n}) \stackrel{\text{eq:pdffrac_jaceigvecsBYfstate_comp4}}{=} \begin{bmatrix} 0 & \mathbf{n}^T & 0 \end{bmatrix}^T \quad (144)$$

$$\frac{\partial \lambda_4}{\partial \tilde{\mathbf{w}}}(\tilde{\mathbf{w}}, \mathbf{n}) = \left[-\frac{c}{2\rho} \quad \mathbf{n}^T \quad \frac{c}{2p} \right]^T \quad (145)$$

$$\frac{\partial \lambda_5}{\partial \tilde{\mathbf{w}}}(\tilde{\mathbf{w}}, \mathbf{n}) = \left[\frac{c}{2\rho} \quad \mathbf{n}^T \quad -\frac{c}{2p} \right]^T \quad (146)$$

$$\frac{\partial \mathbf{P}}{\partial \tilde{\mathbf{w}}}(\tilde{\mathbf{w}}, \mathbf{n}) \cdot b = \begin{bmatrix} \frac{\partial l_1^T}{\partial \tilde{\mathbf{w}}}(\tilde{\mathbf{w}}, \mathbf{n}) \cdot b \\ \frac{\partial l_2^T}{\partial \tilde{\mathbf{w}}}(\tilde{\mathbf{w}}, \mathbf{n}) \cdot b \\ \frac{\partial l_3^T}{\partial \tilde{\mathbf{w}}}(\tilde{\mathbf{w}}, \mathbf{n}) \cdot b \\ \frac{\partial l_4^T}{\partial \tilde{\mathbf{w}}}(\tilde{\mathbf{w}}, \mathbf{n}) \cdot b \\ \frac{\partial l_5^T}{\partial \tilde{\mathbf{w}}}(\tilde{\mathbf{w}}, \mathbf{n}) \cdot b \end{bmatrix} \text{eq:pdfrac_jaceigvalsBYfstate_comp1 (147)}$$

$$\frac{\partial l_1}{\partial \tilde{\mathbf{w}}}(\tilde{\mathbf{w}}, \mathbf{n}) = \begin{bmatrix} -\frac{n_1(\gamma-1)\|\mathbf{v}\|^2}{2\rho c^2} & -\frac{n_1(\gamma-1)v_1}{c^2} & -\frac{n_1(\gamma-1)v_2}{c^2} & -n_3 & -\frac{n_1(\gamma-1)v_3}{c^2} + n_2 & \frac{n_1(\gamma-1)\|\mathbf{v}\|^2}{2pc^2} \\ \frac{n_1(\gamma-1)v_1}{\gamma p} & \frac{n_1\rho(\gamma-1)}{\gamma p} & 0 & 0 & -\frac{n_1v_1\rho(\gamma-1)}{\gamma p^2} & \\ \frac{n_1(\gamma-1)v_2}{\gamma p} & 0 & \frac{n_1\rho(\gamma-1)}{\gamma p} & 0 & -\frac{n_1v_2\rho(\gamma-1)}{\gamma p^2} & \\ \frac{n_1(\gamma-1)v_3}{\gamma p} & 0 & 0 & \frac{n_1\rho(\gamma-1)}{\gamma p} & -\frac{n_1v_3\rho(\gamma-1)}{\gamma p^2} & \\ -\frac{n_1\gamma-1}{pc^2} & 0 & 0 & 0 & \frac{n_1\gamma-1}{pc^2} & \end{bmatrix} \text{eq:pdfrac_jaceigvalsBYfstate_comp1 (148)}$$

$$\frac{\partial l_2}{\partial \tilde{\mathbf{w}}}(\tilde{\mathbf{w}}, \mathbf{n}) = \begin{bmatrix} -\frac{n_2(\gamma-1)\|\mathbf{v}\|^2}{2\rho c^2} & -\frac{n_2(\gamma-1)v_1}{c^2} + n_3 & -\frac{n_2(\gamma-1)v_2}{c^2} & -\frac{n_2(\gamma-1)v_3}{c^2} - n_1 & \frac{n_2(\gamma-1)\|\mathbf{v}\|^2}{2pc^2} \\ \frac{n_2(\gamma-1)v_1}{\gamma p} & \frac{n_2\rho(\gamma-1)}{\gamma p} & 0 & 0 & -\frac{n_2v_1\rho(\gamma-1)}{\gamma p^2} \\ \frac{n_2(\gamma-1)v_2}{\gamma p} & 0 & \frac{n_2\rho(\gamma-1)}{\gamma p} & 0 & -\frac{n_2v_2\rho(\gamma-1)}{\gamma p^2} \\ \frac{n_2(\gamma-1)v_3}{\gamma p} & 0 & 0 & \frac{n_2\rho(\gamma-1)}{\gamma p} & -\frac{n_2v_3\rho(\gamma-1)}{\gamma p^2} \\ -\frac{n_2\gamma-1}{pc^2} & 0 & 0 & 0 & \frac{n_2\gamma-1}{pc^2} \end{bmatrix} \text{eq:pdfrac_jaceigvalsBYfstate_comp2 (149)}$$

$$\frac{\partial l_3}{\partial \tilde{\mathbf{w}}}(\tilde{\mathbf{w}}, \mathbf{n}) = \begin{bmatrix} -\frac{n_3(\gamma-1)\|\mathbf{v}\|^2}{2\rho c^2} & -\frac{n_3(\gamma-1)v_1}{c^2} - n_2 & -\frac{n_3(\gamma-1)v_2}{c^2} + n_1 & -\frac{n_3(\gamma-1)v_3}{c^2} & \frac{n_3(\gamma-1)\|\mathbf{v}\|^2}{2\rho c^2} \\ \frac{n_3(\gamma-1)v_1}{\gamma p} & \frac{n_3\rho(\gamma-1)}{\gamma p} & 0 & 0 & -\frac{n_3v_1\rho(\gamma-1)}{\gamma p^2} \\ \frac{n_3(\gamma-1)v_2}{\gamma p} & 0 & \frac{n_2\rho(\gamma-1)}{\gamma p} & 0 & -\frac{n_3v_2\rho(\gamma-1)}{\gamma p^2} \\ \frac{n_3(\gamma-1)v_3}{\gamma p} & 0 & 0 & \frac{n_2\rho(\gamma-1)}{\gamma p} & -\frac{n_3v_3\rho(\gamma-1)}{\gamma p^2} \\ -\frac{n_3\gamma-1}{\rho c^2} & 0 & 0 & 0 & \frac{n_3\gamma-1}{pc^2} \end{bmatrix}$$

eq:pdfrac_jaceigvalsBYfstate_comp3
(150)

$$\frac{\partial l_4}{\partial \tilde{\mathbf{w}}}(\tilde{\mathbf{w}}, \mathbf{n}) = \begin{bmatrix} \frac{c}{2\rho} \mathbf{v} \cdot \mathbf{n} & (\gamma-1)v_1 - cn_1 & (\gamma-1)v_2 - cn_2 & (\gamma-1)v_3 - cn_3 & -\frac{c}{2p} \mathbf{v} \cdot \mathbf{n} \\ -\frac{cn_1}{2\rho} & -(\gamma-1) & 0 & 0 & \frac{cn_1}{2p} \\ -\frac{cn_2}{2\rho} & 0 & -(\gamma-1) & 0 & \frac{cn_2}{2p} \\ -\frac{cn_3}{2\rho} & 0 & 0 & -(\gamma-1) & \frac{cn_3}{2p} \\ 0 & 0 & 0 & 0 & 0 \end{bmatrix}$$

eq:pdfrac_jaceigvalsBYfstate_comp4
(151)

$$\frac{\partial l_5}{\partial \tilde{\mathbf{w}}}(\tilde{\mathbf{w}}, \mathbf{n}) = \begin{bmatrix} \frac{c}{2\rho} \mathbf{v} \cdot \mathbf{n} & (\gamma-1)v_1 - cn_1 & (\gamma-1)v_2 - cn_2 & (\gamma-1)v_3 - cn_3 & -\frac{c}{2p} \mathbf{v} \cdot \mathbf{n} \\ \frac{cn_1}{2\rho} & -(\gamma-1) & 0 & 0 & -\frac{cn_1}{2p} \\ \frac{cn_2}{2\rho} & 0 & -(\gamma-1) & 0 & -\frac{cn_2}{2p} \\ \frac{cn_3}{2\rho} & 0 & 0 & -(\gamma-1) & -\frac{cn_3}{2p} \\ 0 & 0 & 0 & 0 & 0 \end{bmatrix}$$

eq:pdfrac_jaceigvalsBYfstate_comp5
(152)

Therefor, the numerical roe flux (127) can therefore be derived by the primitive state vector as:

$$\frac{\partial \tilde{\phi}}{\partial \tilde{\mathbf{w}}_i} = \frac{1}{2} \mathcal{A}(\tilde{\mathbf{w}}_i, \tilde{\mathbf{w}}_j) \quad (153)$$

$$- \frac{1}{2} \left[\left(\frac{\partial \mathbf{P}^{-1}}{\partial \tilde{\mathbf{w}}}(\sim) \frac{\partial \mathbf{M}}{\partial \tilde{\mathbf{w}}}(\sim) \right) |\Lambda(\sim)| \mathbf{P}(\sim) (\tilde{\mathbf{w}}_j - \tilde{\mathbf{w}}_i) \right] \quad (154)$$

$$+ \mathbf{P}^{-1}(\sim) \left(\frac{\partial |\Lambda|}{\partial \tilde{\mathbf{w}}}(\sim) \frac{\partial \mathbf{M}}{\partial \tilde{\mathbf{w}}}(\sim) \right) \mathbf{P}(\sim) (\tilde{\mathbf{w}}_j - \tilde{\mathbf{w}}_i) \quad (155)$$

$$+ \mathbf{P}^{-1}(\sim) |\Lambda(\sim)| \left(\frac{\partial \mathbf{P}}{\partial \tilde{\mathbf{w}}}(\sim) \frac{\partial \mathbf{M}}{\partial \tilde{\mathbf{w}}}(\sim) \right) (\tilde{\mathbf{w}}_j - \tilde{\mathbf{w}}_i) \quad (156)$$

$$- \mathbf{P}^{-1}(\sim) |\Lambda(\sim)| \mathbf{P}(\sim) \left] \right. \quad (157)$$

where the full analytic expression can be obtained by backward substitution of equations (128) to (152).

This derivative, along with the derivative of the viscous term, which will be derived in Section ??, will be a key component in the Sensitivity calculations as shown in Section 7 and 9. This is due to the fact that will follow the procedere of discretization before derivation as justified in Section 7.1.

8.3 Derivative with respect to the abstract variable $\frac{\partial \mathbf{R}}{\partial s}$

Since the fluid Jacobian is also required in every standard fluid solve, the important term, unique to [SA](#) is the partial derivative of the residual with respect to the design variable s .

Similar to the previously discussed fluid Jacobian, the computation of $\frac{\partial \mathbf{R}}{\partial s}$ can be splitted into convective and viscous part. We again focus on the special case of an intersected cell in the following two subsections, since the standard case of a standard cell far from the interface follows trivially from that.

It shall also be noted that in most cases, the derivative $\frac{\partial \mathbf{R}}{\partial s}$ is non-zero only at a few fluid nodes. For shape-sensitivity, for example, only the nodes at the interface have a non-zero contribution here. Looking at equation (109) one can therefor interpret the solution of the linear system, or the multiplication with the inverse Jacobian, as a propagation operation.

8.3.1 Convective contribution $\frac{\partial \mathbf{R}^c}{\partial s}$

Generally, one can write the convective fluid residual as

$$\mathbf{R}_{ij}^{c,i} = \phi_{ij}^i(\tilde{\mathbf{w}}_{ij}, \tilde{\mathbf{w}}_{ij}^*(s), \mathbf{n}_{ij}) \quad (158)$$

The most important factor here, is of course the dependency of the half Riemann solution on the abstract variable. This dependency becomes obvious in the case of shape sensitivity, since the intersection point used for the Riemann solution depends

upon the interface shape.

The derivative can be obtained straightforwardly as

$$\mathbf{R} \mathbf{R}_{ij}^{c,i} s = \frac{\partial \mathbf{R}_{ij}^{c,i}}{\partial \mathbf{w}_{ij}^*} \frac{\partial \mathbf{w}_{ij}^*}{\partial s} \quad (159)$$

here, the analytical derivative of the first term can be taken from section 8.1. The second derivative is more cumbersome. The issue is visualized in Figure 9.

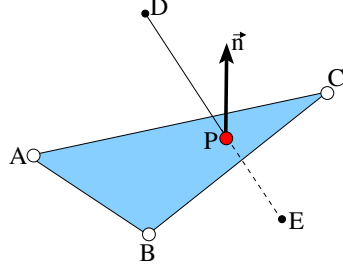


Figure 9: Visualization of the intersection of a fluid mesh edge ($D - E$) with an element of the embedded surface ($A - B - C$). For a shape-sensitivity analysis, SDesign returns the derivatives of the embedded surface nodes A, B, C position with respect to the shape parameter. This is done by first computing the intersection point P . Together with the element normal \mathbf{n} , the intersection point is used to reconstruct the shape derivatives at nodes D and E . **TODO**

Based on the consideration above, we find the following dependency for the

$$\frac{\partial \mathbf{w}_{ij}^*}{\partial s} = \frac{\partial \mathbf{w}_{ij}^*}{\partial s} \left(\frac{\partial \mathbf{w}_i}{\partial s} \Big|_{i=A,B,C}, \xi, \mathbf{n} \right) \quad (160)$$

The derivatives of the geometrical quantities with respect to s are found as

$$\frac{\partial \xi}{\partial s} = \frac{\partial \xi}{\partial \mathbf{x}} \frac{\partial \mathbf{x}}{\partial s} \quad (161)$$

$$\frac{\partial \mathbf{n}_{wall}}{\partial s} = \frac{\partial \mathbf{n}_{wall}}{\partial \mathbf{x}} \frac{\partial \mathbf{x}}{\partial s} \quad (162)$$

8.3.2 Viscous contribution $\frac{\partial \mathbf{R}^v}{\partial s}$

The derivative of the viscous contribution is derived very similarly to the viscous Jacobian. Looking at equation **TODO** one can derive

$$\begin{aligned} \frac{\partial \mathbf{R}^v(s, \tilde{\mathbf{w}}^a(s), \tilde{\mathbf{w}}^g(\tilde{\mathbf{w}}^a(s)), \mathbf{x}(s))}{\partial s} &= \underbrace{\frac{\partial \mathbf{R}^v}{\partial \tilde{\mathbf{w}}^a} \frac{\partial \tilde{\mathbf{w}}^a}{\partial s}}_{\text{can be re-used from ALE after the ghost-point population}} + \underbrace{\frac{\partial \mathbf{R}^v}{\partial \tilde{\mathbf{w}}^g} \cdot \widehat{\frac{\partial \tilde{\mathbf{w}}^g}{\partial \tilde{\mathbf{w}}^a}}}_{\text{obtained during the population process}} \frac{\partial \tilde{\mathbf{w}}^a}{\partial s} \\ &+ \underbrace{\frac{\partial \mathbf{R}^v}{\partial \mathbf{x}} \frac{\partial \mathbf{x}}{\partial s}}_{=0 \text{ for embedded}} \end{aligned} \quad (163)$$

9 Aero-elastic Sensitivity Analysis

The previous chapter dealt with the SA of a pure fluid problem. Boundary, or respectively mesh-movement in general, was only induced due to shape variation via design variables itself. However, one can easily decieve a system, where the fluid interacts with an elastic structure. This would introduce an additional dependency of the structure shape, and thus fluid-structure interface, on the fluid solution. Also, a fully coupled system introduces a direct connection between the stress resultants in the structure with the fluid solutions. This chapter therfore investigates the SA of such a coupled system of equations. Considerations are build upon the derivations in chapter 7 and the coupled three-field FSI formulation described in chapter 5.1. The SA approach applied in this thesis is based on the work of [?], for deriving the Global Sensitivity Equations (GSE) of coupled systems. As introduced by the authors of [?], we utilize the three-field formulation of [?].

The derivative of the optimization criterion q_j , as introduced in Equation (77), with respect to the optimization variable s_i gives:

$$\frac{dq_j}{ds_i} = \frac{\partial q_j}{\partial s_i} + \frac{\partial q_j}{\partial \mathbf{u}} \frac{d\mathbf{u}}{ds_i} + \frac{\partial q_j}{\partial \dot{\mathbf{x}}} \frac{d\dot{\mathbf{x}}}{ds_i} + \frac{\partial q_j}{\partial \mathbf{w}} \frac{d\mathbf{w}}{ds_i} \quad (164)$$

$$= \frac{\partial q_j}{\partial s_i} + \begin{bmatrix} \frac{\partial q_j}{\partial \mathbf{u}} \\ \frac{\partial q_j}{\partial \dot{\mathbf{x}}} \\ \frac{\partial q_j}{\partial \mathbf{w}} \end{bmatrix}^T \cdot \begin{bmatrix} \frac{d\mathbf{u}}{ds_i} \\ \frac{d\dot{\mathbf{x}}}{ds_i} \\ \frac{d\mathbf{w}}{ds_i} \end{bmatrix} \quad (165)$$

where the partial derivatives, $\frac{\partial q_j}{\partial \mathbf{u}}$, $\frac{\partial q_j}{\partial \dot{\mathbf{x}}}$ and $\frac{\partial q_j}{\partial \mathbf{w}}$ can be directly evaluated within the discretized structure and fluid model through the relation between structural, aerodynamic design and abstract optimization parameters defied in the design model 6.2. The cumbersome part are the derivatives $\frac{d\mathbf{u}}{ds_i}$, $\frac{d\dot{\mathbf{x}}}{ds_i}$ and $\frac{d\mathbf{w}}{ds_i}$. To obtain them, the governing equations (??) TODO write down governing equations have to be derived:

$$\underbrace{\begin{bmatrix} \frac{\partial \mathcal{S}_{gov}}{\partial s_i} \\ \frac{\partial \mathcal{D}_{gov}}{\partial s_i} \\ \frac{\partial \mathcal{F}_{gov}}{\partial s_i} \end{bmatrix}}_A + \underbrace{\begin{bmatrix} \frac{\partial \mathcal{S}_{gov}}{\partial \mathbf{u}} & \frac{\partial \mathcal{S}_{gov}}{\partial \dot{\mathbf{x}}} & \frac{\partial \mathcal{S}_{gov}}{\partial \mathbf{w}} \\ \frac{\partial \mathcal{D}_{gov}}{\partial \mathbf{u}} & \frac{\partial \mathcal{D}_{gov}}{\partial \dot{\mathbf{x}}} & \mathbf{0} \\ \mathbf{0} & \frac{\partial \mathcal{F}_{gov}}{\partial \dot{\mathbf{x}}} & \frac{\partial \mathcal{F}_{gov}}{\partial \mathbf{w}} \end{bmatrix}}_{\text{eq:governing_equations_derivative}} \begin{bmatrix} \frac{\partial \mathbf{u}}{\partial s_i} \\ \frac{\partial \dot{\mathbf{x}}}{\partial s_i} \\ \frac{\partial \mathbf{w}}{\partial s_i} \end{bmatrix} = \mathbf{0} \quad (166)$$

In this equations $\frac{\partial \mathcal{S}_{gov}}{\partial s_i}$ and $\frac{\partial \mathcal{F}_{gov}}{\partial s_i}$ can be again directly evaluated using the relation specified in the design model. The matrix of first derivatives \mathbf{A} is from now on denoted as the "Jacobian of the optimization problem".

Combining the previous two equations, it follows that the total derivative of the optimization criterion with respect to the abstract variables can be expressed as:

$$\frac{dq_j}{ds_i} = \frac{\partial q_j}{\partial s_i} - \underbrace{\begin{bmatrix} \frac{\partial q_j}{\partial \mathbf{u}} \\ \frac{\partial q_j}{\partial \dot{\mathbf{x}}} \\ \frac{\partial q_j}{\partial \mathbf{w}} \end{bmatrix}}_{n_q \times n_{eq}}^T \underbrace{\mathbf{A}^{-1}}_{n_{eq} \times n_{eq}} \begin{bmatrix} \frac{\partial \mathcal{S}_{gov}}{\partial s_i} \\ \frac{\partial \mathcal{D}_{gov}}{\partial s_i} \\ \frac{\partial \mathcal{F}_{gov}}{\partial s_i} \end{bmatrix} \quad \text{deriv_optcritBYabsvar (167)}$$

Where n_{eq} is the total number of equations(e.g. five fluid state equations for the compressible NSG in 3D, three equations of the mesh motions and another three equations for the structure motion), n_q is the number of optimization criteria and n_s is the number of abstract variables.

9.1 Direct vs. adjoint approach

Equation 167 suggests, that there are two alternatives to compute vector-matrix-vector product above.

Direct approach Firstly, one could first compute the derivatives of the aeroelastic response for each abstract variable and perform the matrix product with \mathbf{A} :

$$\begin{bmatrix} \frac{d\mathbf{u}}{ds_i} \\ \frac{d\dot{\mathbf{x}}}{ds_i} \\ \frac{d\mathbf{w}}{ds_i} \end{bmatrix} = -\mathbf{A}^{-1} \begin{bmatrix} \frac{\partial \mathcal{S}_{gov}}{\partial s_i} \\ \frac{\partial \mathcal{D}_{gov}}{\partial s_i} \\ \frac{\partial \mathcal{F}_{gov}}{\partial s_i} \end{bmatrix} \quad \text{and then eq:direct_approach (168)}$$

$$\frac{dq_j}{ds_i} = \frac{\partial q_j}{\partial s_i} - \begin{bmatrix} \frac{\partial q_j}{\partial \mathbf{u}} \\ \frac{\partial q_j}{\partial \dot{\mathbf{x}}} \\ \frac{\partial q_j}{\partial \mathbf{w}} \end{bmatrix}^T \begin{bmatrix} \frac{d\mathbf{u}}{ds_i} \\ \frac{d\dot{\mathbf{x}}}{ds_i} \\ \frac{d\mathbf{w}}{ds_i} \end{bmatrix} \quad (169)$$

Where the total complexity can be approximated as $\mathcal{O}(n_{eq}^2 n_s + n_q n_{eq} n_s)$

Adjoint approach Secondly, one could also first compute the derivatives of the optimization criteria and multiply with the Jacobian before substituting this into Equation (167):

$$\begin{aligned} \begin{bmatrix} \mathbf{a}_u \\ \mathbf{a}_{\dot{x}} \\ \mathbf{a}_w \end{bmatrix} &= \mathbf{A}^{-T} \begin{bmatrix} \frac{\partial q_j}{\partial \mathbf{u}} \\ \frac{\partial q_j}{\partial \dot{\mathbf{x}}} \\ \frac{\partial q_j}{\partial \mathbf{w}} \end{bmatrix} && \text{eq: firststep_adjoint (170)} \\ \frac{dq_j}{ds_i} &= \frac{\partial q_j}{\partial s_i} - \begin{bmatrix} \mathbf{a}_u \\ \mathbf{a}_{\dot{x}} \\ \mathbf{a}_w \end{bmatrix}^T \begin{bmatrix} \frac{\partial \mathcal{S}_{gov}}{\partial s_i} \\ \frac{\partial \mathcal{D}_{gov}}{\partial s_i} \\ \frac{\partial \mathcal{F}_{gov}}{\partial s_i} \end{bmatrix} && (171) \end{aligned}$$

Where the total complexity can be approximated as $\mathcal{O}(n_{eq}^2 n_q + n_q n_{eq} n_s)$

If one or the other approach is to be preferred depends in on the optimization setup, particularly the number of optimization criteria and the number of optimization variables. Looking at the orders above, one can conclude that if the number of abstract parameters n_s is smaller than the number of optimization criteria, the direct approach is more efficient, otherwise the adjoint approach is to be preferred. Additionally one can argue, that the relevant term in the orders above is the one with n_{eq}^2 since it dominates the sum. Therefore, depending on whether n_s or n_q is bigger, the direct or the adjoint method is to be preferred.

9.1.1 Direct Sensitivity Analysis for the Euler equations

The A matrix for the direct approach in ALE formulation looks like

$$\mathbf{A} = \begin{bmatrix} \frac{\partial \mathcal{S}_{gov}}{\partial \mathbf{u}} & \frac{\partial \mathcal{S}_{gov}}{\partial \dot{\mathbf{x}}} & \frac{\partial \mathcal{S}_{gov}}{\partial \mathbf{w}} \\ \frac{\partial \mathcal{D}_{gov}}{\partial \mathbf{u}} & \frac{\partial \mathcal{D}_{gov}}{\partial \dot{\mathbf{x}}} & \mathbf{0} \\ \mathbf{0} & \frac{\partial \mathcal{F}_{gov}}{\partial \dot{\mathbf{x}}} & \frac{\partial \mathcal{F}_{gov}}{\partial \mathbf{w}} \end{bmatrix} = \begin{bmatrix} \mathbf{K} & \frac{\partial \mathbf{P}_T}{\partial \dot{\mathbf{x}}} & \frac{\partial \mathbf{P}_T}{\partial \mathbf{w}} \\ \begin{bmatrix} \mathbf{K}_{\Omega\Gamma} \mathbf{T}_u \\ \mathbf{T}_u \end{bmatrix} & \begin{bmatrix} \mathbf{K}_{\Omega\Omega} & \mathbf{0} \\ \mathbf{0} & \mathbf{I} \end{bmatrix} & \begin{bmatrix} \mathbf{0} & \frac{\partial \mathbf{F}_2}{\partial \dot{\mathbf{x}}_\Omega} & \mathbf{H}_2 \end{bmatrix} \end{bmatrix} \quad \text{eq: Amatrix_ALE (172)}$$

Where, \mathbf{H}_2 is the Jacobian of the second order row flux. It shall be noted that constructing this Jacobian is not a trivial issue and takes up a lot of computational resources, especially for **FV**, as described in [?]. Investigation into whether this term can be approximated at first order were carried out in [?] and [?].

Furthermore, [?] considered replacing the two mesh motion related matrices $\frac{\partial \mathbf{P}_T}{\partial \dot{\mathbf{x}}}$ and $\frac{\partial \mathbf{F}_2}{\partial \dot{\mathbf{x}}_\Omega}$ by a transpirational boundary condition. The consequences of this approach are also investigated in [?] and [?].

This thesis, however, does not use any of this simplifications.

The derivation of the sensitivities, can be achieved in a staggered scheme, very similar to the one, described in ??TODO. It consists of five steps.

1) Update the structural displacement sensitivity to a new time step
BY differentiating equations (57) and (61) and applying an under relaxation, we can obtain

$$\frac{d\mathbf{u}^{(n)}}{ds_i} = (1 - \theta) \frac{d\mathbf{u}^{(n)}}{ds_i} + \theta \frac{d\bar{\mathbf{u}}}{ds_i} \quad \text{eq:underrelax_structdisp} \quad (173)$$

where $\bar{\mathbf{u}}$ is obtained from:

$$\mathbf{K} \frac{d\bar{\mathbf{u}}}{ds_i} = \frac{\partial T O D O}{\partial s_i} + \frac{\partial \mathbf{T}_u^{(n)}}{\partial s_i} - \frac{\partial \mathbf{K}}{\partial s_i} \mathbf{u} \quad \text{eq:fictitious_structdisp} \quad (174)$$

2) Transfer sensitivity of structure motion to the interface

$$\frac{d\mathbf{u}_T^{(n)}}{ds_i} = \mathbf{T}_u \frac{d\mathbf{u}^{(n)}}{ds_i} \quad \text{eq:interface_projections} \quad (175)$$

3) Compute derivative of fluid mesh motion The fluid mesh motion is computed by solving the pseudo Dirichlet problem as described in [?]. By design, the fictitious stiffness matrix $\bar{\mathbf{K}}$ does not depend on the abstract optimization variables \mathbf{s}

$$\bar{\mathbf{K}}_{\Omega\Omega} \frac{d\dot{\mathbf{x}}_\Omega^{(n)}}{ds_i} = -\bar{\mathbf{K}}_{\Omega\Gamma} \frac{d\dot{\mathbf{x}}_\Gamma^{(n)}}{ds_i} \quad \text{eq:mms_domain} \quad (176)$$

with

$$\frac{d\dot{\mathbf{x}}_\Gamma^{(n)}}{ds_i} = \frac{d\dot{\mathbf{x}}_\Gamma^{(n)}}{ds_i} \quad (177)$$

4) Compute the sensitivity of the fluid state variables The derivatives of the fluid state variables are computed by

$$\mathbf{H}_2 \frac{d\mathbf{w}^{(n+1)}}{ds_i} = \frac{\partial \mathbf{F}_2}{\partial s_i} - \frac{\partial \mathbf{F}_2}{\partial \dot{\mathbf{x}}} \frac{d\dot{\mathbf{x}}^{(n)}}{ds_i} \quad (178)$$

5) Compute the sensitivity of the structure load vector The derivative of the fluid load with respect to the abstract variables can be computed by the third of Equations (168) with the definition of \mathbf{A} as specified in (172).

$$\frac{\partial \mathbf{P}_F^{(n+1)}}{\partial s_i} = \frac{\partial \mathbf{P}_F^{(n+1)}}{\partial \dot{\mathbf{x}}} \frac{d\dot{\mathbf{x}}^{(n)}}{ds_i} + \frac{\partial \mathbf{P}_F^{(n+1)}}{\partial \mathbf{w}} \frac{d\text{loadByAbsVar}^{(n)}}{ds_i} \quad (179)$$

and compute project it onto the structure via

$$\frac{\partial \mathbf{P}_T^{(n+1)}}{\partial s_i} = \mathbf{T}_p \frac{\partial \mathbf{P}_F^{(n+1)}}{\partial s_i} \quad (180)$$

The convergence of the staggered algorithm can be monitored via

$$\left\| \mathbf{K} \frac{d\bar{\mathbf{u}}^{(n+1)}}{ds_i} - \frac{\partial \text{TODO}}{\partial s_i} - \frac{\partial \mathbf{P}_T^{(n+1)}}{\partial s_i} + \frac{\partial \mathbf{K}}{\partial s_i} \right\|_2 \leq \epsilon^{SA} \left\| \mathbf{K} \frac{d\bar{\mathbf{u}}^{(0)}}{ds_i} - \frac{\partial \text{TODO}}{\partial s_i} - \frac{\partial \mathbf{P}_T^{(0)}}{\partial s_i} + \frac{\partial \mathbf{K}}{\partial s_i} \right\|_2 \quad (181)$$

$$\left\| \mathbf{H}_2 \frac{d\mathbf{w}^{(n+1)}}{ds_i} + \frac{\partial \mathbf{F}_2}{\partial s_i} + \frac{\partial \mathbf{F}_2}{\partial \dot{\mathbf{x}}} \frac{d\dot{\mathbf{x}}^{(n+1)}}{ds_i} \right\|_2 \leq \epsilon^{SA} \left\| \mathbf{H}_2 \frac{d\mathbf{w}^{(0)}}{ds_i} + \frac{\partial \mathbf{F}_2}{\partial s_i} + \frac{\partial \mathbf{F}_2}{\partial \dot{\mathbf{x}}} \frac{d\dot{\mathbf{x}}^{(0)}}{ds_i} \right\|_2 \quad (182)$$

9.1.2 Adjoint Sensitivity Analysis for the Euler equations

The adjoint SA follows the same scheme as the direct one
Equation (170) can be written as:

$$\begin{bmatrix} \mathbf{K} & \begin{bmatrix} \frac{\partial \mathbf{P}_T}{\partial \dot{\mathbf{x}}_\Omega} & \frac{\partial \mathbf{P}_T}{\partial \dot{\mathbf{x}}_\Gamma} \end{bmatrix} & \frac{\partial \mathbf{P}_T}{\partial \mathbf{w}} \\ \begin{bmatrix} \mathbf{K}_{\Omega\Gamma} \mathbf{T}_u \\ \mathbf{T}_u \end{bmatrix} & \begin{bmatrix} \mathbf{K}_{\Omega\Omega} & \mathbf{0} \\ \mathbf{0} & \mathbf{I} \end{bmatrix} & \mathbf{0} \\ \mathbf{0} & \begin{bmatrix} \frac{\partial \mathbf{F}_2}{\partial \dot{\mathbf{x}}_\Omega} & \frac{\partial \mathbf{F}_2}{\partial \dot{\mathbf{x}}_\Gamma} \end{bmatrix} & \mathbf{H}_2 \end{bmatrix}^T \begin{bmatrix} \mathbf{a}_u \\ \mathbf{a}_{\dot{\mathbf{x}}_\Omega} \\ \mathbf{a}_{\dot{\mathbf{x}}_\Gamma} \\ \mathbf{a}_w \end{bmatrix} = \begin{bmatrix} \frac{\partial q_j}{\partial \mathbf{u}} \\ \frac{\partial \mathbf{q}}{\partial \dot{\mathbf{x}}_\Omega} \\ \frac{\partial \mathbf{q}}{\partial \dot{\mathbf{x}}_\Gamma} \\ \frac{\partial q_j}{\partial \mathbf{w}} \end{bmatrix} \quad \text{eq:adjoint_equation} \quad (183)$$

TODO check if the index j is really required here! A stated earlier, the matrices $\frac{\partial \mathbf{q}}{\partial \dot{\mathbf{x}}}$ and $\frac{\partial \mathbf{q}}{\partial \mathbf{w}}$ can be computed analytically. As for \mathbf{H}_2 , we follow the methodology outlined in [?] for evaluating and storing it efficiently as the product of flux operators. Again the staggered procedure for solving the adjoint state problem shares the same computational kernels with the partitioned aeroelastic scheme described in [?]

1) Update the adjoint structure displacement to the new time step

$$\mathbf{a}_u^{(n+1)} = (1 - \theta)\mathbf{a}_u^{(n)} + \theta\mathbf{a}_u^{-{(n+1)}} \quad (184)$$

$$(185)$$

where $\mathbf{a}_u^{-{(n+1)}}$ is obtained from

$$\mathbf{K}\mathbf{a}_u^{-{(n+1)}} = \frac{\partial \mathbf{q}}{\partial \mathbf{u}} - \mathbf{K}_{\Omega\Gamma} \mathbf{T}_u \mathbf{a}_{x\Omega}^{(n)} + \mathbf{T}_u \mathbf{a}_{x\Gamma}^{(n)} \quad (186)$$

TODO derive this equation

2) Compute the adjoint fluid state by solving

$$\mathbf{H}_2^T \mathbf{a}_w^{(n+1)} = \frac{\partial \dot{\mathbf{x}}}{\partial \mathbf{w}} + \frac{\partial \mathbf{P}_T}{\partial \mathbf{w}^T} \mathbf{a}_u^{(n+1)} \quad (187)$$

TODO derive this equation Again, $\frac{\partial \mathbf{q}}{\partial \mathbf{w}}$ is computed analytically from the relations defined in the design and aeroelastic model.

3) Compute adjoint mesh motion in domain and on the interface

$$\bar{\mathbf{K}}_{\Omega\Omega} \mathbf{a}_{x\Omega}^{(n+1)} = \frac{\partial \mathbf{q}}{\partial \dot{\mathbf{x}}_\Omega} - \frac{\partial \mathbf{P}_T}{\partial \dot{\mathbf{x}}_\Omega} \mathbf{a}_u^{(n+1)} - \frac{\partial \mathbf{F}_1^T}{\partial \dot{\mathbf{x}}_\Omega} \mathbf{a}_{x\Omega}^{(n+1)} \text{ in } \Omega \quad (188)$$

TODO check equations And the adjoint mesh motion on the interface is computed as $\mathbf{a}_{x\Gamma}^{(n+1)}$

$$\mathbf{a}_{x\Gamma}^{(n+1)} = \frac{\partial \mathbf{q}}{\partial \dot{\mathbf{x}}_{\text{Gamma}}} + \frac{\partial \mathbf{P}_T}{\partial \dot{\mathbf{x}}_\Gamma} \mathbf{a}_u^{(n+1)} - \frac{\partial \mathbf{F}_2^T}{\partial \dot{\mathbf{x}}_\Gamma} \text{ on } \Gamma \quad (189)$$

where $\frac{\partial \mathbf{q}}{\partial \mathbf{w}}$ is computed analytically.

The convergence of the staggered adjoint optimization algorithm can be monitored via

$$\left\| \mathbf{R}_q - \mathbf{A}^T \mathbf{a}^{(n+1)} \right\| \leq \epsilon^{SA} \|\mathbf{R}_q\| \quad (190)$$

10 The Embedded Boundary Method

It was already outlined in Section 2, that using an Eulerian approach in the context of an aeroelastic simulation leads to a so-called embedded formulation, where the interface of the structure mesh no longer coincides with the fluid mesh. This was appealing, since it allowed for the usage of fixed meshes and an Eulerian formulation, on the other hand as explained in Section ??, an error of the order $\mathcal{O}(\frac{h}{2})$ is introduced. A possible solution to recover second order convergence rate is quickly described in section **TODO**.

10.1 Setup

In this thesis, we consider embedded structure interfaces only. Whether the structure is deformable or rigid does not really make a difference for the subsequent considerations.

The basic setup is depicted in Figure 10.

Several issues have to be addressed in an embedded framework. Firstly, the interface may move during the simulation. In fact, large deformations of the structure have been one of the primary aspects for the development of an embedded framework in the first place. The question thus becomes how to track the interface during the simulation. This is addressed in section 10.5.

Secondly, the evaluation of the inviscid (191) and viscous (201) term becomes cumbersome for cells that are being intersected. We address this issue separate for the inviscid and the viscous term in sections 10.2 and 10.3.

Finally, in an FSI simulation we are typically interested in integral quantities over the structure surface, e.g. the lift and drag values of an airfoil. We now have several possibilities to define the structure surface to perform integration on in an embedded simulation. This issue will be discussed in section 10.4.

10.2 Evaluation of the inviscid term at the interface

For this section as well as for section 10.3 we consider Figure 10.

A question, that arises when looking at equation (40) is how to evaluate those terms for node i , where some of the vertices in $\kappa(i)$ are inactive ghost nodes.

We will answer this question for the inviscid term in this subsection and look at the viscous term in the subsequent one.

First, we notice that we can split the summation as follows

$$\sum_{j \in \kappa(i)} \phi_{ij}(\mathbf{w}_i, \mathbf{w}_j, \boldsymbol{\nu}_{ij}) = \sum_{j \in \kappa(i)^a} \phi_{ij}(\mathbf{w}_i, \mathbf{w}_j, \boldsymbol{\nu}_{ij}) + \sum_{j \in \kappa(i) \setminus \kappa(i)^a} \phi_{ij}^{\text{eq:five_inviscid_split}}(\mathbf{w}_i, \mathbf{w}_*, \boldsymbol{\nu}_{ij}) \quad (191)$$

where \mathbf{w}_* is the fluid state at the auxiliary intersection between edge ij and the auxiliary interface. To obtain \mathbf{w}_* a one-sided Riemann problem is defined

$$\frac{\partial \tilde{\mathbf{w}}}{\partial t} = \frac{\partial \mathcal{F}}{\partial s}(\tilde{\mathbf{w}}) = \mathbf{0} \quad (192)$$

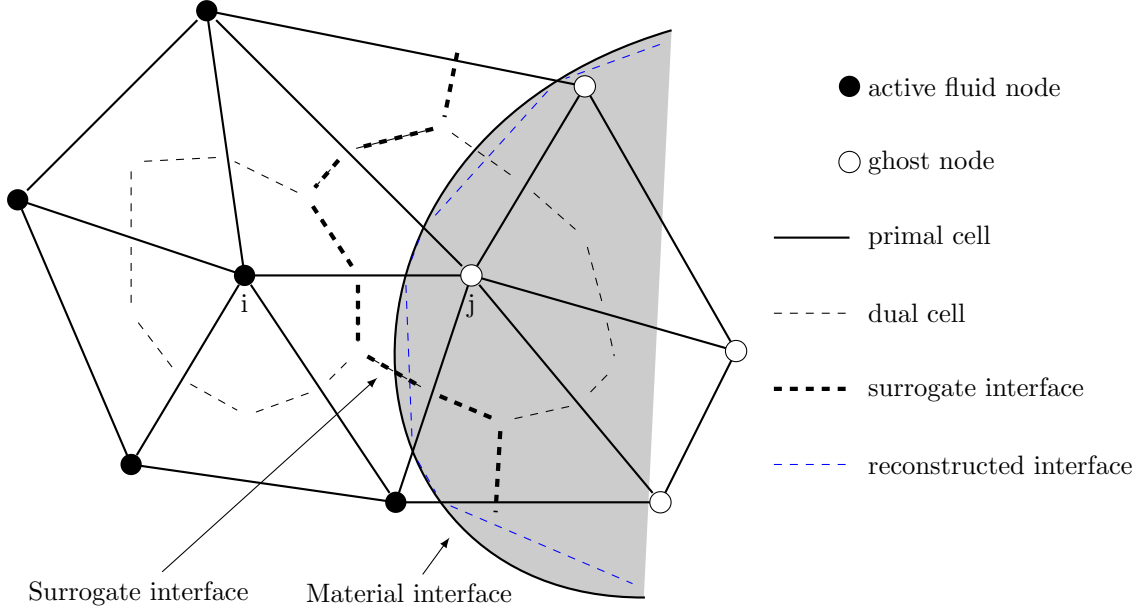


Figure 10: Sketch of an embedded simulation setup. The primal grid is intersected by a material interface. In FIVER, the material interface is replaced by a surrogate interface that is created by connecting the dual-grid interfaces closest to the embedded surface. By connecting the intersection points of the embedded surface with the primal grid, we can also create a so-called, reconstructed surface that is particularly useful for the calculation of forces on the surface.

where s is the local abscissa along the direction ij , that has its origin in M_{ij} . The one sided Riemann problem can then be initialized with

$$\tilde{\mathbf{w}}_L = \begin{bmatrix} \rho_i & \mathbf{v}_i & p_i \end{bmatrix} \quad (193)$$

The exact solution of the one-sided, one-dimensional Riemann problem contains a constant (in time) state at the fluid-structure interface which is denoted here by

$$\mathbf{w}_* = \begin{bmatrix} \rho_* & \mathbf{v}_* & p_* \end{bmatrix} \quad (194)$$

which can then be used in equation (191)

10.2.1 FIVER-1

$$\begin{aligned} \frac{\partial \tilde{\mathbf{w}}^*}{\partial \tau} + \frac{\partial \tilde{f}(\tilde{\mathbf{w}}^*)}{\partial \xi} &= \mathbf{0} \\ \tilde{f}^*(\xi, 0) &= \tilde{\mathbf{w}}_{ij} \\ \mathbf{v}(0, \tau) \cdot \mathbf{n}_{wall} &= \mathbf{v}_{wall} \cdot \mathbf{n}_{wall} \end{aligned} \quad \begin{array}{l} \xi < 0 \\ \text{eq:half riemann_problem} \\ \{ t \leq \tau \} \end{array} \quad (195)$$

$$\phi_{ij} = \phi_{ij}(\tilde{\mathbf{w}}_{ij}, \tilde{\mathbf{w}}_b^*, \mathbf{n}_{ij}) \quad (196)$$

10.3 Evaluation of the viscous terms at the interface

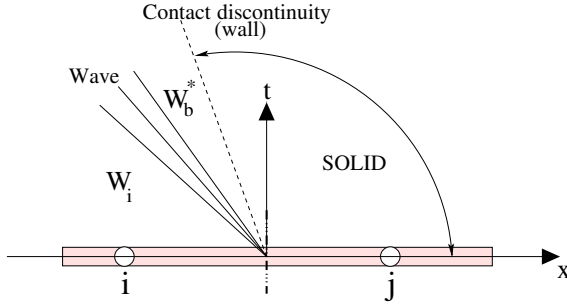


Figure 11: Solution of the 1D half Riemann problem around edge $i-j$ described in equation (195). The obtained fluid state at the interface is then used to evaluate the flux function, see equation (??)

10.2.2 FIVER-2

The Fluid state is extrapolated to the material interface

$$\mathbf{w}_\Gamma = \mathbf{w}_i + \nabla \mathbf{w}_i (\mathbf{x}_\Gamma - \mathbf{x}_i) \quad (197)$$

The one-dimensional half-Riemann problem is solved at the material interface Γ

$$\tilde{\mathbf{w}}_\Gamma^* = \tilde{\mathbf{w}}^*(\tilde{\mathbf{w}}_\Gamma, \mathbf{v}_{wall}, \mathbf{n}_{wall}) \quad (198)$$

The fluid state is inter/extrapolated at the control volume interface C_{ij}

$$\tilde{\mathbf{w}}_{ij}^* = \tilde{\mathbf{w}}_{ij}^*(\mathbf{w}_\Gamma^*, \mathbf{w}_i) \quad (199)$$

Numerical flux at the control volume interface:

$$\mathbf{R}_{ij}^c = \mathbf{R}_{ij}^c(\mathbf{w}_{ij}, \mathbf{w}_{ij}^*, \mathbf{n}_{ij}) \quad (200)$$

It has been proven in **TODO** that this approach recovers second order convergence int the vicinity of the interface.

10.3 Evaluation of the viscous terms at the interface

If one wants to keep the FE-like evaluation of the second term, (40) can be splitted as

$$\sum_{T_i \in \lambda(i)} \int_{T_i} \mathbb{K} \nabla \mathbf{w} \nabla \phi_i dx = \sum_{T_i \in (\lambda(i^a))} \int_{T_i} \mathbb{K} \nabla \mathbf{w} \nabla \phi_i dx + \sum_{\substack{T_i \in (\lambda(i) \setminus \lambda(i^a)) \\ \text{eq:fiver_viscous_split}}} \int_{T_i} \mathbb{K} \nabla \mathbf{w}^R \nabla \phi_i dx = \quad (201)$$

where $\lambda(i^a)$ is the set of triangles that can be build from the active nodes around node i and $\lambda(i) \setminus \lambda(i^a)$ are all the triangles where at least one node is inactive(ghost).

The only difficulty now becomes the evaluation of the last term, meaning the integration over cutted elements, where at least on node is inactive, and thus does not

have a fluid state solution.

We did not have that problem for the inviscid term of equation (40), since a **FV** approximation was chosen, and therefore we could construct a flux at the interface thanks to the piston problem. No inactive node had to be considered.

For the viscous part, however, we want to keep the **FE** like formulations described in 3.3 to avoid re-writing large portions of the code. If a triangle is cut by the interface, one or two nodes will therefore be labeled inactive, and be denoted as ghost-nodes. Clearly, the fluid state vector at this ghost nodes is not defined. The question thus becomes how to evaluate this terms (last part in equation (201)).

The approach we take, that is also outlined in **TODO ask for reference** is to reconstruct a pseudo fluid-state at the ghost points, such that the boundary conditions at the wall are full-filled.

10.3.1 Reconstruction of the fluid-state at ghost-nodes

TODO ask Farhat if this is really how it is done To explain the reconstruction at the ghost nodes, it again helps to consider Figure 10.

We also notice that the viscous flux, as defined in Equation 19, only depends on the fluid velocity and the temperature. Reconstruction of the velocity at the ghost node is straight forward. Assuming a linear interpolation inside the elements, the velocity at node i is reconstructed such, that the stick condition is fulfilled at the interface.

As far as the reconstruction of the temperature is concerned, two different cases have to be considered: adiabatic walls and isothermal walls.

For an adiabatic wall, the temperature gradient at the wall is zeros, which can be achieved by setting the temperature of the ghost note equal to that of node i . An isothermal wall boundary condition enforces a certain, constant temperature at the wall. Similar to the velocity boundary condition, this can be achieved by finding an appropriate ghost point value such that the condition is enforced.

The issue is depicted in detail in figure 12. The figure also reveals that there is no unique solution for the ghost point value. Multiple active node connect to the ghost node and the above described relations can be formulated for every one of them. **FIVER** therefore solves a least square system to chose an appropriate value.

The elegance of this approach is that once the ghost point state have been found, the evaluation of the viscous contribution can be done with the standard code routines. No adaption is required to make them work in the embedded framework.

10.4 Evaluation of forces

Another issue that arises for embedded simulations is the appropriaite evaluation of the forces on an embedded interface. This is especially important if the embedded framework is used in an **FSI** setup to get an approriate resultant on the structure. Sensitivity Analysis is another application, where approriate evaluation of Lift and

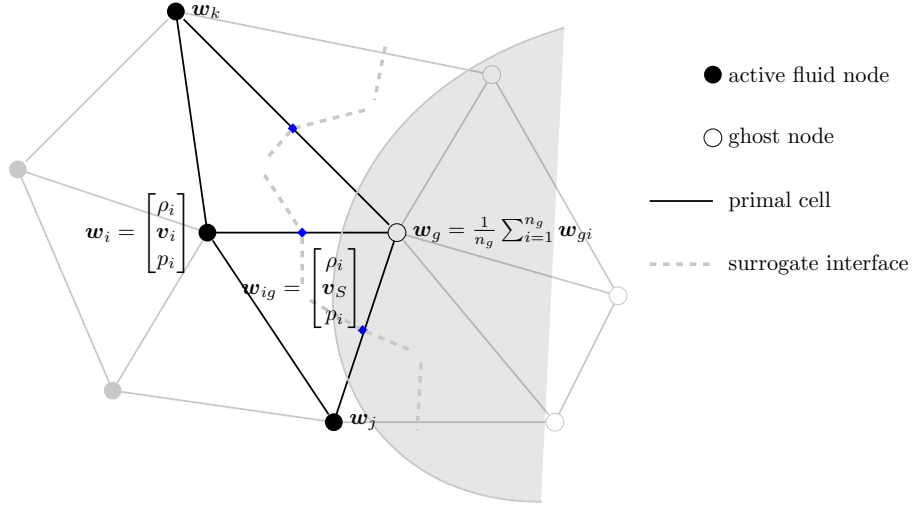


Figure 12: Illustration of the ghost point population process. States at nodes i, j, k are known from computation. States at mid-edges kg, ig, jg are the states we want to impose at the interface. The pressure and density are constantly extrapolated from the fluid states, whereas the velocity is set to the structure velocity at the interface. A linear extrapolation is then performed from the active states over the stated at the intersection points to obtain the interpolated ghost states. Since the interpolated ghost state values are typically ambiguous, due to multiple edges connecting to one ghost node, a least-square algorithm or a simple averaging can be performed to obtain a final value for the ghost state w_g .

Drag integrals are crucial.

This problem has been analyzed in **REF** **REF** **MOST** importantly, the question becomes whether to evaluate the pressure integral **REF** over the auxiliary control volume interface **Ref** or over the so called reconstructed interface, which can be obtained by creating auxiliary surfaces inside the intersected elements through the knowledge about intersection points at the edges.

10.5 Level-set method

The issue of interface tracking is extensively discussed in **CITEWangGretarsson2012** and TODO.

Since the interface in an embedded simulation typically moves, an appropriate interface tracking approach is required.

For **FIVER**, the popular level set method [?] was chosen.

The level set approach is characterized by the following equation:

$$\frac{\phi}{t} + \mathbf{v} \cdot \nabla \phi = 0 \quad \text{eq:level_set (202)}$$

where ϕ is a function designed to track the material interface. Particularly, ϕ is initialized such that the interface is characterized by $\phi = 0$. The interface

can then be tracked via a simple time integration of equation (202). Details of this approach, which was developed for computer visualization purposes, can be found in [?].

TODO

11 Verification

After chapter 2 described the basic equation of fluid mechanics, discretization of this equations with **FV** and **FE** schemes in section 3, and an introduction to **SA**, the expressions for the actual derivatives have been derived in section 7. This has been done for both the body-fitted and the embedded ?? framework of AERO-F. This section is denoted to a thorough validation of the obtained derivatives. As described in REF, AERO-F handles both sensitivities with respect to far-field variables(e.g. angle of attack) as well as shape sensitivities. Both types require to be handled fundamentally differently. While the first type leads to derivatives mainly in the far field boundary conditions, the latter one interferes with the wall treatment. More importantly, as shown in section TODO, in the embedded case, doing shape sensitivities leads to additional derivatives with regards to the intersector. For all those reasons, the verification provided in this chapter deals with both M_∞ -sensitivity as well as shape-sensitivity. More over we will provide plots for both the body-fitted and the embedded case.

11.1 Verification approach

The question of how to verify the obtained sensitivities is cumbersome anything but straightforward.

To begin with, what quantity can we verify anyway?

If we have a look at equation **TODO**, one can see, that there are two main derivatives: $\frac{\partial \mathbf{R}}{\partial \mathbf{w}}$ and $\frac{\partial \mathbf{R}}{\partial \mathbf{w}}$.

The basic idea that we exploit for verification is to compute a reference solution for the Sensitivities by a **FD** of two steady-state simulation. The advantage is, that the sensitivity-module does not have to be used at all to obtain those references, thus it is ensured that potential bugs are not carried over.

However, for both of the above quantities, computing a finite difference solution is cumbersome. For the Jacobian $\frac{\partial \mathbf{R}}{\partial \mathbf{w}}$ a simple forward difference would look as follows:

$$\left. \frac{\partial \mathbf{R}_i}{\partial \mathbf{w}_j} \right|_{\mathbf{w}_0} = \frac{\mathbf{R}_i(\mathbf{w}_0 + \epsilon \mathbf{e}_j) - \mathbf{R}_i(\mathbf{w}_0) - \epsilon \mathbf{e}_j}{2\epsilon} \quad (203)$$

which would entail an $\mathcal{O}(N)$ number of residual evaluations.

As far as $\frac{\partial \mathbf{R}}{\partial \mathbf{w}}$ goes, a **FD** verification would be feasible:

$$\begin{aligned} \frac{\partial \mathbf{R}_i}{\partial M_\infty} &= \frac{\mathbf{R}(\mathbf{w}_i^+) - \mathbf{R}(\mathbf{w}_i^-)}{2\epsilon} \\ \mathbf{w}_i^\pm &= \begin{cases} \mathbf{w}_i|_0 & \text{for internal nodes} \\ \mathbf{w}_i|_{\mathbf{w}_i(M_i=M_0+\epsilon)} & \text{for boundary nodes} \end{cases} \end{aligned} \quad (204)$$

which could be done cheaply, and is in fact done in AERO-F if the parameter `SensitivityAnalysis.SensitivityComputation` is set to `FiniteDifference` however, it requires the fluid-state to be updated according to the mach-number change at the fluid boundary and thus introduced the potential for new bugs.

Instead, the first quantity to be validated in this thesis is the solution of the linear system described in equation [REF](#), $\frac{\partial \mathbf{w}}{\partial s}$.

this can be done easily by performing a simple [FD](#) difference on the solution of two steady-state simulations;

$$\frac{d\mathbf{w}}{ds} = \frac{\mathbf{w}(s + \epsilon) - \mathbf{w}(s - \epsilon)}{2\epsilon} \quad (205)$$

which involves no extra coding and can be done with a standard steady state solver.

Additionally, since the optimization will run on lift and drag, we also validate them with steady state results.

$$\frac{dq}{ds} = \frac{q(s + \epsilon) - q(s - \epsilon)}{2\epsilon} \quad (206)$$

The validation of integrated forces is provided in figures ??-?? for body-fitted computations and in figures ??-?? for embedded.

12 Verification of mach-sensitivity

For the body-fitted case, the verification of $\frac{d\mathbf{w}}{dM_\infty}$ for ALE simulations is provided in figure [13](#) for Euler equation, figure [14](#) for full [NSE](#) and in figure [15](#) for [NSE](#) equations with an additional Spallart-Almaraes turbulence model. Additionally, a side by side comparison of the analytic results between all three equation types is also provided in figure [19](#) in order to ensure that the additional viscous and turbulent terms actually account for a visible difference.

For the embedded case, we provide the verification of $\frac{d\mathbf{w}}{dM_\infty}$ in figure [16](#) for Euler equation, figure [17](#) for full [NSE](#) and in figure [18](#) for [NSE](#) equations with an additional Spallart-Almaraes turbulence model. Again, a side by side comparison of the analytic results between all three equation types is also provided in figure [20](#) in order to ensure that the additional viscous and turbulent terms actually account for a visible difference.

13 Verification shape sensitivity

The verification of $\frac{d\mathbf{w}}{ds}$ for ALE simulations is provided in figure [21](#) for Euler equation, figure [22](#) for full [NSE](#) and in figure [23](#) for [NSE](#) equations with an additional Spallart-Almaraes turbulence model. Additionally, a side by side comparison of the

Verification $\frac{d\mathbf{w}}{dM_\infty}$ for Euler equations and a body-fitted framework

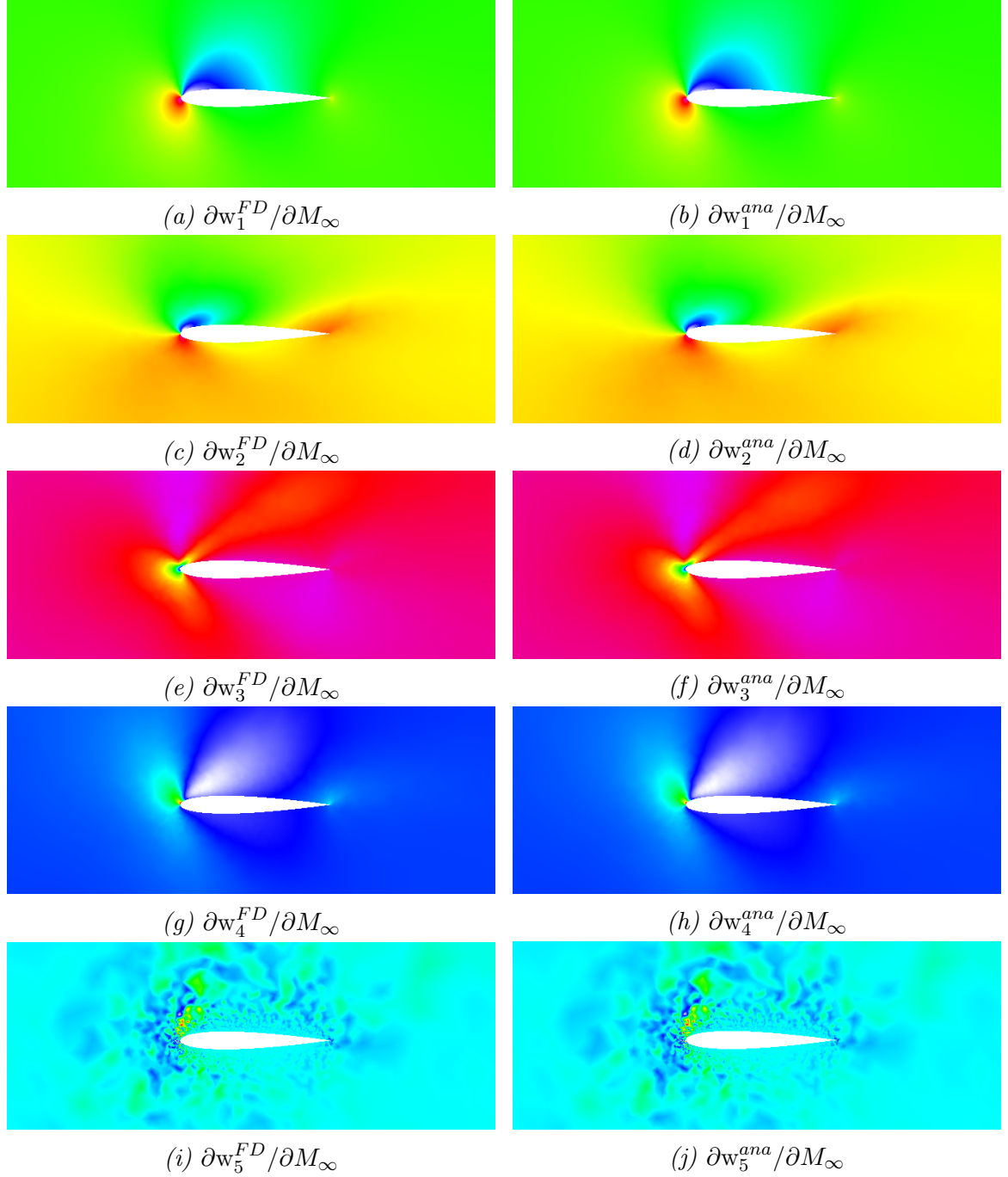


*Figure 13: Verification of $\frac{d\mathbf{w}}{dM_\infty}$ for Euler equations in the body-fitted framework. The **FD** reference solution as described in section 11.1 is provided in the left column, the newly implemented analytic derivatives are visualized in the right column. **FD** and analytic solution are plotted using the same color-scheme.*

Verification $\frac{d\mathbf{w}}{dM_\infty}$ for Laminar equations and a body-fitted framework

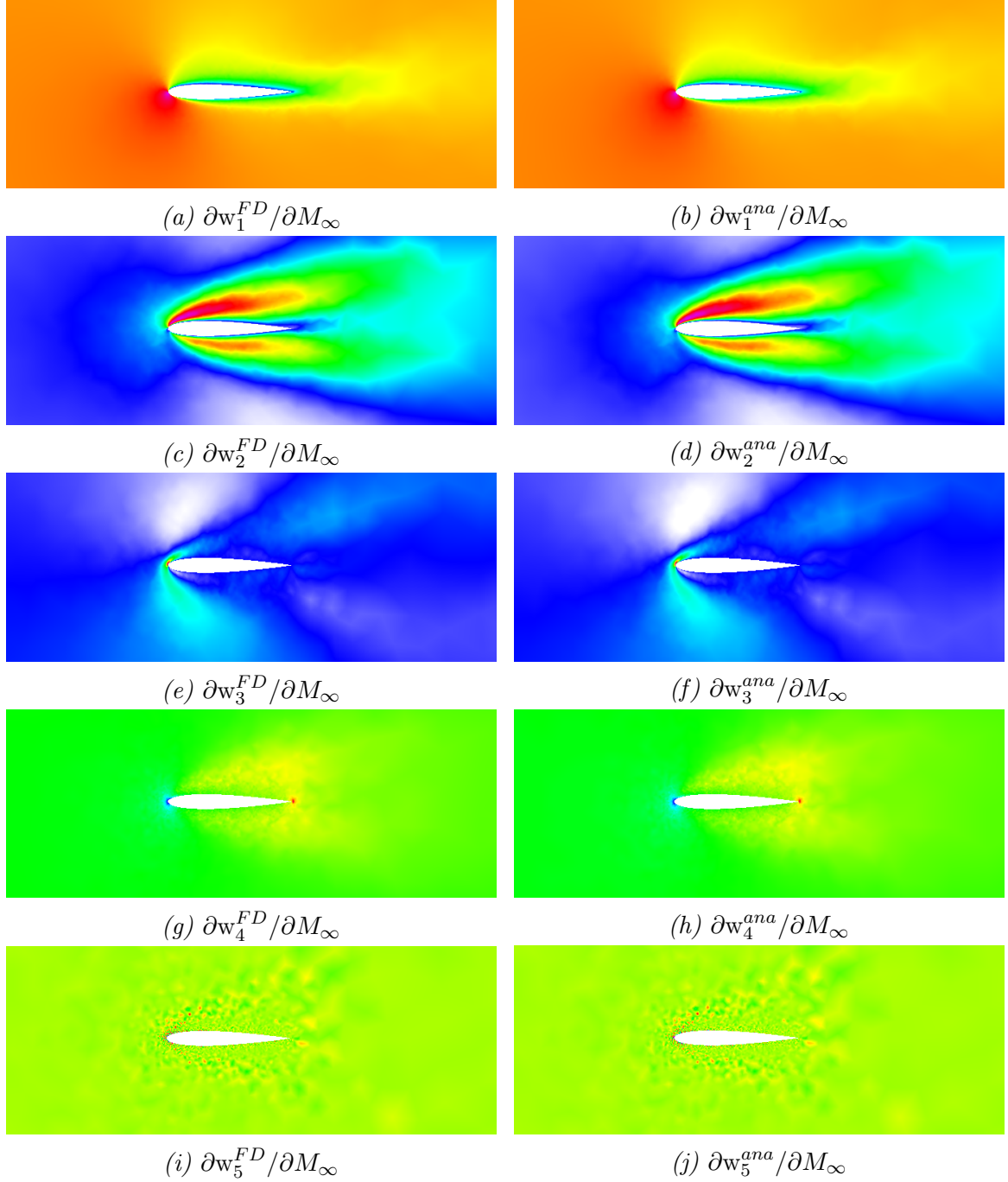


Figure 14: Verification of $\frac{d\mathbf{w}}{dM_\infty}$ for Laminar equations in the body-fitted framework. The **FD** reference solution as described in section 11.1 is provided in the left column, the newly implemented analytic derivatives are visualized in the right column. **FD** and analytic solution are plotted using the same color-scheme.

Verification $\frac{d\mathbf{w}}{dM_\infty}$ for RANS equations and a body-fitted framework

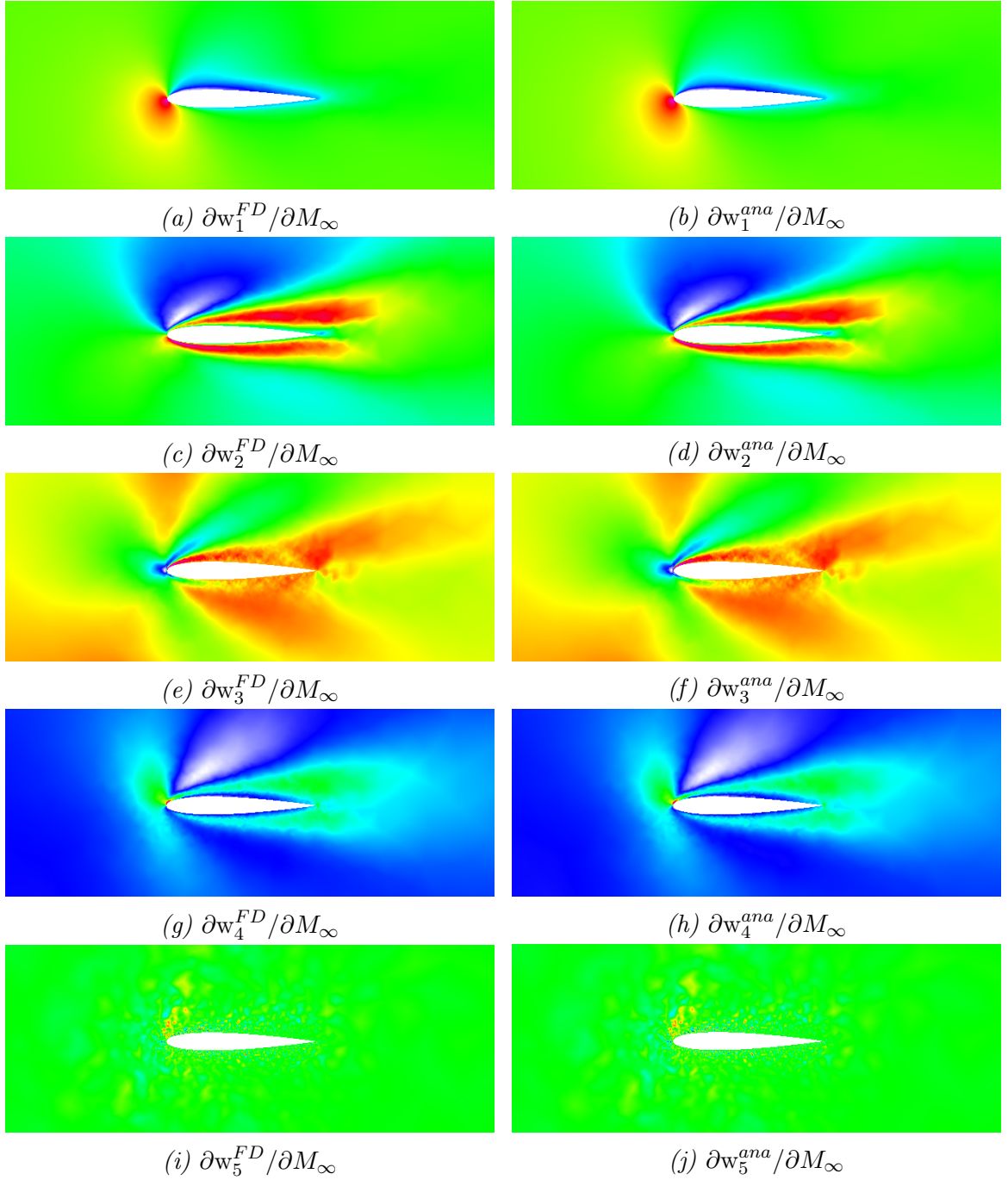


Figure 15: Verification of $\frac{d\mathbf{w}}{dM_\infty}$ for RANS equations in the body-fitted framework. The FD reference solution as described in section 11.1 is provided in the left column, the newly implemented analytic derivatives are visualized in the right column. FD and analytic solution are plotted using the same color-scheme.

Verification $\frac{d\mathbf{w}}{dM_\infty}$ for Euler equations and a embedded framework

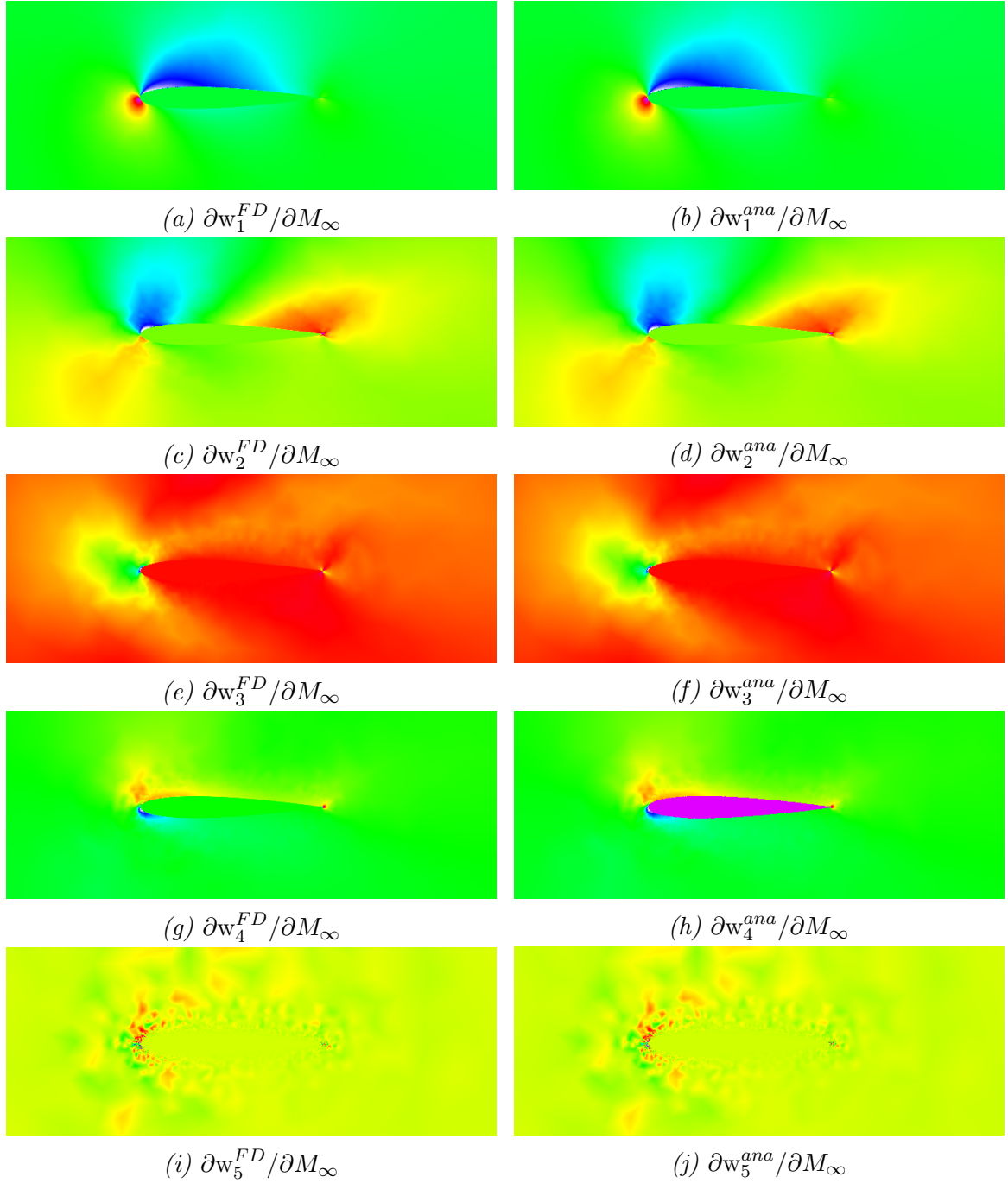


Figure 16: Verification of $\frac{d\mathbf{w}}{dM_\infty}$ for Euler equations in the embedded framework. The **FD** reference solution as described in section 11.1 is provided in the left column, the newly implemented analytic derivatives are visualized in the right column. **FD** and analytic solution are plotted using the same color-scheme.

Verification $\frac{d\mathbf{w}}{dM_\infty}$ for Laminar equations and a embedded framework

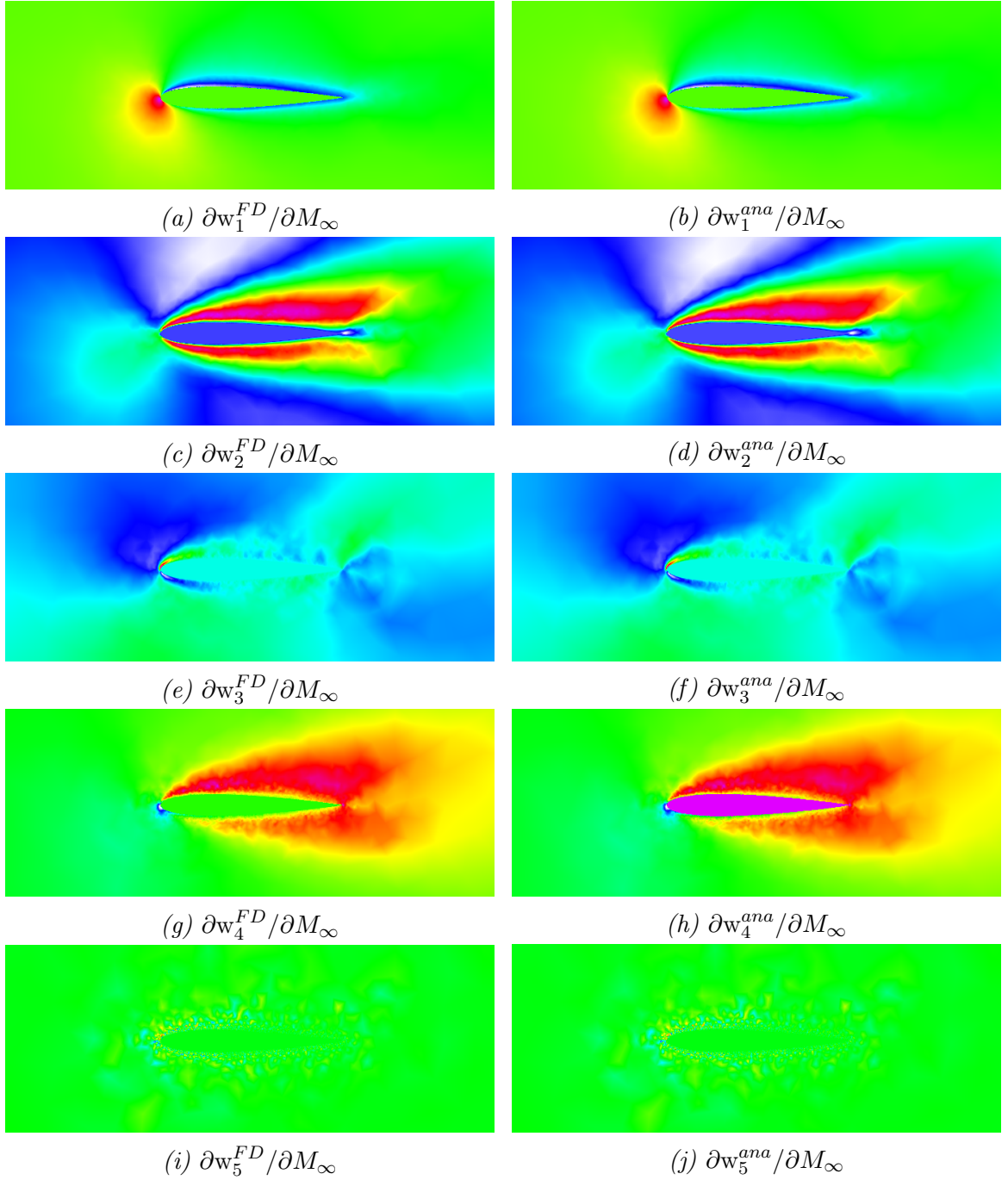


Figure 17: Verification of $\frac{d\mathbf{w}}{dM_\infty}$ for Laminar equations in the embedded framework. The FD reference solution as described in section 11.1 is provided in the left column, the newly implemented analytic derivatives are visualized in the right column. FD and analytic solution are plotted using the same color-scheme.

Verification $\frac{d\mathbf{w}}{dM_\infty}$ for RANS equations and a embedded framework

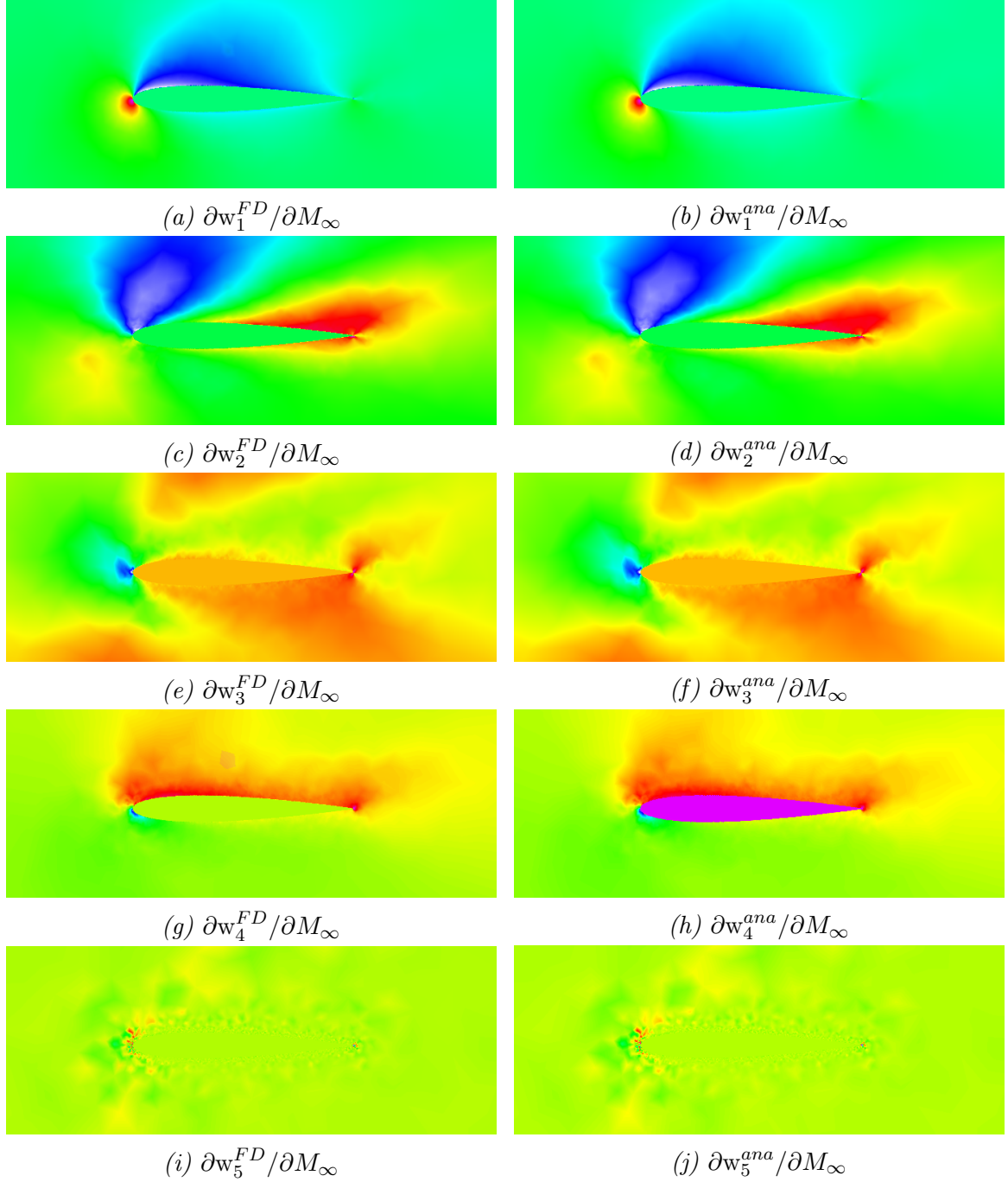


Figure 18: Verification of $\frac{d\mathbf{w}}{dM_\infty}$ for RANS equations in the embedded framework. The **FD** reference solution as described in section 11.1 is provided in the left column, the newly implemented analytic derivatives are visualized in the right column. **FD** and analytic solution are plotted using the same color-scheme.

Comparison of $\frac{d\mathbf{w}}{dM_\infty}$ in the body-fitted framework for all 3 equation types

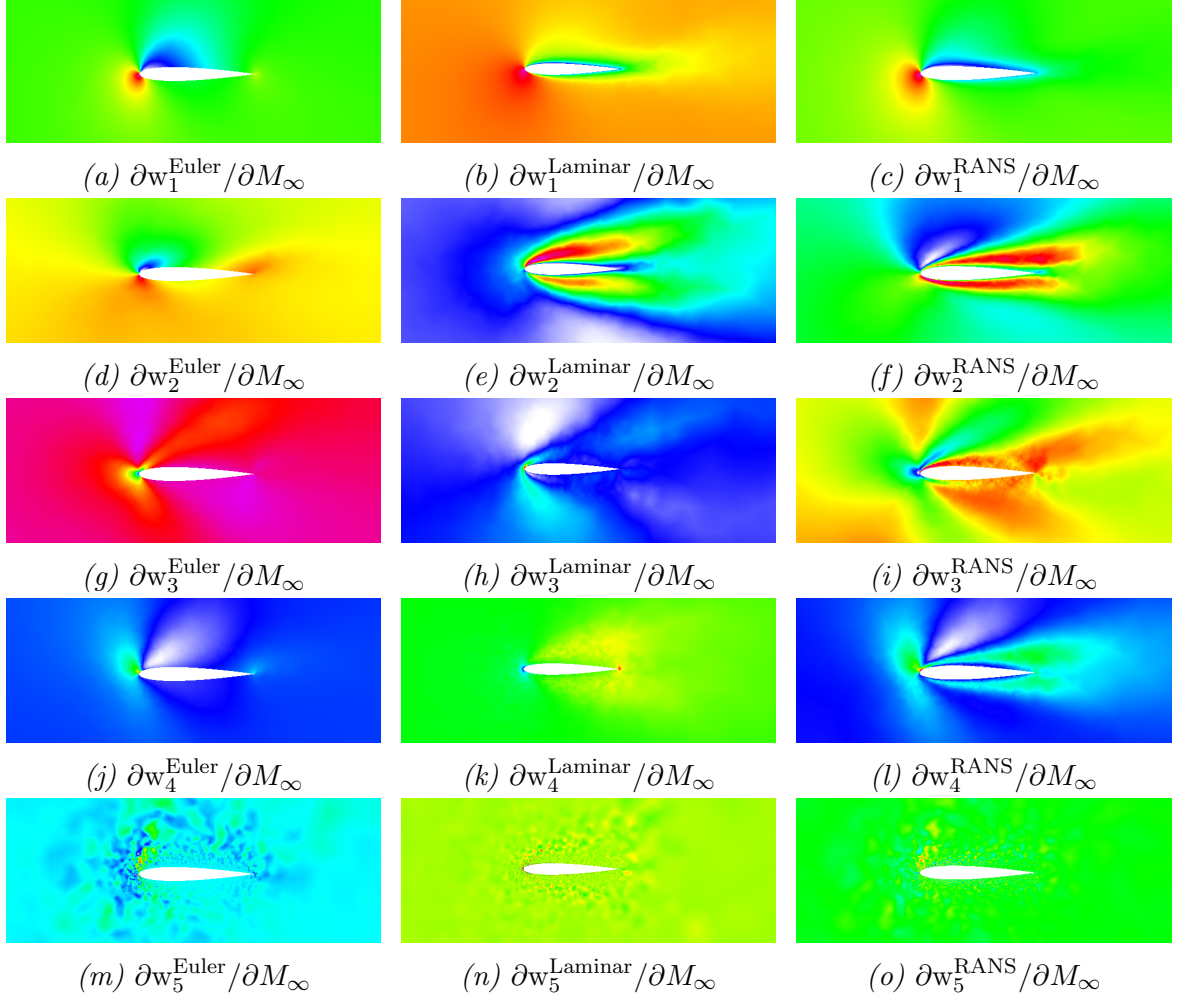


Figure 19: Comparison of analytic $\frac{d\mathbf{w}}{dM_\infty}$ for Euler equations(left column), laminar [NSE](#) equations (center column) and [NSE](#) equations with turbulence models (right column) in the body-fitted framework.

analytic results between all three equation types is also provided in figure 27 in order to ensure that the additional viscous and turbulent terms actually account for a visible difference.

For the embedded case, we provide the verification of $\frac{d\mathbf{w}}{ds}$ in figure 24 for Euler equation, figure 25 for full [NSE](#) and in figure 26 for [NSE](#) equations with an additional Spallart-Almaraes turbulence model. Again, a side by side comparison of the analytic results between all three equation types is also provided in figure 28 in order to ensure that the additional viscous and turbulent terms actually account for a visible difference.

Comparison of $\frac{d\mathbf{w}}{dM_\infty}$ in the embedded framework for all 3 equation types

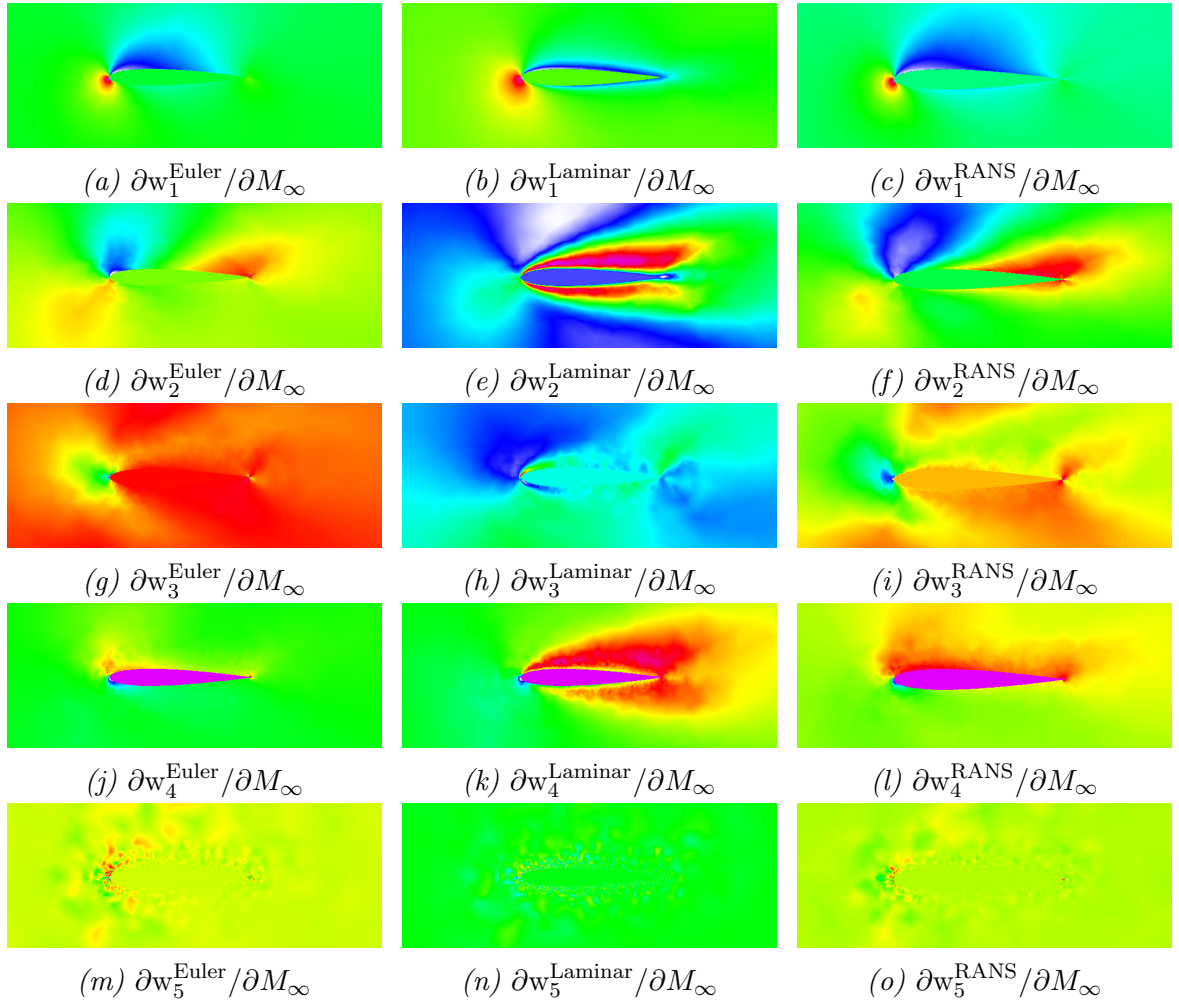
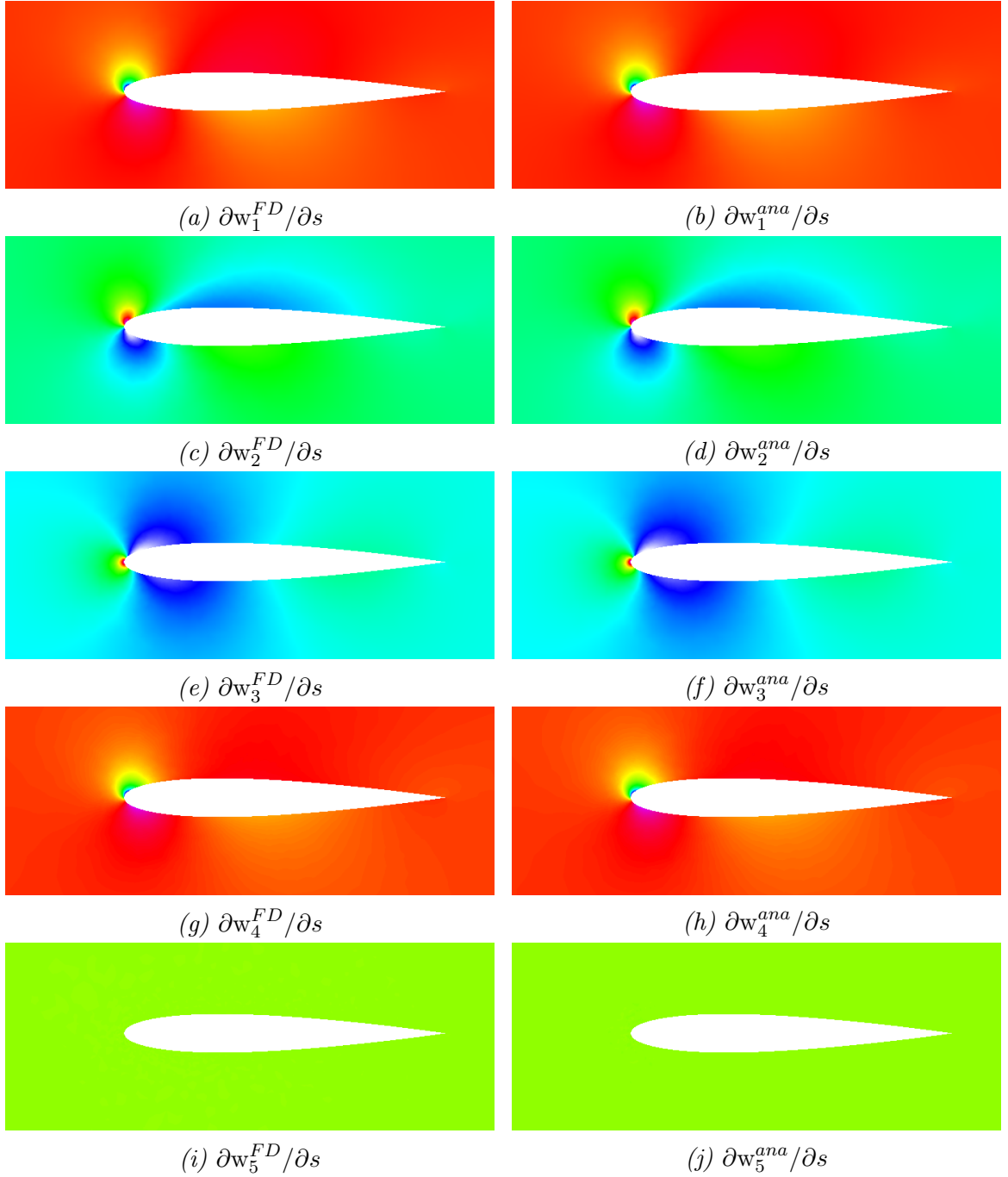


Figure 20: Comparison of analytic $\frac{d\mathbf{w}}{dM_\infty}$ for Euler equations (left column), laminar NSE equations (center column) and NSE equations with turbulence models (right column) in the embedded framework.

Verification $\frac{d\mathbf{w}}{ds}$ for Euler equations and a body-fitted framework



*Figure 21: Verification of $\frac{d\mathbf{w}}{ds}$ for Euler equations in the body-fitted framework. The **FD** reference solution as described in section 11.1 is provided in the left column, the newly implemented analytic derivatives are visualized in the right column. **FD** and analytic solution are plotted using the same color-scheme.*

Verification $\frac{d\mathbf{w}}{ds}$ for Laminar equations and a body-fitted framework

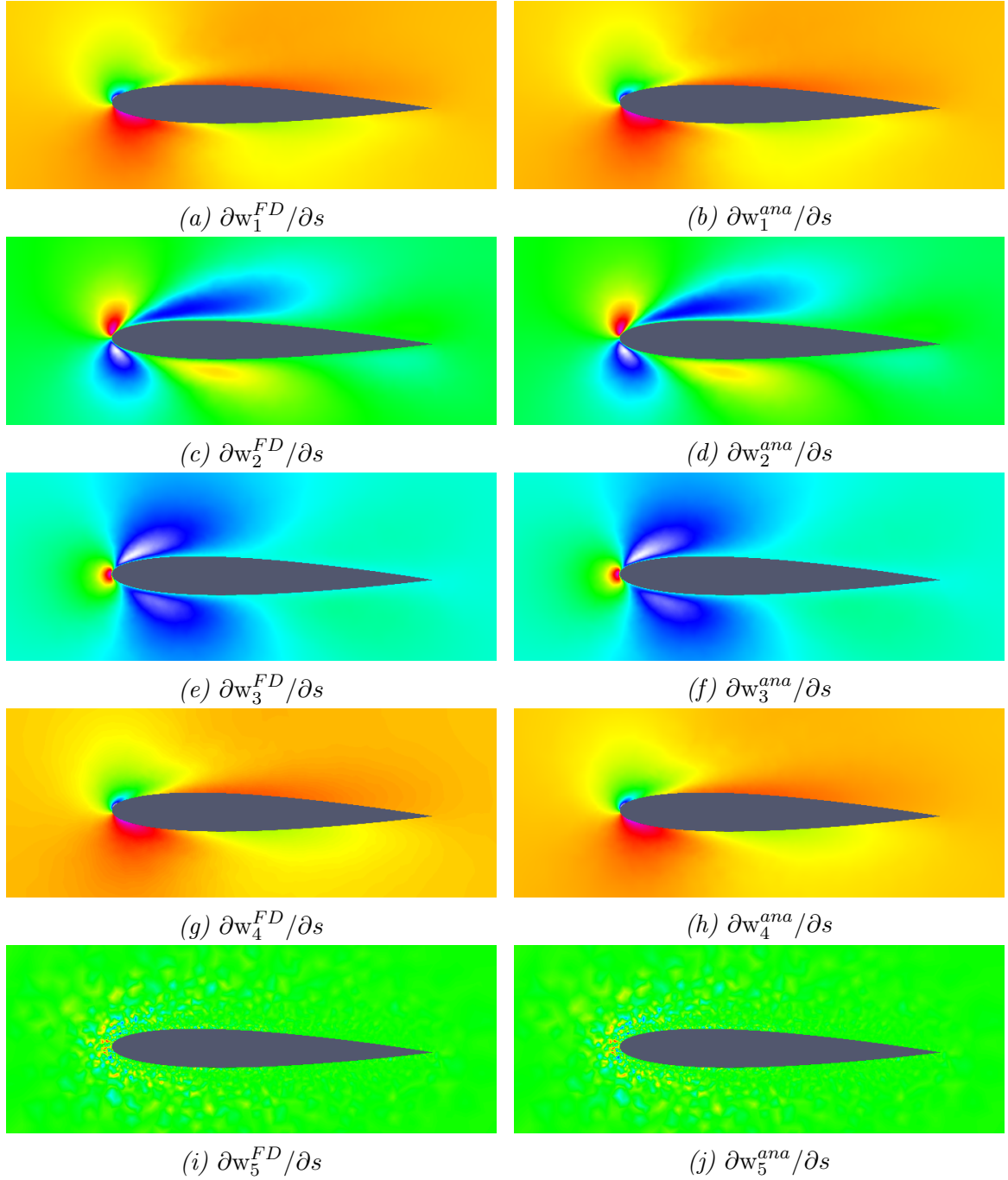
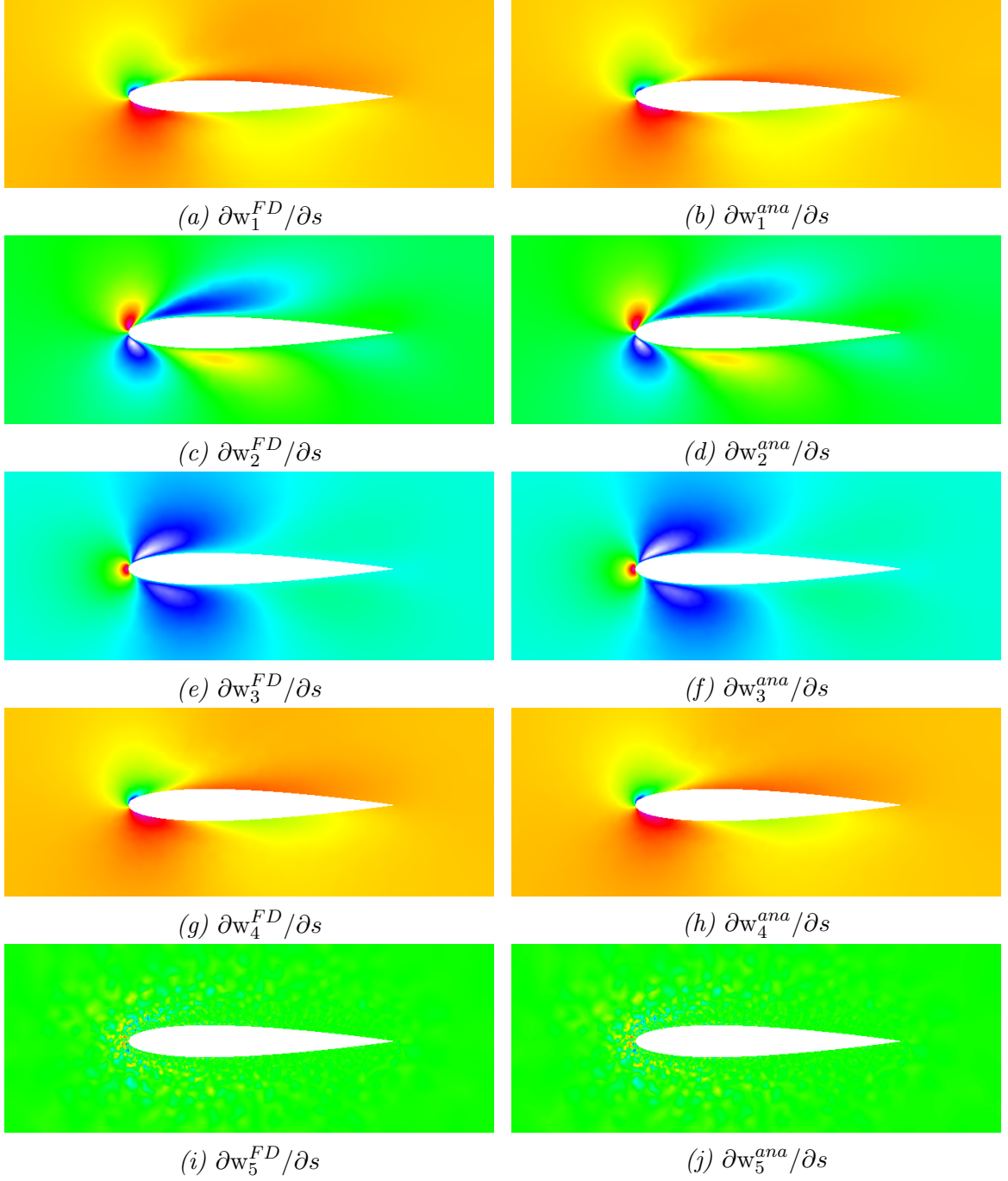


Figure 22: Verification of $\frac{d\mathbf{w}}{ds}$ for Laminar equations in the body-fitted framework. The **FD** reference solution as described in section 11.1 is provided in the left column, the newly implemented analytic derivatives are visualized in the right column. **FD** and analytic solution are plotted using the same color-scheme.

Verification $\frac{d\mathbf{w}}{ds}$ for RANS equations and a body-fitted framework



*Figure 23: Verification of $\frac{d\mathbf{w}}{ds}$ for RANS equations in the body-fitted framework. The **FD** reference solution as described in section 11.1 is provided in the left column, the newly implemented analytic derivatives are visualized in the right column. **FD** and analytic solution are plotted using the same color-scheme.*

Verification $\frac{d\mathbf{w}}{ds}$ for Euler equations and a embedded framework

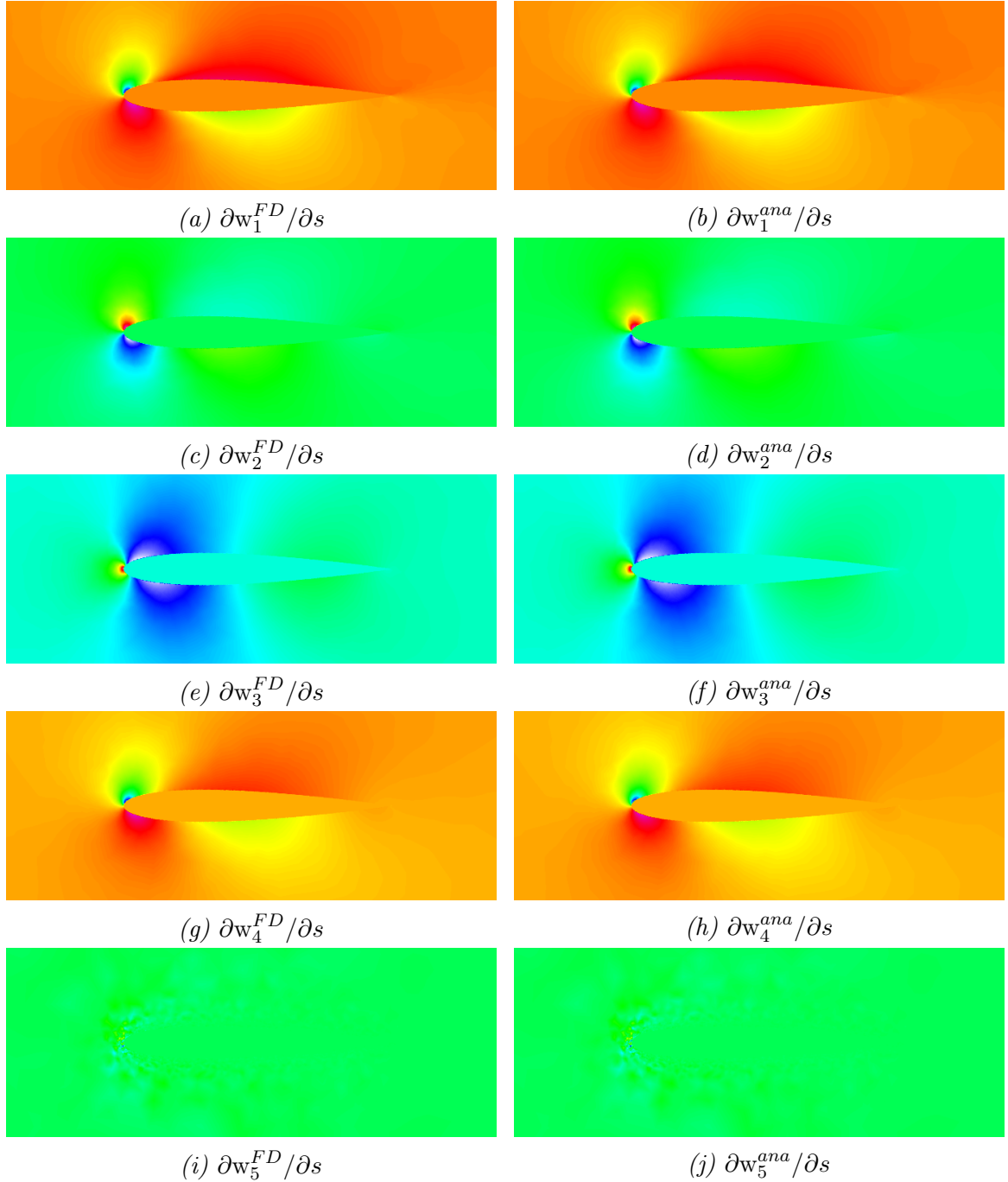


Figure 24: Verification of $\frac{d\mathbf{w}}{ds}$ for Euler equations in the embedded framework. The **FD** reference solution as described in section 11.1 is provided in the left column, the newly implemented analytic derivatives are visualized in the right column. **FD** and analytic solution are plotted using the same color-scheme.

Verification $\frac{d\mathbf{w}}{ds}$ for Laminar equations and a embedded framework

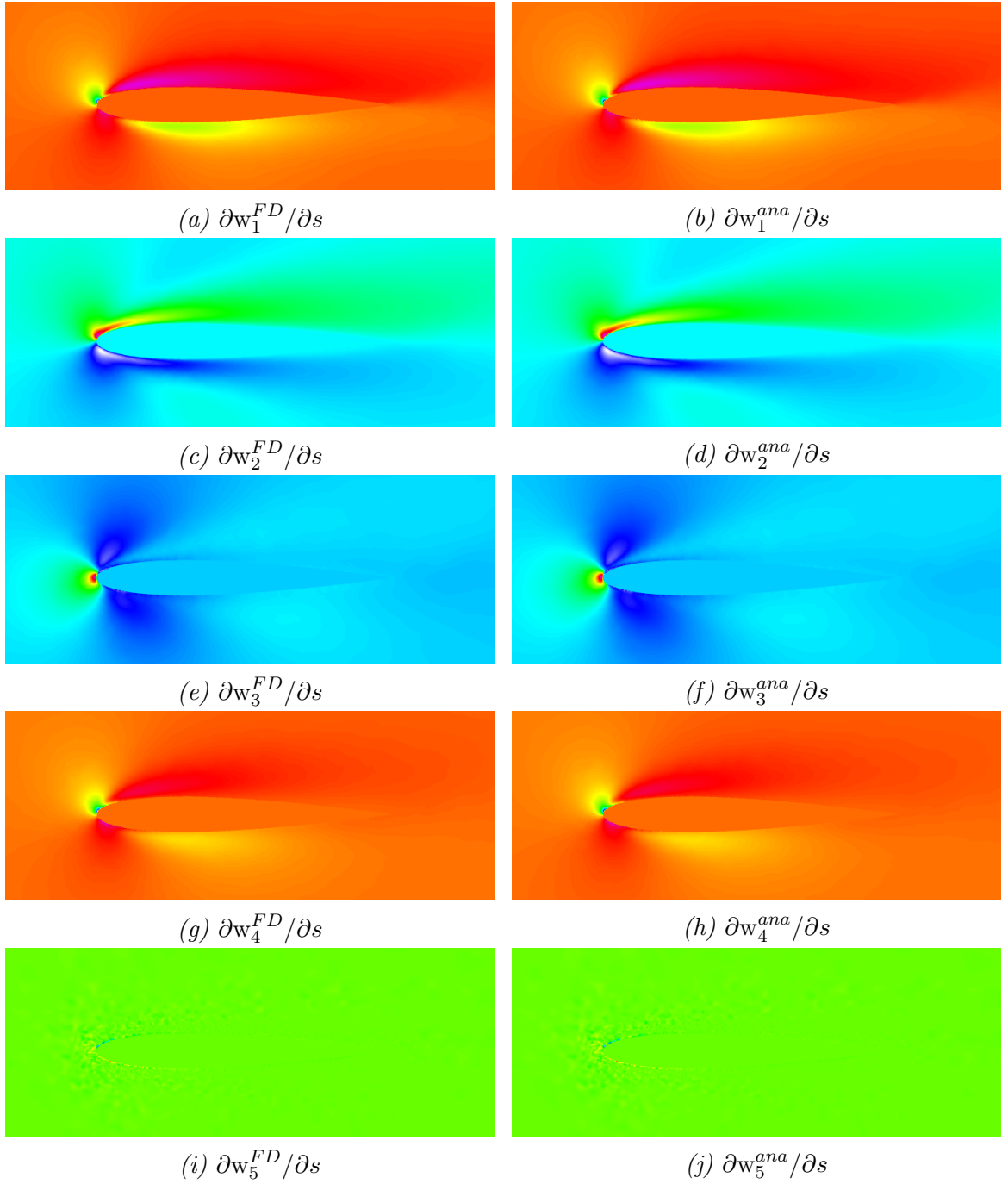


Figure 25: Verification of $\frac{d\mathbf{w}}{ds}$ for Laminar equations in the embedded framework. The **FD** reference solution as described in section 11.1 is provided in the left column, the newly implemented analytic derivatives are visualized in the right column. **FD** and analytic solution are plotted using the same color-scheme.

Verification $\frac{d\mathbf{w}}{ds}$ for RANS equations and a embedded framework

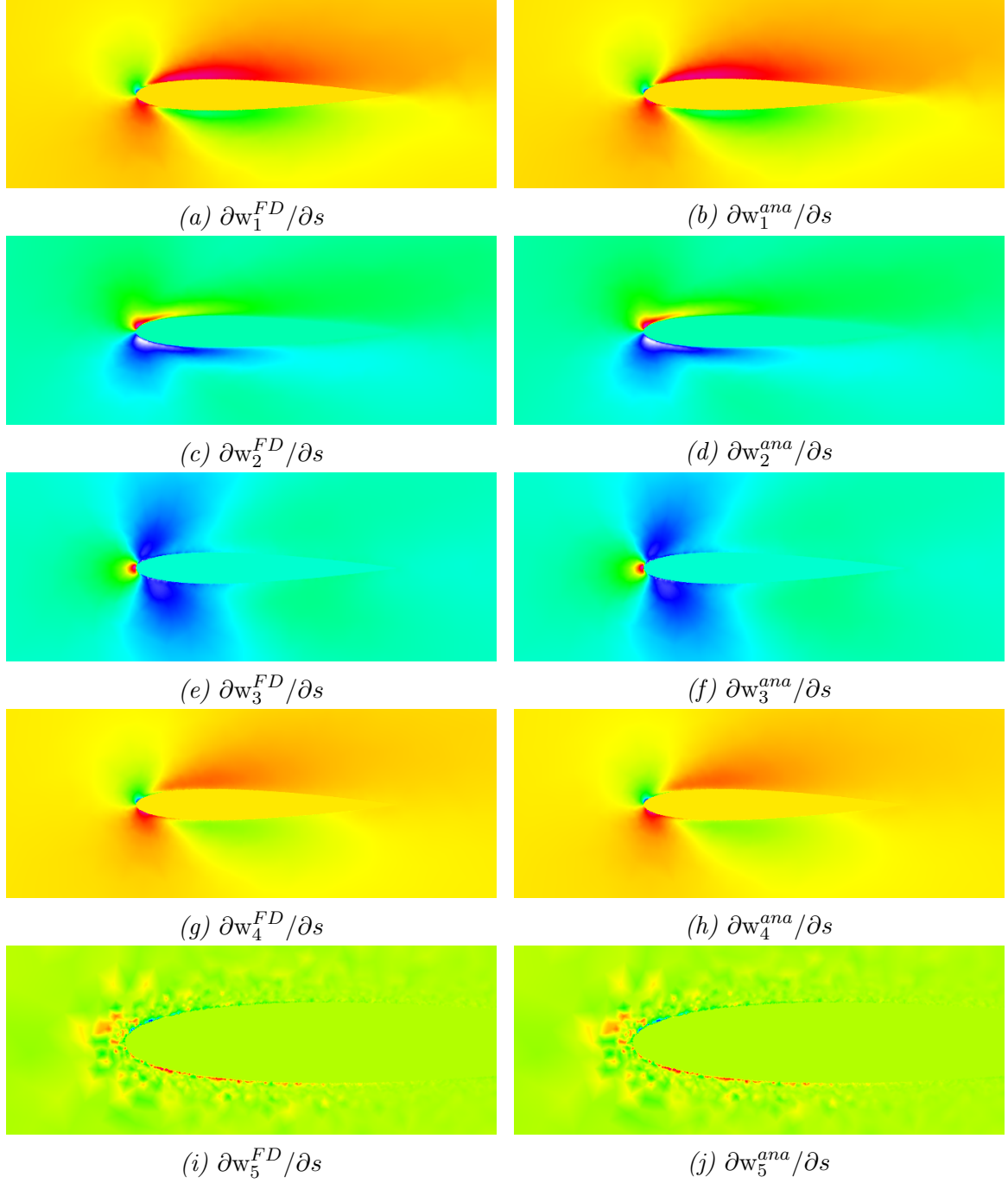


Figure 26: Verification of $\frac{d\mathbf{w}}{ds}$ for RANS equations in the embedded framework. The **FD** reference solution as described in section 11.1 is provided in the left column, the newly implemented analytic derivatives are visualized in the right column. **FD** and analytic solution are plotted using the same color-scheme.

Comparison of $\frac{d\mathbf{w}}{ds}$ in the body-fitted framework for all 3 equation types

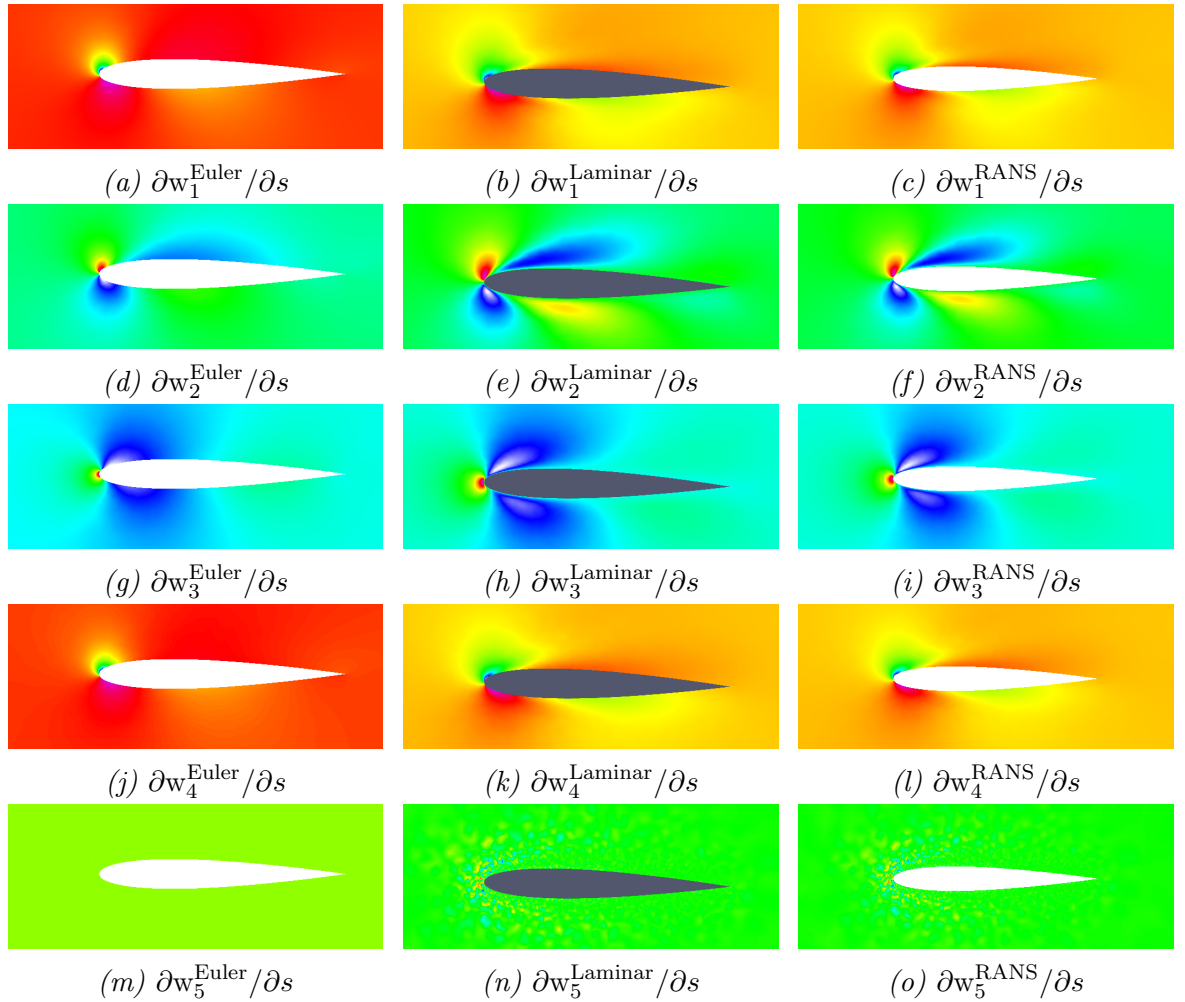


Figure 27: Comparison of analytic $\frac{d\mathbf{w}}{dM_\infty}$ for Euler equations(left column), laminar NSE equations (center column) and NSE equations with turbulence models (right column) in the body-fitted framework.

Comparison of $\frac{d\mathbf{w}}{ds}$ in the embedded framework for all 3 equation types

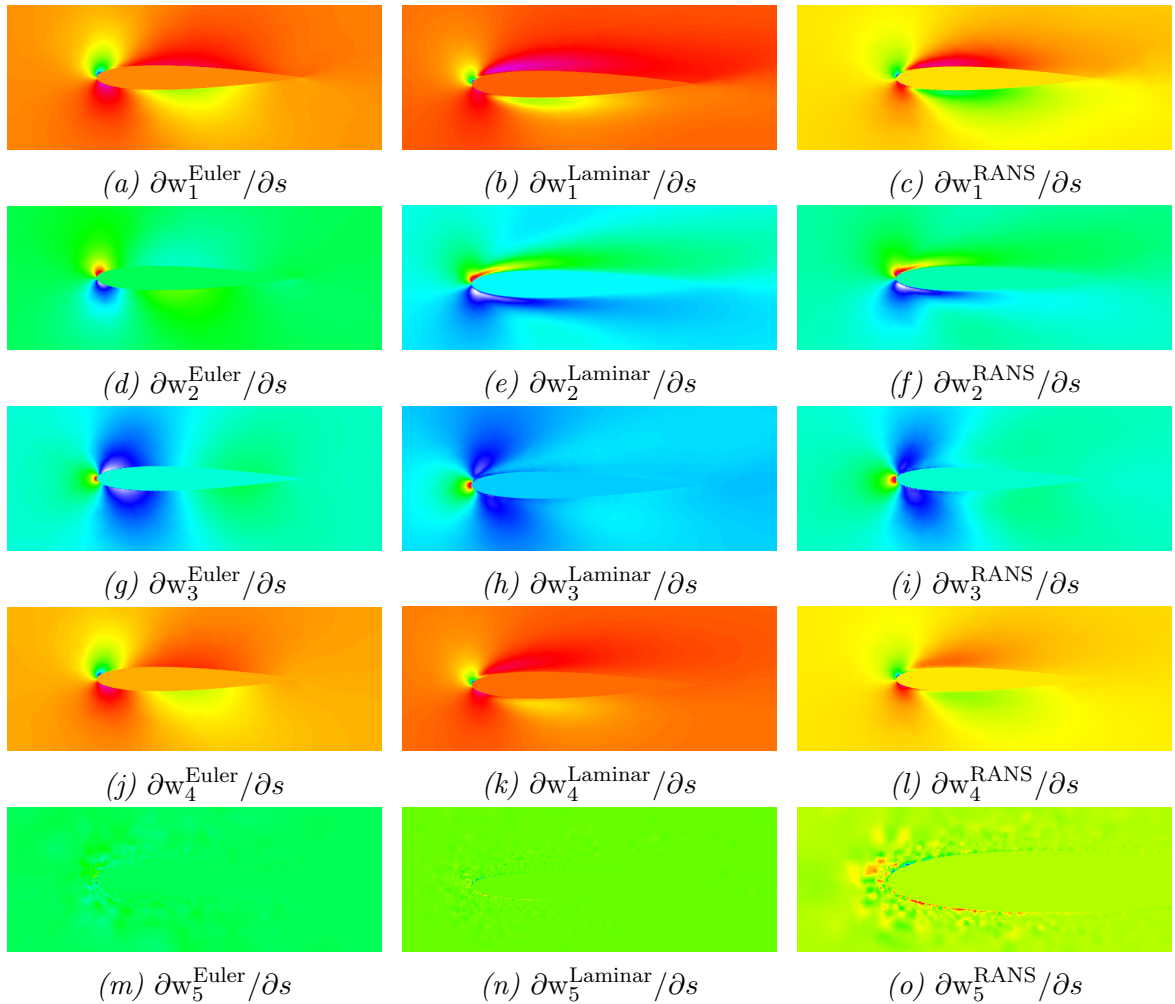


Figure 28: Comparison of analytic $\frac{d\mathbf{w}}{dM_\infty}$ for Euler equations(left column), laminar **NSE** equations (center column) and **NSE** equations with turbulence models (right column) in the embedded framework.

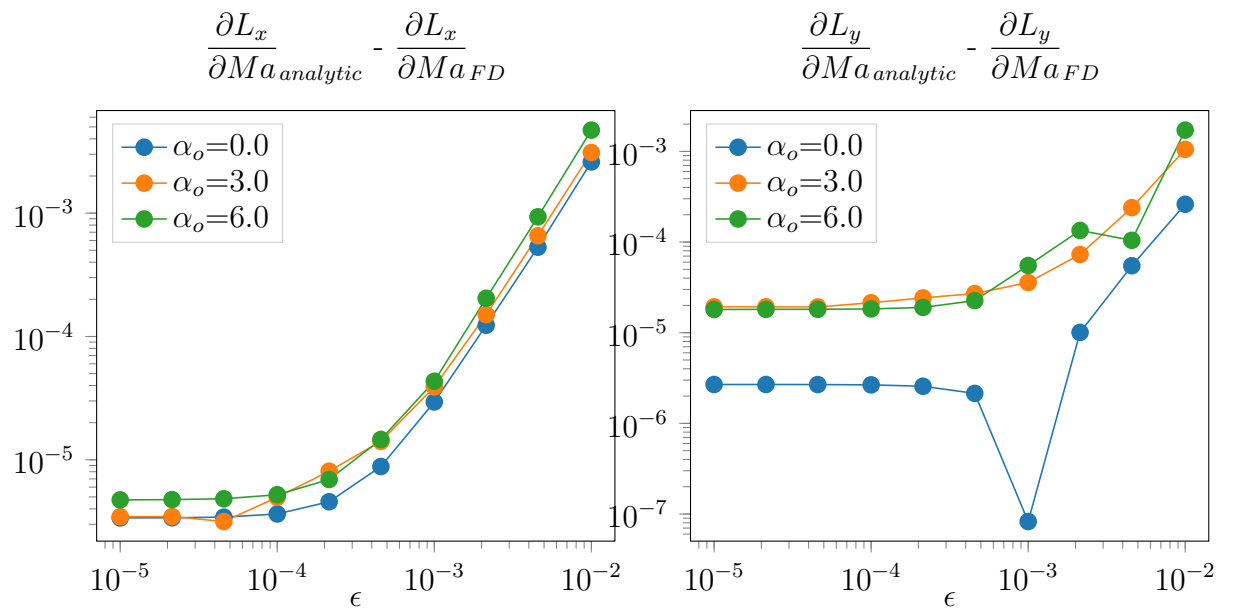


Figure 29: The graph shows the relative error between the Lift and Drag mach-sensitivities obtained by **FD** of two steady states, compared to the mach-sensitivity obtained by analytic direct evaluation. Please note that a **FD** Jacobian has been used here, which introduces an approximation error. Furthermore, the finite precision of the obtained steady states is another error source. This explains why the error levels off. For all practical optimization purposes, the obtained accuracy is more than enough.

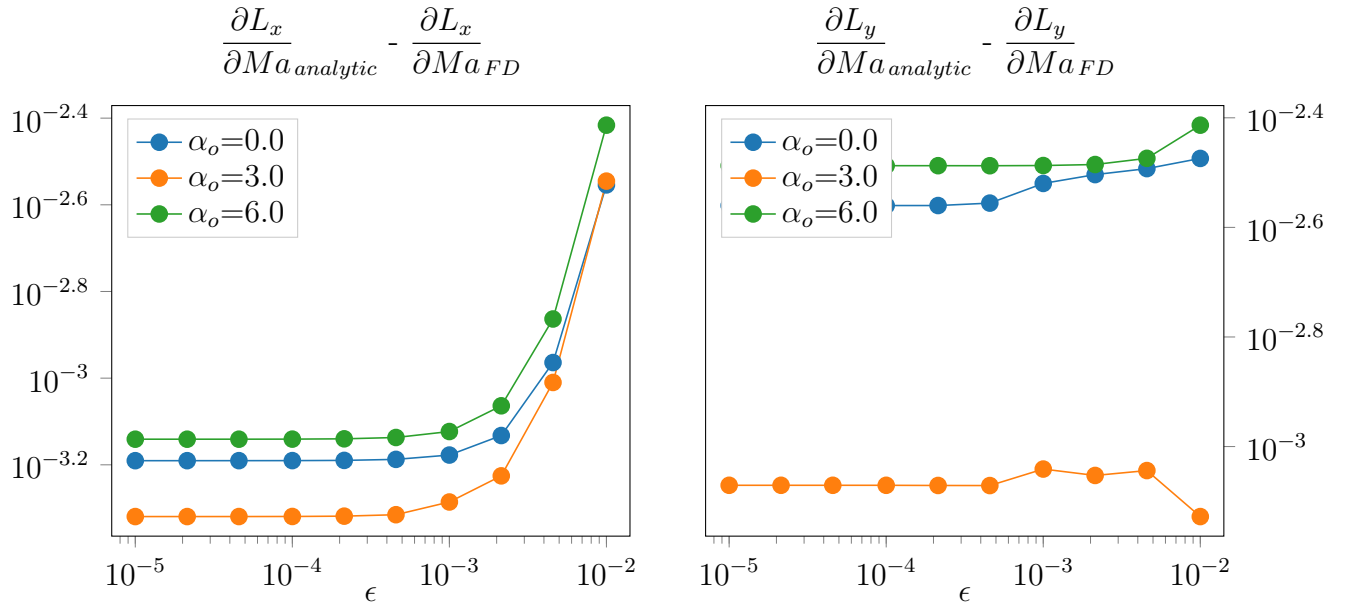


Figure 30: The graph shows the relative error between the Lift and Drag mach-sensitivities obtained by FD of two steady states, compared to the mach-sensitivity obtained by analytic direct evaluation. Please note that a FD Jacobian has been used here, which introduces an approximation error. Furthermore, the finite precision of the obtained steady states is another error source. This explains why the error levels off. For all practical optimization purposes, the obtained accuracy is more than enough.

Validation of the Lift and Drag results for shape-sensitivity: body-fitted Eulerequations

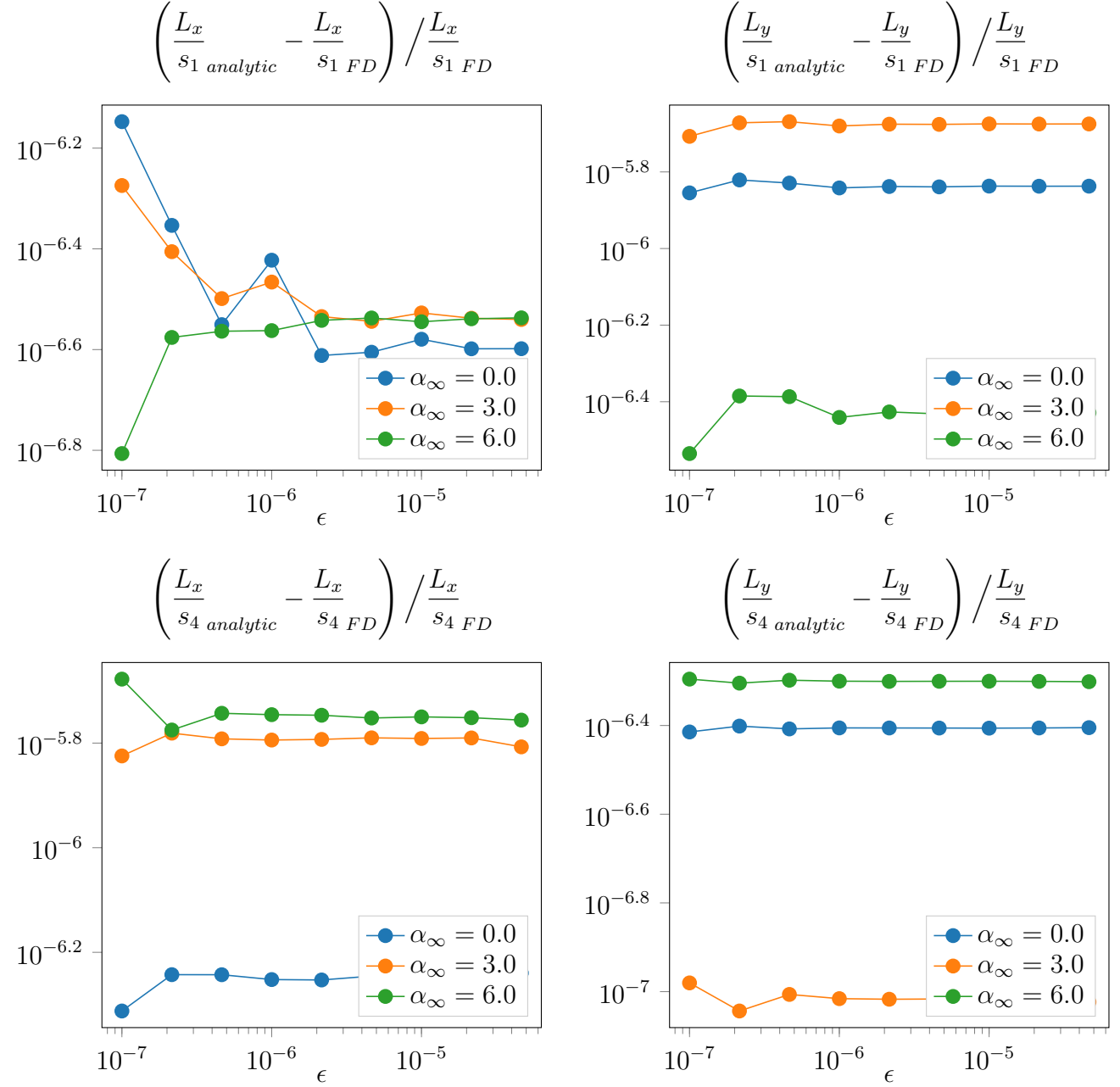


Figure 31: The graph shows the relative error between the Lift and Drag shape-sensitivities obtained by **FD** of two steady states, compared to the sensitivity obtained by analytic direct evaluation. Please note that a **FD** Jacobian has been used here, which introduces an approximation error. Furthermore, the finite precision of the obtained steady states is another error source. This explains why the error levels off. For all practical optimization purposes, the obtained accuracy is more than enough.

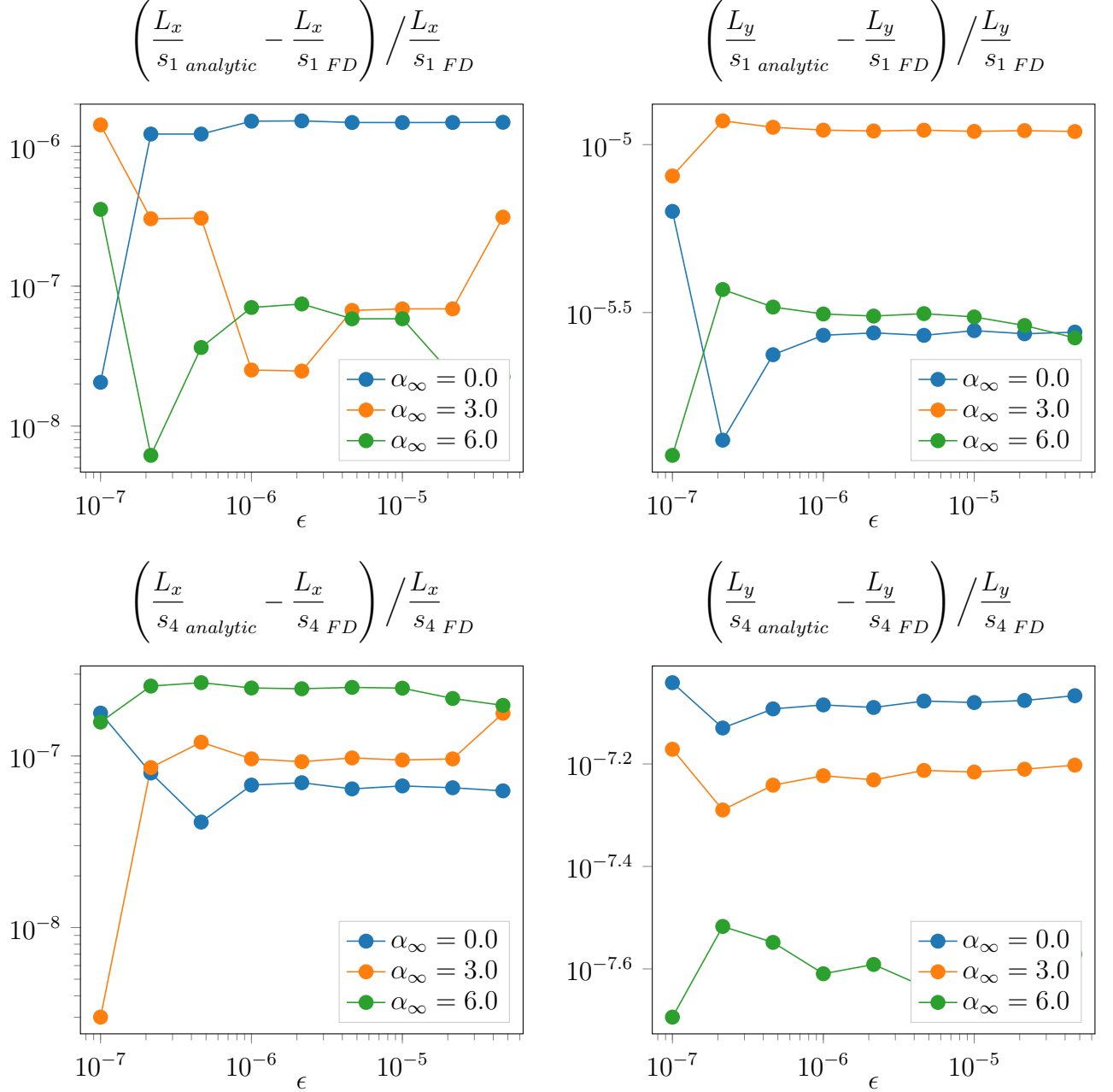
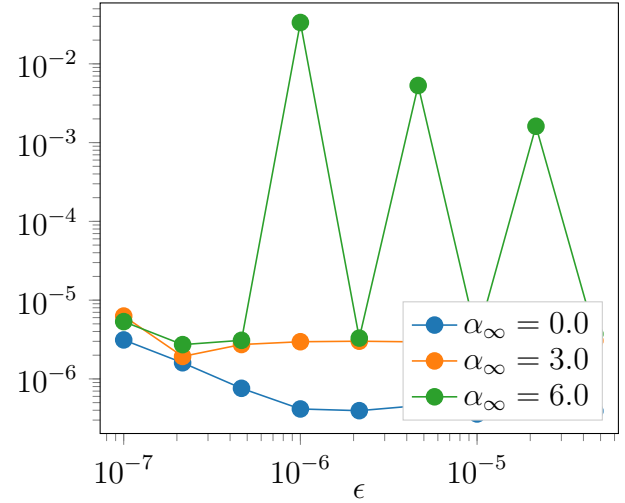
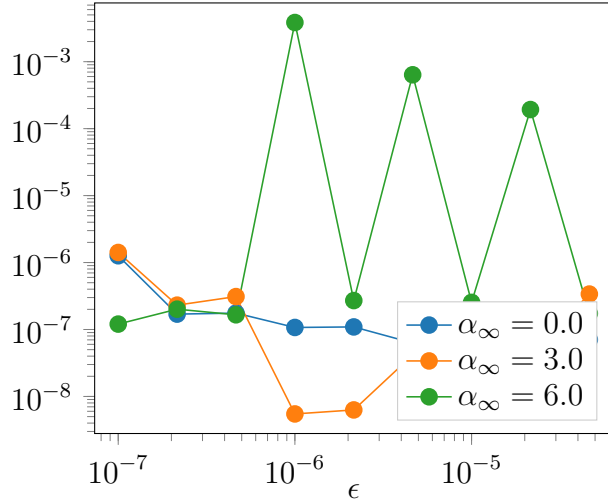
Validation of the Lift and Drag results for shape-sensitivity: body-fitted Laminarequations


Figure 32: The graph shows the relative error between the Lift and Drag shape-sensitivities obtained by FD of two steady states, compared to the sensitivity obtained by analytic direct evaluation. Please note that a FD Jacobian has been used here, which introduces an approximation error. Furthermore, the finite precision of the obtained steady states is another error source. This explains why the error levels off. For all practical optimization purposes, the obtained accuracy is more than enough.

Validation of the Lift and Drag results for shape-sensitivity: body-fitted RANSequations

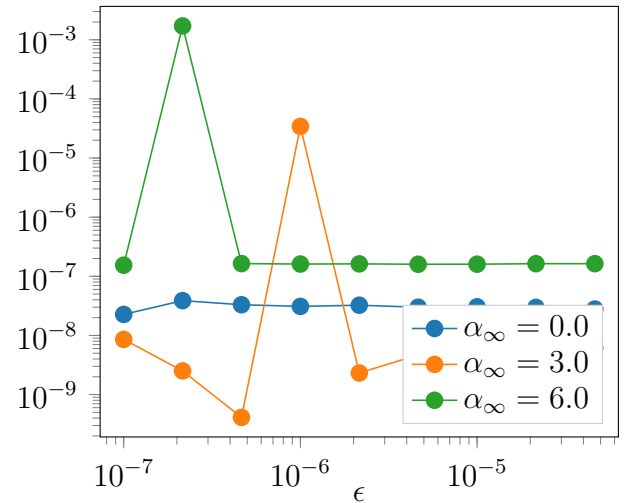
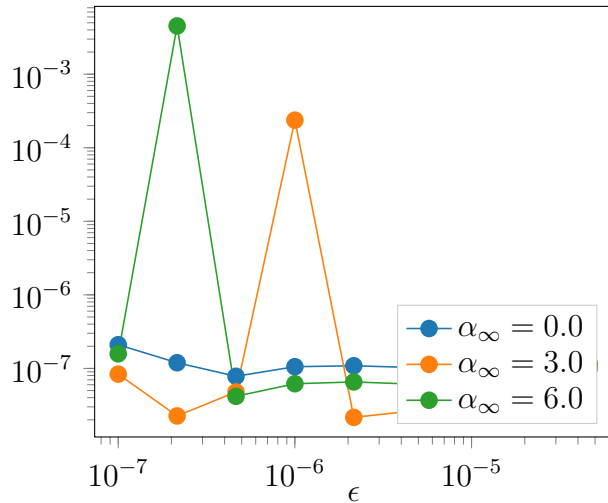
$$\left(\frac{L_x}{s_1 \text{ analytic}} - \frac{L_x}{s_1 \text{ FD}} \right) / \frac{L_x}{s_1 \text{ FD}}$$

$$\left(\frac{L_y}{s_1 \text{ analytic}} - \frac{L_y}{s_1 \text{ FD}} \right) / \frac{L_y}{s_1 \text{ FD}}$$



$$\left(\frac{L_x}{s_1 \text{ analytic}} - \frac{L_x}{s_1 \text{ FD}} \right) / \frac{L_x}{s_1 \text{ FD}}$$

$$\left(\frac{L_y}{s_1 \text{ analytic}} - \frac{L_y}{s_1 \text{ FD}} \right) / \frac{L_y}{s_1 \text{ FD}}$$



$$\left(\frac{L_x}{s_1 \text{ analytic}} - \frac{L_x}{s_1 \text{ FD}} \right) / \frac{L_x}{s_1 \text{ FD}}$$

$$\left(\frac{L_y}{s_1 \text{ analytic}} - \frac{L_y}{s_1 \text{ FD}} \right) / \frac{L_y}{s_1 \text{ FD}}$$

